MULTIMODAL IMAGING IN PARKINSON'S DISEASE:
EXPLORING IRON–, NEUROMELANIN-SENSITIVE MRI AND FDOPA PET RELATIONSHIPS

Thèse présentée en vue de l'obtention du titre de
Docteur en Sciences médicales

Frédérique Depierreux, M. D.

– Année Académique 2020-2021 –

COVER PICTURE

Penelope and the Suitors. John William Waterhouse, 1912
© Aberdeen City Council (Art Gallery & Museums Collections). Painting reproduced by kind permission of Aberdeen Art Gallery and Museums, United Kingdom.

BACK COVER

'I am half sick of shadows,' said The Lady of Shalott. John William Waterhouse, 1915 © Art Gallery of Ontario. Painting reproduced by kind permission of Art Gallery of Ontario, Canada.

SUPERVISOR

Professor Gaëtan GARRAUX
University of Liège

ASSESSMENT COMMITTEE

Professor Pierre MAQUET
President of the Committee
University of Liège

Professor Christophe PHILLIPS
University of Liège

Ms Evelyne BALTEAU
University of Liège

Professor Alain MAERTENS de NOORDHOUT
University of Liège

Professor Eric SALMON
University of Liège

Professor Patrick SANTENS
University of Gent

Professor Stéphane LEHERICY
Institut du Cerveau et de la Moëlle Epinière, Paris

© *Frédérique Depierreux, 2021*

Ce travail a été réalisé grâce au soutien financier du Fonds National de la Recherche Scientifique (FRS-FNRS) et du Fonds Rahier.

Nothing ever becomes real till it is experienced.

John Keats, Letters, 1819

In truth, whatever is worth doing at all, is
worth doing well; and nothing can be
done well without attention.

Philip Stanhope, 4th Earl of Chesterfield, Letters, 1774

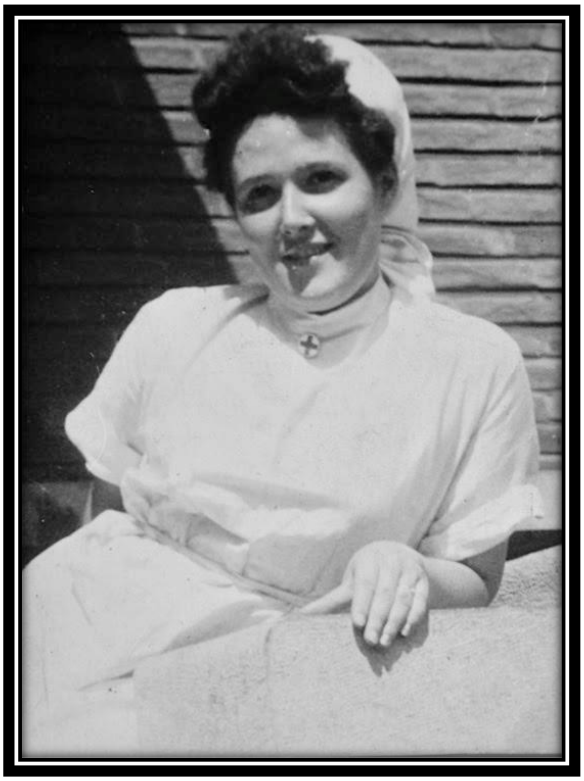

This work is dedicated to the memory of my beloved grand-mother Maria, depicted here when she was volunteering as a nurse during World War II.

REMERCIEMENTS

My first thoughts are naturally dedicated to my supervisor, the one and only Pr Garraux, whom I would like to thank for his absolutely unique mentorship and important role in this PhD.

This work would not have been possible without the precious help of the members of the MoVeRe group (Katherine Baquero, Tamara Daelemans, Laurane Mackels, Eric Parmentier) and the Cyclotron Research Centre members (Olivier Bodart, Sophie Lalou, Annick Claes, Brigitte Herbillon, Benjamin Lauricella, Patrick Hawotte, Mohamed Ali Bahri, Eric Salmon, Christian Degueldre, Christophe Philips and Evelyne Balteau). I will neither forget the inestimable organising talents of Laura Lambert and Lucia Canale, nor the optimism and comfort offered by the young and promising generation of neurologists, François Meyer, Solène Dauby, Lindsay Vogel, Emilie Drion, Florence Forte, Ibrahim Ben Razek and Nicolas Lambert. I will always remember and appreciate the support of two unique, clever and brilliant men, my eternal *binôme*, Haroun Jedidi, and my faithful *partner in crime* Eric Parmentier.

I am extremely grateful to my supervisor, the extraordinary and outstanding Prof. Pierre Maquet, for his invaluable advice, continuous support, and patience during my PhD study. His boundless knowledge and immense experience have encouraged me in all the time of my academic research. The endless hours spent coding together in Matlab will always remain a fond memory of mine. Most importantly, he taught me, *with magnanimous meekness, what strength was.*

I will never forget my first professor of Neurology, the "*greatest among the great*" Prof. Gustave Moonen, who continuously inspires me. As the first to believe in me, he shared with me his passion about neurology and passed on to me the taste for scientific research.

Finally, I would like to express my gratitude to my dearest and peaceful husband Pierre-Yves, and friends Martine Voos and Gilles Ghyssen for their encouragement and support all through my studies, especially regarding the tameless, swift and proud West Wind – *Zéphyr* – breeze and sometimes wild flurry.

CONTENT

CHAPTER 3 NEUROIMAGING OF PARKINSON'S DISEASE

PART 2 – PERSONAL CONTRIBUTION

CHAPTER 6 DISCUSSION

PART 3 – APPENDICES

LIST OF FIGURES

LIST OF TABLES

APPENDIX

LIST OF ABBREVIATIONS

AADC	Aromatic L-amino-acid decarboxylase
CBD	Corticobasal degeneration
DAT	Dopamine transporter
[^{18}F]DOPA	6-[^{18}F]fluoro-L-dopa
GPi	Globus pallidus pars interna
LC	Locus coeruleus
LEDD	Levodopa equivalent daily dose
MSA	Multiple system atrophy
MR	Magnetic resonance
MRI	Magnetic resonance imaging
NM	Neuromelanin
PD	Parkinson's disease
PET	Positron emission tomography
PSP	Progressive supranuclear palsy
RBD	REM sleep behavior disorder
REM	Rapid eye movement sleep
SCA	Spinocerebellar atrophy
SN	Substantia nigra
SNpc	Substantia nigra pars compacta
SNr	Substantia nigra pars reticulata
SPECT	Single photon emission computed tomography
TH	Tyrosine hydroxylase
UPDRS	Unified Parkinson's disease rating scale
VBM	Voxel based morphometry
VBQ	Voxel based quantification
VMAT2	Vesicular monoamine transporter 2

ABSTRACT

Parkinson's disease is a progressive neurodegenerative synucleinopathy characterised by a selective degeneration of neuromelanin-containing dopaminergic neurons and a deposition of iron in the substantia nigra pars compacta, beyond that observed in healthy brains of a similar age. However, the mutual interactions between neuromelanin loss, iron accumulation and nigro-striatal dysfunction still need to be clarified.

In the present work, we designed a study to assess the relationships between the dopaminergic function as measured by [^{18}F]DOPA PET and neuromelanin content and iron load in the substantia nigra, using respectively neuromelanin- and iron-sensitive MRI (R2*). Forty-six participants [23 Parkinson's disease patients and 23 healthy control participants, individually matched for age and sex] received on a single day a [^{18}F]DOPA PET, a qualitative neuromelanin-sensitive MRI, and a multiparameter protocol allowing for quantifying R2*. Data analysis consisted of voxelwise multiple regressions testing the group effect and, when relevant, its interaction with neuromelanin or iron signals. Substantia nigra values of R2* and neuromelanin were extracted automatically from regions of interest derived from an independent atlas of basal ganglia. Clinical asymmetry was taken into account in the analyses.

In Parkinson's disease patients, R2* was selectively increased in left lateral substantia nigra as compared to healthy participants, suggesting a local accumulation of iron in Parkinson's disease. By contrast, neuromelanin signal differed between Parkinson's disease patients and healthy controls but without specific regional distribution within substantia nigra. Dopaminergic function in posterior putamen, measured by [^{18}F]DOPA PET, decreased as R2* increased in lateral substantia nigra, indicating that dopaminergic function impairment, characteristic of PD, progresses with iron accumulation in the

substantia nigra. Putaminal dopaminergic function was also positively correlated with neuromelanin signal in lateral substantia nigra, indicating that dopaminergic function impairment parallels the depigmentation in the substantia nigra. A complex relationship was detected between R2* in the lateral substantia nigra and neuromelanin signal in the medial substantia nigra.

Multimodal imaging reveals regionally-specific relationships between iron accumulation and depigmentation within the substantia nigra of Parkinson's disease and provides in vivo insights in its neuropathology. Our results confirm the relevance of iron-sensitive and NM-sensitive MRI as biomarkers for Parkinson's disease diagnosis.

RESUME

La maladie de Parkinson est une pathologie neurodégénérative progressive appartenant au groupe des synucléinopathies, caractérisée, au sein de la substance noire (pars compacta), par une dégénérescence sélective de neurones dopaminergiques contenant de la neuromélanine et par une accumulation de fer, au-delà de ce qui est observé avec l'âge chez les sujets normaux. Cependant, les relations entre disparition de la neuromélanine, accumulation de fer et dysfonction des voies nigrostriées doivent encore être clarifiées.

Dans le présent travail, nous avons choisi d'étudier les relations entre, d'une part, la fonction dopaminergique mesurée par la TEP cérébrale à la [^{18}F]DOPA et, d'autre part, le contenu en neuromélanine et la charge en fer de la substance noire, en utilisant respectivement des séquences IRM spécifiques sensibles au contenu en neuromélanine et en fer (R2* - taux de relaxation transverse effective). Quarante-six participants (23 patients souffrant d'une maladie de Parkinson idiopathique et 23 sujets contrôles sains, appariés individuellement pour l'âge et le sexe) ont subi le même jour une TEP à la [^{18}F]DOPA, et une IRM cérébrale comportant des séquences neuromélanine (qualitatives) ainsi qu'un protocole de séquences « multiparamétriques » permettant notamment la quantification du taux effectif de relaxation transverse, R2*. L'analyse des données a été effectuée voxel par voxel (« voxelwise ») par des régressions multiples univariées testant l'effet de groupe, et le cas échéant, ses interactions avec les signaux neuromélanine et R2*. Les valeurs de R2* et de neuromélanine de la substance noire ont été extraites de façon automatique de régions d'intérêt définies en utilisant un atlas indépendant des noyaux gris de la base. L'asymétrie des manifestations cliniques a été prise en compte dans les analyses statistiques.

Chez les patients parkinsoniens, les valeurs de R2* étaient plus élevées dans la substance noire latérale gauche par comparaison aux sujets contrôles, suggérant une accumulation locale de fer liée à la maladie de Parkinson. En revanche, le signal extrait des séquences neuromélanine différait entre patients parkinsoniens et contrôles, mais sans que ne soit mise en évidence une distribution régionale spécifique au sein de la substance noire. La fonction dopaminergique mesurée par TEP à la [^{18}F]DOPA dans le putamen postérieur était réduite lorsque le signal R2* de la substance noire latérale augmentait, indiquant que l'altération du fonctionnement dopaminergique des voies nigrostriées progresse avec l'accumulation de fer au sein de la substance noire. Une corrélation positive entre la fonction dopaminergique putaminale et le signal extrait des séquences neuromélanine dans la substance noire latérale a également été mis en évidence, indiquant que la dysfonction dopaminergique progresse parallèlement à la dépigmentation de la substance noire. Enfin, une relation complexe entre le signal R2* de la substance noire latérale et le signal neuromélanine de la substance noire médiale a également été détectée.

L'imagerie multimodale révèle ainsi des relations régionales spécifiques entre l'accumulation de fer et la dépigmentation de la substance noire dans la maladie de Parkinson, permettant d'entrevoir in vivo les processus neuropathologiques à l'œuvre durant la progression de cette affection dégénérative. Les résultats de notre étude confirment la pertinence des séquences IRM sensibles à la neuromélanine et aux dépôts de fer en tant que biomarqueurs potentiels du diagnostic de la maladie de Parkinson.

PART 1

Introduction

CHAPTER 1

1 CLINICAL OVERVIEW OF PARKINSON'S DISEASE

1 GENERAL CONSIDERATIONS

Parkinson's disease (PD) is a progressive neurodegenerative disease, classically characterised by bradykinesia, rigidity, tremor at rest and postural instability (Fahn et al., 2011). In addition to the motor symptoms, a variety of non-motor symptoms develops over the course of the disease (and often precedes motor symptoms), including sleep dysfunction, hyposmia, cognitive impairment, autonomic dysfunction, etc. Although the aetiology of idiopathic PD is largely unknown, its neuropathological hallmarks are well specified as the degeneration of the nigrostriatal pathway, resulting in motor symptoms, and deposits of alpha-synuclein throughout peripheral and central nervous systems.

2 EPIDEMIOLOGY

PD is the second most frequent adult-onset neurodegenerative disorder worldwide (Hirtz *et al.*, 2007) and a growing public health issue given population aging, as age is a major risk factor. In Europe, prevalence of PD is estimated from 1267 to 1535 per 100 000 inhabitants, depending on the age and sex group studied (Pringsheim *et al.*, 2014) , and the incidence is usually comprised between 8 and 18 per 100,000 persons a year (de Lau and Breteler, 2006). PD

prevalence increases with age, and is usually affecting more men than women, with a male-to-female ratio of about 1.5 (Tysnes and Storstein, 2017). However, this sex ratio varies according the age group and the geographic location considered (Pringsheim *et al.*, 2014).

3 DIAGNOSIS CRITERIA

A definite diagnosis of PD requires pathological examination of the brain at autopsy (Postuma et al., 2015). Unfortunately, there is currently no laboratory test or imaging technique that can reliably diagnose PD during life. The diagnosis of PD in vivo is still largely based on the correct identification of its clinical features, relying on medical history and neurological examination (Berardelli et al., 2013).

However, clinical diagnosis remains uncertain at initial presentation, and many patients initially diagnosed with PD will later on receive another diagnosis (e.g. atypical Parkinsonism). Diagnostic accuracy varies according to the expertise of the clinician, disease duration, age, etc. (Postuma et al., 2015). In 1992, Hugues et al. demonstrated in a clinico-pathological correlation study of PD that 76% of cases diagnosed with idiopathic PD during life satisfied the established neuropathological criteria for idiopathic PD (Hughes et al., 1992) ("depletion of brain stem pigmented neurons with Lewy bodies in some of the remaining nerve cells"). More recent studies showed that between 75% and 95% of patients diagnosed with PD by experts have their diagnosis confirmed by autopsy (Litvan et al., 1998; Adler et al., 2014).

Until recently, the most widely used clinical criteria for the diagnosis of PD were the UK Parkinson's Disease Society Brain Bank clinical diagnostic criteria (UKBBC) (Gibb and Lees, 1988) **(see Table 1)**. However, they were superseded by new diagnostic criteria, which support the clinical diagnosis by selected investigations (genetic,

olfactory, neuropsychological tests and neuroimaging studies, like transcranial sonography, etc.) (Berardelli et al., 2013).

Novel diagnostic criteria were proposed by the International Parkinson and Movement Disorder Society (MDS) in 2015 [Clinical Diagnostic Criteria for Parkinson's disease (MDS-PD Criteria), **see Table 2**] in order to codify the expert clinical diagnostic process and to help standardise diagnosis in research and clinical settings. A recent validation study using these criteria demonstrated high sensitivity and specificity but the gold standard used for the comparison was expert clinical diagnosis, not pathologic examination. The overall accuracy for "probable PD" diagnosis was estimated at 92.6%. According to this validation study, sensitivity and specificity of MDS-PD Criteria are both higher than those achieved using United Kingdom Brain Bank criteria (Postuma et al., 2018).

TABLE 1 - UK Parkinson's Disease Society Brain Bank clinical diagnostic criteria (Gibb and Lees, 1988)

STEP 1 – DIAGNOSIS OF PARKINSONIAN SYNDROME
BRADYKINESIA (slowness of initiation of voluntary movement with progressive reduction in speed and amplitude of repetitive actions) and at least one of the following: a. muscular rigidity b. 4-6 Hz rest tremor c. postural instability not caused by primary visual, vestibular, cerebellar or proprioceptive dysfunction.
STEP 2 - EXCLUSION CRITERIA FOR PARKINSON'S DISEASE
- history of repeated strokes with stepwise progression of Parkinsonian features - history of repeated head injury - history of definite encephalitis - oculogyric crises - neuroleptic treatment at onset of symptoms - more than one affected relative - sustained remission - strictly unilateral features after three years - supranuclear gaze palsy - cerebellar signs - early severe autonomic involvement - early severe dementia with disturbances of memory, language and praxis - Babinski sign - presence of a cerebral tumour or communicating hydrocephalus on CT scan. - negative response to large doses of levodopa (if malabsorption excluded) - MPTP exposure
STEP 3 - SUPPORTIVE PROSPECTIVE POSITIVE CRITERIA FOR PARKINSON'S DISEASE.
Three or more required for diagnosis of definite Parkinson's disease. - unilateral onset - rest tremor present - progressive disorder - persistent asymmetry affecting the side of onset - most excellent response (70-100%) to levodopa - severe levodopa-induced chorea - levodopa response for 5 years or more - clinical course of 10 years or more

TABLE 2 – MDS (Movement Disorders Society) Clinical Diagnostic Criteria for Parkinson's disease (Postuma *et al.*, 2015)

	The first essential criterion is parkinsonism, which is defined as bradykinesia, in combination with at least 1 of rest tremor or rigidity. Examination of all cardinal manifestations should be carried out as described in the MDS–Unified Parkinson Disease Rating Scale. Once parkinsonism has been diagnosed: **Diagnosis of Clinically Established PD requires:** 1. Absence of absolute exclusion criteria 2. At least two supportive criteria, and 3. No red flags **Diagnosis of Clinically Probable PD requires:** 1. Absence of absolute exclusion criteria 2. Presence of red flags counterbalanced by supportive criteria If 1 red flag is present, there must also be at least 1 supportive criterion If 2 red flags, at least 2 supportive criteria are needed No more than 2 red flags are allowed for this category
SUPPORTIVE CRITERIA	1. Clear and dramatic beneficial response to dopaminergic therapy. During initial treatment, patient returned to normal or near-normal level of function. In the absence of clear documentation of initial response a dramatic response can be classified as: a) Marked improvement with dose increases or marked worsening with dose decreases. Mild changes do not qualify. Document this either objectively (>30% in UPDRS III with change in treatment), or subjectively (clearly-documented history of marked changes from a reliable patient or caregiver). b) Unequivocal and marked on/off fluctuations, which must have at some point included predictable end-of-dose wearing off. 2. Presence of levodopa-induced dyskinesia 3. Rest tremor of a limb, documented on clinical examination (in past, or on current examination) 4. The presence of either olfactory loss or cardiac sympathetic denervation on MIBG scintigraphy

ABSOLUTE EXCLUSION CRITERIA	The presence of any of these features rules out PD: 1. Unequivocal cerebellar abnormalities, such as cerebellar gait, limb ataxia, or cerebellar oculomotor abnormalities (eg, sustained gaze evoked nystagmus, macro square wave jerks, hypermetric saccades) 2. Downward vertical supranuclear gaze palsy, or selective slowing of downward vertical saccades 3. Diagnosis of probable behavioural variant frontotemporal dementia or primary progressive aphasia, defined according to consensus criteria within the first 5 years of disease 4. Parkinsonian features restricted to the lower limbs for more than 3 years 5. Treatment with a dopamine receptor blocker or a dopamine-depleting agent in a dose and time-course consistent with drug-induced parkinsonism 6. Absence of observable response to high-dose levodopa despite at least moderate severity of disease 7. Unequivocal cortical sensory loss (ie, graphesthesia, stereognosis with intact primary sensory modalities), clear limb ideomotor apraxia, or progressive aphasia 8. Normal functional neuroimaging of the presynaptic dopaminergic system 9. Documentation of an alternative condition known to produce parkinsonism and plausibly connected to the patient's symptoms, or, the expert evaluating physician, based on the full diagnostic assessment feels that an alternative syndrome is more likely than PD
RED FLAGS	1. Rapid progression of gait impairment requiring regular use of wheelchair within 5 y of onset 2. A complete absence of progression of motor symptoms or signs over 5 or more y unless stability is related to treatment 3. Early bulbar dysfunction: severe dysphonia or dysarthria (speech unintelligible most of the time) or severe dysphagia (requiring soft food, NG tube, or gastrostomy feeding) within first 5 years 4. Inspiratory respiratory dysfunction: either diurnal or nocturnal inspiratory stridor or frequent inspiratory sighs 5. Severe autonomic failure in the first 5 years of disease. This can include: a) Orthostatic hypotension—orthostatic decrease of blood pressure within 3 min of standing by at least 30 mm Hg systolic or 15 mm Hg diastolic, in the absence of dehydration, medication, or other diseases that could plausibly explain autonomic dysfunction, or

RED FLAGS	b) Severe urinary retention or urinary incontinence in the first 5 years of disease (excluding long-standing or small amount stress incontinence in women), that is not simply functional incontinence. In men, urinary retention must not be attributable to prostate disease, and must be associated with erectile dysfunction 6. Recurrent (>1/y) falls because of impaired balance within 3 years of onset 7. Disproportionate anterocollis (dystonic) or contractures of hand or feet within the first 10 years 8. Absence of any of the common nonmotor features of disease despite 5 years disease duration. These include sleep dysfunction (sleep-maintenance insomnia, excessive daytime somnolence, symptoms of REM sleep behavior disorder), autonomic dysfunction (constipation, daytime urinary urgency, symptomatic orthostasis), hyposmia, or psychiatric dysfunction (depression, anxiety, or hallucinations) 9. Otherwise-unexplained pyramidal tract signs, defined as pyramidal weakness or clear pathologic hyperreflexia (excluding mild reflex asymmetry and isolated extensor plantar response) 10. Bilateral symmetric parkinsonism. The patient or caregiver reports bilateral symptom onset with no side predominance, and no side predominance is observed on objective examination

In these new criteria, the motor syndrome (parkinsonism) remains the core feature by which clinical PD is defined, but non-motor manifestations are now included as well. The MDS criteria use a two-step process: first, parkinsonism must be identified (bradykinesia in combination with either rest tremor, rigidity, or both), then the clinician has to establish whether this parkinsonism is attributable to PD.

Indeed, misdiagnoses generally include other pathologies causing neurodegenerative or secondary parkinsonism (progressive supranuclear palsy, multiple system atrophy, cortico-basal syndrome, basal ganglia vascular disease, etc.) or other diseases presenting with similar clinical features, without authentic parkinsonian disorder (essential tremor, dystonic tremor, etc.).

In 2016, Rizzo et al. proposed a meta-analysis regarding the accuracy of clinical diagnosis of PD, as reported in the last 25 years. Twenty studies have been reviewed, most of them using pathologic examination as the gold standard for PD diagnosis. Based on the latter, the pooled diagnostic accuracy was 80.6%. Authors concluded that the validity of clinical diagnosis of PD did not improve in the last 25 years, and that reliable biomarkers are urgently needed to improve the accuracy of clinical diagnosis in vivo (Rizzo *et al.*, 2016*a*).

4 CLINICAL ASSESSMENT

4.1 RATING SCALES

In order to quantify the severity of parkinsonian symptoms and signs, various scales have been proposed over the past forty years. Most studies used the Unified Parkinson's Disease Rating Scale (UPDRS), originally developed in the 1980s (Fahn, S.; Elton, 1987), or Hoehn and Yahr staging scale (Hoehn and Yahr, 1967). In order to improve some of the limitations of the original scale, the Movement Disorders Society (MDS) commissioned a revision of the UPDRS scale, resulting

in 2008 in a new version, named the MDS–sponsored UPDRS revision (MDS-UPDRS) (Goetz *et al.*, 2008).

In our study, we used the third section of MDS-UPDRS scale, dedicated to motor examination **(see Appendix 1, Table 1)**. Hoehn and Yahr staging scale was also used **(see Table 3)** to get a general idea about Parkinson's disease progression.

TABLE 3 - Hoehn and Yahr staging scale (Hoehn and Yahr, 1967)

STAGE	
0	Asymptomatic
1	Unilateral involvement only usually (with minimal or no functional disability)
2	Bilateral or midline involvement without impairment of balance
3	Mild to moderate involvement; some postural instability but physically independent, needs assistance to recover from pull test
4	Severely disabling disease; still able to walk or stand unassisted
5	Wheelchair bound or bedridden unless aided

Other scales have been developed for PD studies in an attempt to assess the overall health-related quality of life, such as the Parkinson's disease quality of life questionnaire (PDQL) or the Parkinson's disease questionnaire-39 (PDQ-39, **see Appendix 2, Table 2**) (Jenkinson *et al.*, 1997). Other tools focus on different aspects of the disease, such as the nonmotor symptoms scale (NMSS) (Chaudhuri *et al.*, 2006, 2007) or the gait and balance scale (GABS) (Thomas *et al.*, 2004).

4.2 OTHER MEASURES

In order to account for the effect of treatment, levodopa equivalent dose or LED has also been assessed in our study. The standardised LED formula uses conversion factors that have been calculated for antiparkinsonian drugs in order to estimate a total daily levodopa equivalent dose (Tomlinson *et al.*, 2010), and represents a useful tool to compare doses between clinical studies.

CHAPTER 2

2 NEUROPATHOLOGY OF PARKINSON'S DISEASE

1 OVERVIEW AND HISTORY

As detailed in the next section **(Chapter 2, Section 2)**, the two main pathological features in Parkinson's disease include a progressive neuronal loss in vulnerable cell populations within the substantia nigra and the presence of Lewy body pathology in surviving neurons of the substantia nigra. These two aspects had their own historical developments.

Parkinson's disease was first recognised as a unique clinical entity by James Parkinson in 1817, in his "Essay on the Shaking Palsy". Many decades later, in 1871, Meynert identified the involvement of basal ganglia in movement disorders. By the end of the nineteenth century, Brissaud was the first to suggest that substantia nigra is affected in PD (1895). This discovery was confirmed in 1919 by Tetriakoff, who reported the loss of cells in the substantia nigra, cells that were later shown to contain dopamine. He also showed that each substantia nigra served the motor activity of the contralateral side of the body. Since then, many authors invariably confirmed degenerative lesions in SN (Foix and Nicolesco, 1925) and further demonstrated that the degenerative process involved many other nuclei, such as the locus coeruleus, the raphe nuclei, the nucleus basalis of Meynert, etc. (Hassler, 1938; Greenfield and Bosanquet, 1953; Jellinger, 1987).

Ehringer and Hornykiewicz reported in 1960 that the striatum of PD patients was deficient in dopamine.

The first observations of Lewy bodies dates back to 1912, when Fritz Jacob Heinrich Lewy discovered these then novel cytoplasmic inclusions in dorsal *vagus nucleus* and *substantia innominata* of PD brains (Lewy, 1912, 1914). Lafora was the first to acknowledge Lewy's findings in 1913 and the first to name them 'Lewy bodies' (Lafora, 1913; Engelhardt, 2017). These findings were confirmed by Tretiakoff in his doctoral thesis, who found an important loss of neurons beside the presence of intraneuronal eosinophilic inclusions (designating them as 'corps de Lewy') in the substantia nigra of his patients with typical Parkinson's disease (Tretiakoff, 1919; Lees *et al.*, 2008; Engelhardt, 2017). Since the 1980s, Lewy neurites and Lewy bodies, composed of aggregates of α-synuclein as discovered in 1997 (Polymeropoulos *et al.*, 1997; Spillantini *et al.*, 1997; Stefanis, 2012), are considered as the second neuropathological hallmark of PD (Gibb and Lees, 1988).

Beside these fundamental features of PD pathology, the role of iron in aging and PD has also been studied by scientists since the 1920's (Spatz, 1922; Lhermitte *et al.*, 1924), and its increasing deposition in basal ganglia with age has been highlighted in 1958 by Hallgren and Sourander (Hallgren and Sourander, 1958). After these first studies, the connection between iron and PD [but also its important role in other neurodegenerative diseases (Gerlach *et al.*, 1994; Ward *et al.*, 2014)] became an important field of research, in both PD histopathology and PD neuro-imaging.

2 PATHOLOGICAL CRITERIA FOR THE DIAGNOSIS OF PARKINSON'S DISEASE

The available pathological criteria for PD (Gibb and Lees, 1988; Gelb et al., 1999; Dickson et al., 2009) require two key histopathological features (**see Figure 1**):

1) moderate to severe selective neuronal loss in the substantia nigra pars compacta (SNpc) AND

2) Lewy pathology

The term 'Lewy pathology' includes various α-synuclein immunoreactive neuronal inclusions. Lewy bodies, the most common of them, appear as round eosinophilic inclusions in neuronal perikarya, but other inclusions are also observed, such as intraneuritic Lewy bodies, Lewy neurites, dot-like structures, and axonal spheroids. In normal conditions, α-synuclein is a small presynaptic protein that is unfolded and highly soluble, but in PD, α-synuclein accumulates as highly insoluble aggregates (amyloid fibrils), stabilised by β-sheet protein structure (Spillantini *et al.*, 1997, 1998; Clayton and George, 1999).

As neuronal loss in the SNpc is found in a vast range of parkinsonian disorders, the presence of Lewy pathology is necessary to distinguish PD from other disorders ('non-α-synucleinopathies').

However, it has to be highlighted that the role of α-synuclein in the neurodegeneration observed in PD remains debated. Moreover, some genetic forms of PD are characterised by nigral degeneration without Lewy bodies, as in patients presenting with PARK2 (Takahashi *et al.*, 1994) or various LRRK2 mutations (Hasegawa and Kowa, 1997). The value of the biomarkers based on α-synuclein presence should then be taken with caution.

FIGURE 1 – **Histopathological features characterising Parkinson's disease.** Pigmented dopaminergic neurons density in a normal subject (A), compared to pigmented neurons density in a PD patient (B). Lewy bodies illustration (C), characterised by round eosinophilic inclusions in neuronal perikarya. Histological section in the midbrain, stained with hematoxylin eosin. Enlargement. 200x (A-B); enlargement. 400x (C). Image courtesy Pr M. Deprez and Dr E. Bianchi, University of Liège.

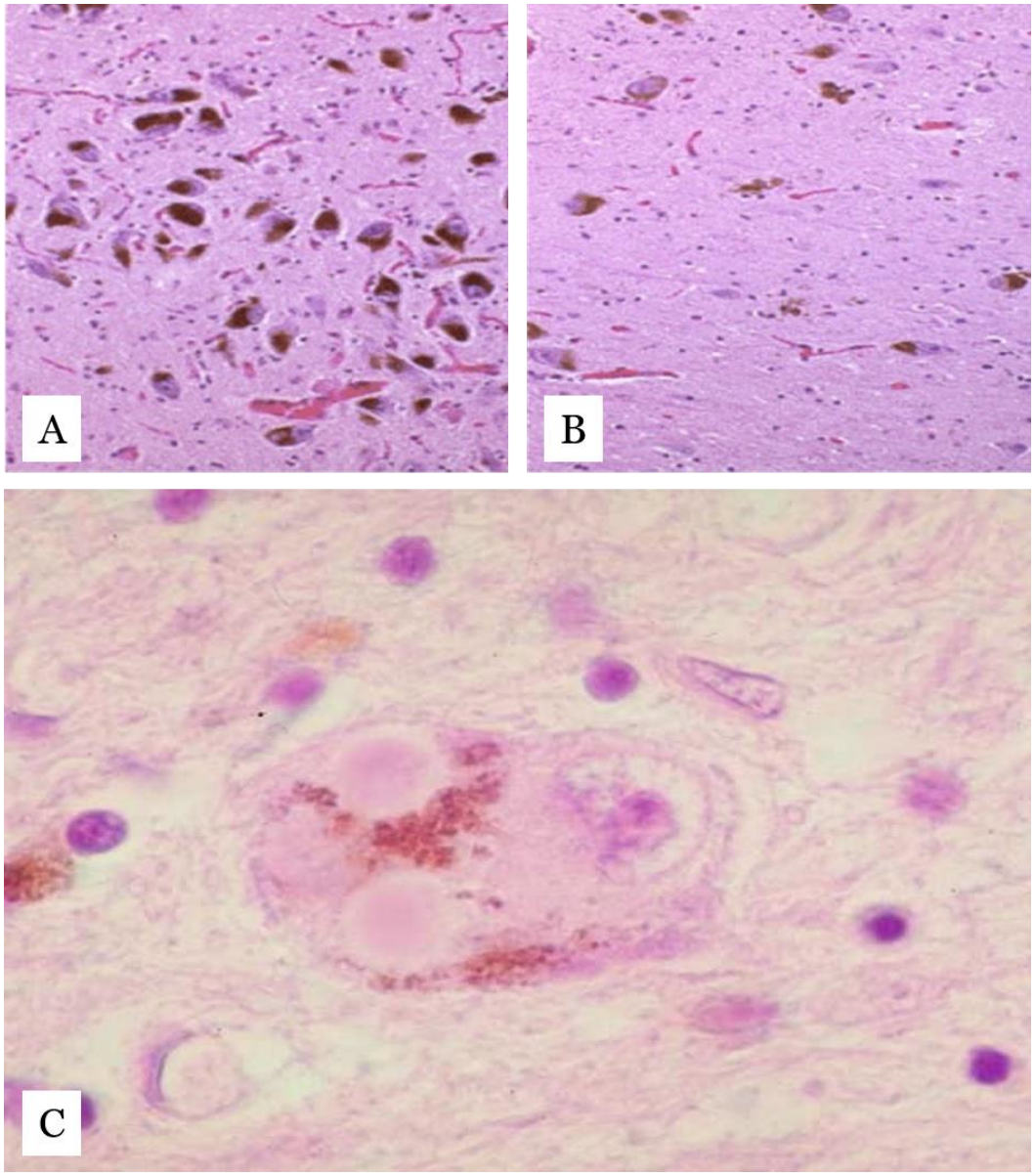

3 THE NIGROSTRIATAL PATHWAY

3.1 ANATOMY AND FUNCTION OF THE BASAL GANGLIA

In order to understand the pathological processes at the origin of PD, it may be appropriate to briefly discuss the normal anatomy and function of the nigrostriatal system. Basal ganglia are a group of nuclei located deep in the brain, including the caudate nucleus and the putamen (the latter two forming the striatum), the globus pallidus, the subthalamic nucleus (in the diencephalon) and the substantia nigra **(see Figures 2 and 3)**. The latter is located in the mesencephalon. Due to their implication in movement disorders, basal ganglia have always been considered to have a predominant motor function, but it is now established that they also play a role in cognitive and emotional functions (Fahn *et al.*, 2011).

SN is divided in two main parts, differing in function and histology. SN pars reticulate (SNr) is very similar to the GPi regarding histology and connectivity. SNr contains sparse neurons, generally without neuromelanin pigment, afferent fibre bundles and thick dendrites. SN pars compacta (SNpc) contains a majority of large dopaminergic neurons (± 50 µm), which are the origin of nigrostriatal projections (Di Lorenzo Alho et al., 2016). These dopaminergic neurons appear as dark cells as they contain a pigment, neuromelanin (NM), giving the name "nigra" to this nucleus **(see Figure 4)**.

In a morphological study of *post-mortem* brains from healthy controls (from 50 to 91 years old) using design-specified stereology, the mean volume of normal SN (both sides) was estimated at 188.3 mm^3 (Di Lorenzo Alho et al., 2016). However, the authors highlighted marked intra- and inter-individual differences regarding shape, volume, asymmetry and neuron density of the SN. Besides, they found a negative correlation between age and total SN volume, whereas the number of neurons remained stable with age.

Finally, the substantia nigra (pars compacta, SNpc) is anatomically in position of profoundly modulating the main motor loops in the basal ganglia. It innervates the striatum via the nigrostriatal pathway and uses dopamine as its main neurotransmitter (for practical considerations, dopamine synthesis is detailed in **Chapter 3, Section 1.2**). The classical model (Crossman, 1987; Albin et al., 1989; Alexander et al., 1990; Alexander, 1994), although admittedly an oversimplification, remains a useful concept to grasp the influence of SN on basal ganglia. It includes two parallel loops, the direct and indirect pathways, coming from the cortex, going through the basal ganglia and going back to the cortex. The direct pathway starts with cortical glutamatergic input which projects to the striatum, then continues to the GPi, then the thalamus and goes back to the cortex. The indirect pathway starts also with cortical input and projects to the striatum and subthalamic nucleus, then to the GPe, GPi and thalamus before going back to the cortex. The putaminal neurons implicated in the direct pathway have D2 dopaminergic receptors and are activated by dopamine, whereas the putaminal neurons implicated in the indirect pathway are characterised by D1 dopaminergic receptors, and are inhibited by the neurotransmitter (Fahn *et al.*, 2011). Overall, SNpc facilitates movement (as it facilitates the direct pathway and inhibits the indirect pathway) but also modulates reward behaviours.

Our understanding of circuitry in basal ganglia is still evolving: this model is a simplification of the basal ganglia physiology, and many novel connections were discovered in the recent years, such as the "hyperdirect pathway". A revised model is currently emerging, taking into account more connections of the basal ganglia and various subcortical and brainstem structures, such as the pedonculo-pontine nucleus (Obeso *et al.*, 2008; Obeso and Lanciego, 2011).

FIGURE 2 – **Anatomy of the basal ganglia**. Coronal section in the brain of a healthy subject, after formaldehyde fixation. Basal ganglia including caudate, putamen, and globus pallidus. Courtesy, Pr M. Deprez and Dr E. Bianchi.

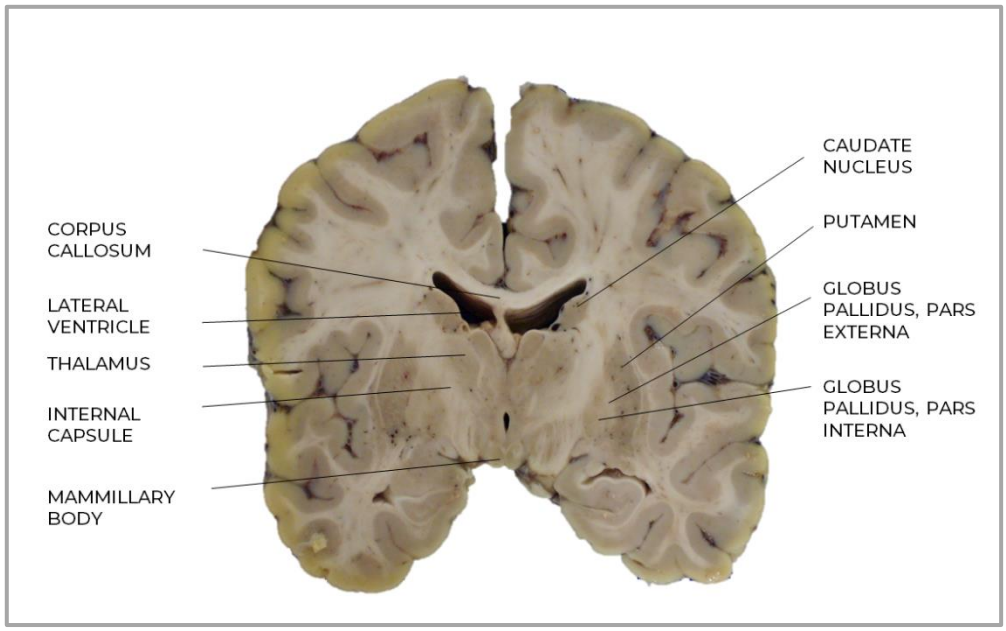

FIGURE 3 – **Anatomy of the midbrain.** Axial section in the midbrain of a healthy subject, after formaldehyde fixation. Brain is seen from below. Courtesy, Pr M. Deprez and Dr E. Bianchi.

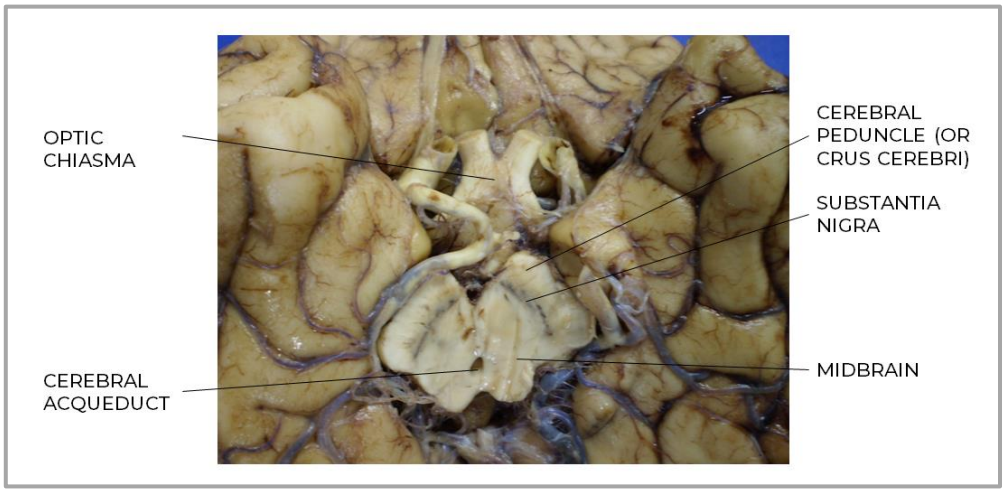

FIGURE 4 – **Dopaminergic pigmented neurons in the substantia nigra.**
Example of histological section of the midbrain, focused on the substantia nigra. The SN was dissected from a healthy brain and stained with cresyl violet. Pigmented neurons can be easily spotted with this type of staining (see arrows pointing pigmented neurons). Zeiss Imager Z1. microscope, coupled with the Mercator device (Mercator Pro 7.00, 2009, Explora Nova, La Rochelle, France), enlargement. 200x (A); enlargement. 30x (B), section thickness: 30 µm. Scale bar = 80 µm (A); 600 µm (B). Personal contribution.

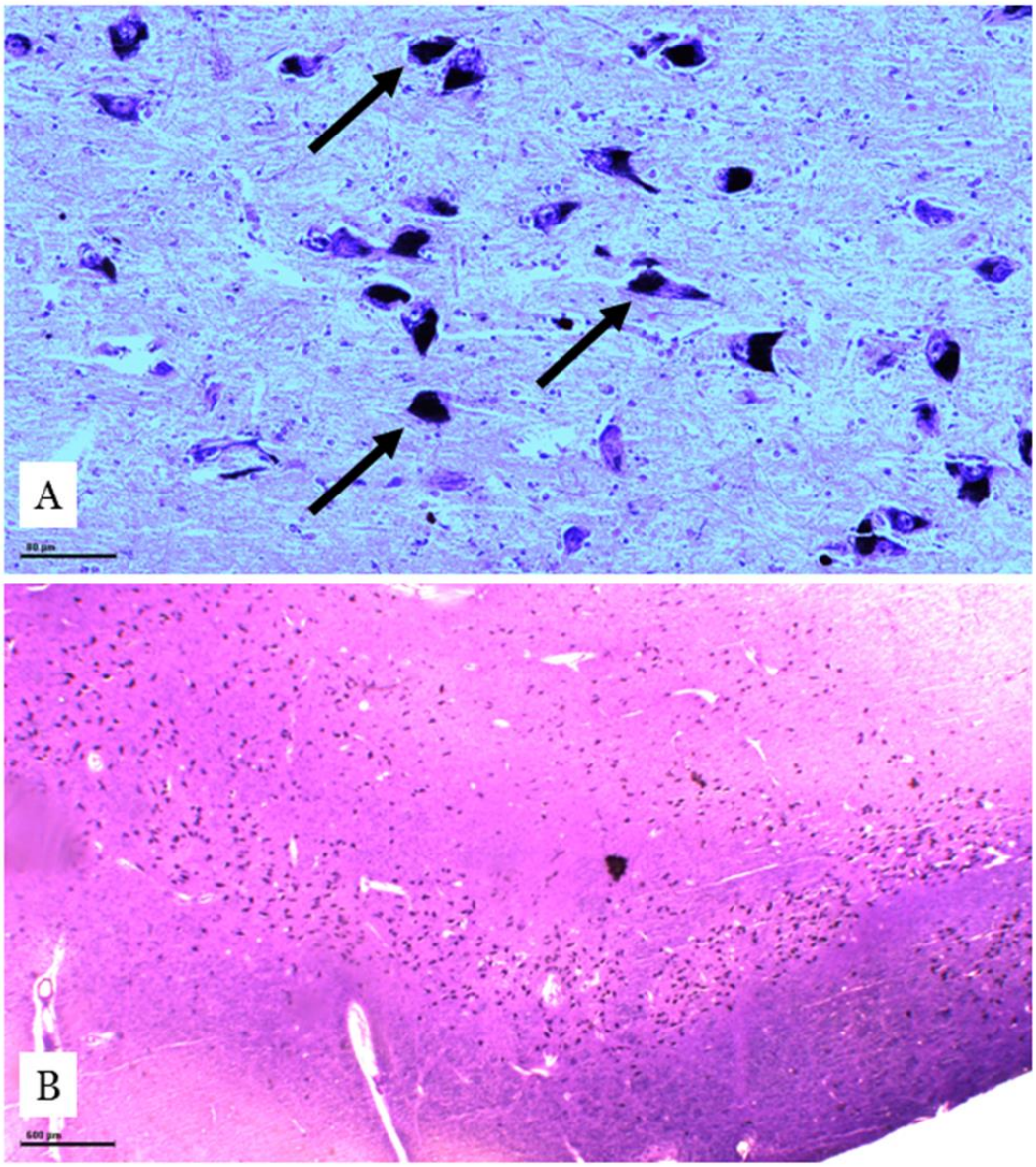

3.2 NEUROMELANIN

Neuromelanin (NM) is a dark cytoplasmic pigment, which is particularly abundant in the dopaminergic neurons of substantia nigra (SN), but also in other several neurons, as the dopaminergic neurons of ventral tegmental area and the noradrenergic neurons of locus coeruleus (LC). In addition, neuronal melanic pigments has been found in the ventrolateral reticular formation, nucleus of the solitary tract in the medulla oblongata, cortex, putamen, and cerebellum (Fedorow et al., 2005; Zecca et al., 2008; Martin-Bastida et al., 2017).

In the SN, more than 95% of the dopaminergic neurons found in the pars compacta contain neuromelanin, but their distribution varies locally: densely packed cells in the ventral tier have a low content of NM and loosely packed cells located in the dorsal tier have a high content of melanin (Gibb, 1992). As demonstrated by Zecca et al., NM pigment concentration in dopaminergic cells of SNpc increases with age because neurons do not excrete nor degrade the pigment (Zecca et al., 2002), beginning its accumulation as early as 3 years of age onwards (Fenichel and Bazelon, 1968). Then, this process linearly progresses with age, with a continuous accumulation through life (Zecca et al., 2002, 2008).

NM pigment appears microscopically as a black and insoluble complex molecule, located within cytoplasmic organelles, and is composed of melanin, proteins, lipids and metal ions. Macroscopically, regions with the highest density of NM-pigmented neurons in the SN and LC are visible as dark areas, as seen on **Figures 3 and 4**.

NM origin is still widely discussed. It derives from the metabolism of excess catecholamines (mostly dopamine in the SN and norepinephrine in the LC), which are not accumulated in synaptic vesicles, but converted by oxidation into semi-quinones and quinones in the cytosol (Sulzer and Zecca, 2000). The subsequent interactions

of these products with undegraded proteins and lipids lead to NM synthesis, which is accumulated afterwards in specialised autolysosomes, 'neuromelanin organelles' (Zucca et al., 2018). NM biosynthesis also involves the iron-mediated auto-oxidation of catecholamines (Zucca et al., 2014), a process activated by an excess of cytosolic catecholamines that are not accumulated into synaptic vesicles by the synaptic vesicular monoamine transporter 2 (VMAT2) (Zucca *et al.*, 2017).

The specialised autolysosomes (or "autophagic organelles") mentioned above cannot catabolise the pigments, and the latter accumulate with age, unless the cell dies. If the cell dies, the pigments are released in the extracellular space and phagocytised by microglia cells, which possess more powerful degradation systems than neurons and are able to destroy NM pigments and organelles (Sulzer et al., 2018). This specific process has been observed by video microscopy studies (Zhang et al., 2011).

In normal conditions, the synthesis of NM is thought to protect dopaminergic neurons from oxidative stress, because it removes excess cytosolic dopamine, and buffers reactive and toxic quinones, generated by the auto-oxidation of catecholamine and promoted by the presence of iron (Sulzer and Zecca, 1999; Zecca et al., 2008). In addition, NM has the ability to chelate metals, such as iron, copper, lead, cadmium, manganese and zinc, and a variety of organic molecules, endogenous and environmental toxins (Zecca et al., 1994, 2002).

Iron is the most abundant of these metal ions, and NM is the main iron storage molecule in the dopaminergic neurons of the substantia nigra (Zucca *et al.*, 2017). Iron binding to the pigment high-affinity sites prevents Fenton's reaction and is therefore protective, but when NM is saturated, iron binds to low-affinity sites, where it is stored in a reactive form and in this situation, promote redox reactions. Therefore, NM could have a toxic function when iron overload is present (Martin-Bastida et al., 2017) whereas a protective role of NM

may be hypothesised when iron is bound under physiological conditions (Zucca *et al.*, 2017).

4 NIGROSTRIATAL DEGENERATION FEATURES IN PARKINSON'S DISEASE

4.1 SUBSTANTIA NIGRA DEGENERATION

As highlighted in the pathological criteria for PD, SN degeneration remains the principal histopathologic feature of the disease, even if it is now proven that the pathological lesions are much more extensive and involve a number of ascending projection pathways in the brainstem and areas of the neocortex (Halliday *et al.*, 2011).

SN degeneration implies the degeneration of dopaminergic neurons in the pars compacta. The fate of NM released in the extracellular space following neuronal death is unclear, but NM is ultimately removed by microglia. These slow processes result in the progressive clearance of NM from the SN, i.e., a "depigmentation" **(see Figure 5)**.

FIGURE 5 – **Substantia Nigra degeneration**. Section through the midbrain, after formaldehyde fixation. Healthy subject (A) compared with Parkinson's disease patient (B). Depigmentation is easily seen in the substantia nigra of Parkinson's disease patient. Courtesy Pr M. Deprez and Dr E. Bianchi.

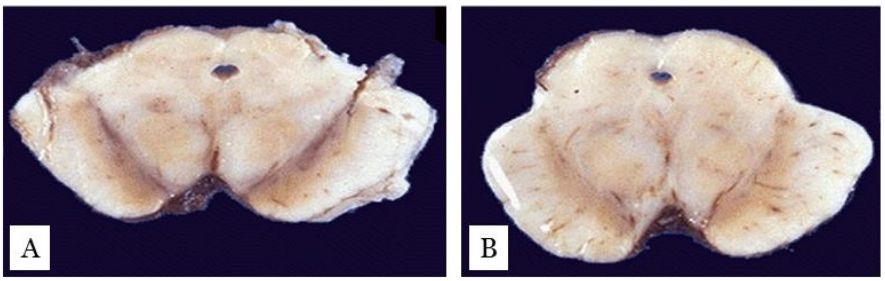

As a result of this degeneration process, nigral and striatal dopamine content decreases. As demonstrated by Kish et al. in a pathology study, there is an uneven pattern of dopamine loss in the striatum: the posterior putamen is affected first and more severely than its anterior counterpart, but as the disease progresses, all striatal regions are

similarly affected (Kish et al., 1988). These findings have also been confirmed by FDOPA PET scans used to study the progression of the disease: FDOPA uptake is lost in a progressive pattern, first and more severely in the posterior putamen (Morrish et al., 1996; Nandhagopal et al., 2009).

Likewise, neurodegeneration is not homogeneous within SN: it predominantly affects the ventrolateral area of the SNpc, as demonstrated in a pathological study by Fearnley and Lees (Fearnley and Lees, 1991), a region that projects to the (posterior) striatum **(see Figure 6)**.

Normal aging is also associated with a reduction of nigral neurons (McGeer et al., 1977) and striatal dopamine (Riederer and Wuketich, 1976), and although PD is associated with increasing age, the pattern of cell loss in the SN and its importance differs from normal aging, as demonstrated by Fearnley and Lees (Fearnley and Lees, 1991).

Another topographical analysis of SN vulnerability has been proposed by Damier et al. (Damier et al., 1999a, b). In order to characterise the pattern of loss of dopaminergic neurons, these authors used calbindin immunostaining to subdivide SN pars compacta into two main compartments: the nigrosomes and the surrounding matrix. Nigrosomes are five calbindin-poor neuronal subgroups, numbered 1 to 5 according their caudo-rostral position. Dopaminergic neurons are sparsely distributed in the matrix, but densely packed in nigrosomes. It was found that neuronal loss, measured and quantified by tyrosine hydroxylase (TH)-immunostaining, was higher in the nigrosomes than in the matrix, nigrosome 1 being the most affected region. This nigrosome 1 is located in the caudal and dorsolateral part of SN pars compacta. Depletion then spreads to other nigrosomes and the matrix according a caudo-rostral gradient.

FIGURE 6 – **Substantia nigra regional pigmented neuronal loss in aging and in Parkinson's disease.** A – normal anatomy. B – Aging. Numbers indicate percentage of neurons lost between age 20 and 90. C – Parkinson's disease. Numbers indicate average percentage loss compared to normal individuals. Picture reproduced from Fearnley and Lees, 1991.

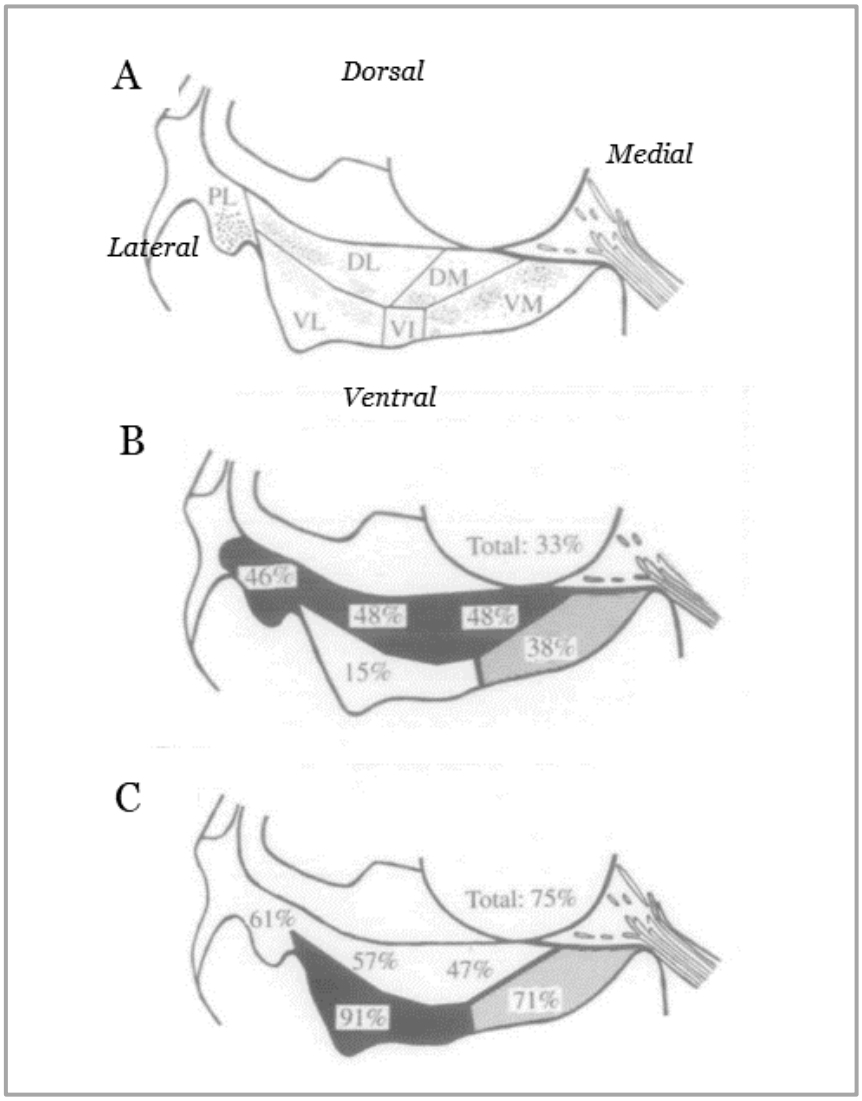

ABBREVIATIONS – Dorsal tier : medial part (DM), lateral part (DL), pars lateralis (PL); Ventral tier: medial part (VM), intermediate part (VI), lateral part (VL).

Clinically manifest parkinsonism appears when approximately 50 to 80% of striatal dopamine concentration (or 30 to 50% of nigral dopaminergic neurons) are lost (Bernheimer et al., 1973; Riederer and Wuketich, 1976; Cheng et al., 2010; Martín-Bastida et al., 2019). This delay is explained by compensatory mechanisms, such as supersensitivity of dopamine receptors, or an increase of neurotransmitter turnover (Fahn et al., 2011). Clinical deficits of PD appear to be more related to the degree of cell loss rather than to the severity of Lewy pathology (Halliday et al., 2011). Besides, it has been demonstrated that nigro-striatal degeneration progressively increases as the duration of illness progresses (Riederer and Wuketich, 1976).

Despite these acknowledged clinical-pathologic correlations, it has to be emphasised that the clinical heterogeneity observed in parkinsonian patients suggests some variations in the distribution of neuropathological changes in the SN and a variable involvement of dopaminergic and other neurotransmitter systems in the brainstem (e.g. cholinergic, noradrenergic, serotoninergic) (Fahn et al., 2011). For example, the tremor-dominant PD seems to be associated with more severe neuronal loss in medial than in lateral SNpc (Jellinger, 1999).

4.2 NEUROMELANIN LOSS IN SUBSTANTIA NIGRA

The specific degeneration of dopamine neurons containing NM in PD, as reported by many authors decades ago (Mann and Yates, 1974), suggests that NM itself is actively involved in the pathology of PD, rather than being just a bystander of cell degeneration. Zecca and colleagues demonstrated that PD is associated with a severe decrease in NM concentration in SN, estimated at 60% when compared to age-matched healthy controls (Zecca et al., 2002). Therefore, the role of NM as a critical factor underlying neuronal vulnerability in PD has long been suspected and widely studied.

In Parkinson's disease, dying dopaminergic neurons of the SN release NM, which is phagocytised and degraded by the activated microglia (Banati et al., 1998). According to current models, this process releases pro-inflammatory cytokines and nitric oxide leading to further neurodegeneration and neuroinflammation (Wilms et al., 2003). In addition, extracellular NM releases reactive iron and other previously accumulated toxins, thus increasing oxidative stress and potentially causing further cell death (Zecca *et al.*, 2004*a*; Zucca *et al.*, 2017).

Some studies provide evidence for a role of NM in neurodegeneration. In the SN of PD patients, the subpopulation of DA neurons containing NM appear to have a specific vulnerability. However, this subject is still a matter of debate, as some studies suggested that neurons with the highest NM content are the most vulnerable (Hirsch et al., 1988; Kastner et al., 1992), while others reported that neurons with a low pigmentation are more susceptible to degenerate (Gibb, 1992). Similarly, in 1991, Gibb and Lees found that lightly pigmented neurons were located in the ventrolateral tiers of SN, whereas heavily pigmented neurons were in the dorsal tiers in healthy controls. They demonstrated that PD patients were characterised by a selective loss of pigmented neurons in the ventrolateral SN group (Gibb and Lees, 1991).

A link between NM and alpha-synuclein has also been highlighted by various authors. Impairment of the ubiquitin-proteasome system has been suggested to contribute to neuronal death in PD (Mandel et al., 2005; Shamoto-Nagai et al., 2006; Martins-Branco et al., 2012). Shamoto-Nagai and colleagues reported that NM inhibits enzymatic activity of 26S proteasome in human dopaminergic neurons (Shamoto-Nagai et al., 2004). In consequence, the reduced activity of proteasome system may prevent protein degradation and cause accumulation of oxidatively-modified and ubiquitinated proteins such as alpha-synuclein aggregates (McNaught et al., 2003). This might be related to the formation of Lewy body.

Therefore, ill-conformed α-synuclein progressing throughout the brainstem through a prion-like mechanism finds, in the SN, conditions promoting its self-perpetuation and the formation of Lewy bodies and neurites.

4.3 THE ROLE OF IRON

The role of iron in aging and PD brain has been studied since the beginning of the twentieth century. The concentration of total brain iron increases with age, and it has been demonstrated that the distribution of iron in the healthy adult brain is heterogeneous, with the highest content found in the globus pallidus, putamen, dentate nucleus and caudate nucleus (Hallgren and Sourander, 1958; Aquino *et al.*, 2009; Péran *et al.*, 2009).

Various factors have been incriminated to explain the increase of iron concentration with aging, including an inflammatory state induced by glial iron accumulation (Xu et al., 2012), increased brain blood barrier permeability (Faucheux et al., 1999), or redistribution of iron within the brain.

Iron is stored in the brain in various molecular complexes (ferritin, NM, transferrin, hemosiderin, and others), and can be found in neurons as well as glial cells.

The NM-iron complex is the main iron compound in catecholaminergic neurons and its concentration increases during aging in the SN, and to a lesser extent in locus coeruleus. In these regions, ferritin-iron complex is only found in glia. However, in the putamen and globus pallidus, deposits of iron are found in fibres, glial cells and neurons where there is no visible NM pigment, while neurons of these structures containing NM do not have detectable iron deposits (Zecca *et al.*, 2004c; Zucca *et al.*, 2017).

In PD, several studies have demonstrated an increase of total iron concentration in the brain of affected individuals, and particularly in the SN, beyond what is observed with age (Lhermitte *et al.*, 1924; Dexter *et al.*, 1987, 1989, Sofic *et al.*, 1988*b*; Sian-Hülsmann *et al.*, 2011), and even a correlation between iron levels and disease severity (Riederer and Wuketich, 1976).

The high levels of iron detected in the SN of PD patients might exceed iron storage capacity of complexes, such as NM and ferritin (Zucca *et al.*, 2017). Various mechanisms explaining iron-mediated damage and neurotoxicity have been proposed. After neuronal degeneration of dopaminergic neurons, cellular debris including NM, iron, and other proteins are phagocytised by activated microglia and macrophages, leading to a perturbation of iron homeostasis. Dying macrophages and glial cells may in turn release their iron, which enters the pool of labile iron, exacerbating iron-mediated oxidative stress and damage of adjacent cells, including neurons (Andersen et al., 2014).

Mutual interactions were also established between iron and alpha-synuclein accumulation. In vitro studies showed that iron induces a conformational change of α-synuclein to the β-sheet conformation, forming fibrils that are present in Lewy bodies (Uversky et al., 2001). Beside, redox-active iron was found to be sequestrated in SN neurons Lewy bodies (Castellani et al., 2000).

CHAPTER 3

3 NEUROIMAGING OF PARKINSON'S DISEASE

1 GENERAL CONSIDERATIONS

1.1 MRI IN ROUTINE CLINICAL PRACTICE

The place of neuroimaging in Parkinson's disease diagnosis remains a subject of debate.

In clinical practice, conventional structural MRI is a well-established method for excluding symptomatic parkinsonisms due to other pathologies (vascular, etc.). Besides, EFNS guidelines currently recommend the use of conventional magnetic resonance imaging at 1,5 T as a tool which can differentiate PD from atypical parkinsonisms and may support the diagnosis of multiple system atrophy (MSA) or progressive supranuclear palsy (PSP), on the basis of regional atrophy or local signal change. Indeed, several findings on conventional structural MRI have been described as diagnostic markers of MSA, such as atrophy of the cerebellum, "hot cross bun" sign in the pons, hyperintensity in the middle cerebellar peduncle, etc., whereas PSP is characterised by midbrain atrophy, "hummingbird" sign, atrophy of the superior cerebellar peduncle, etc. While the specificity of these signs is commonly considered as quite high, their sensitivity is rather low, particularly at the beginning of the disease (Berardelli et al., 2013).

Unfortunately, no such sign detectable at visual inspection of structural MRI has been demonstrated in idiopathic PD, and routine MRI is generally considered as unremarkable **(see Figure 7)** However, during the last ten years, new MRI sequences sensitive to iron, nigral pigments or voxel-based morphometry have been studied in neurodegenerative parkinsonisms, in order to find biomarkers suitable for PD diagnosis, prodromal diagnosis and PD progression evaluation **(see Chapter 3, Section 2)**.

FIGURE 7 – **Conventional MRI in Parkinson's disease.** A–B: T1-weighted MRI, axial slices at the level of midbrain (A) and at the level of basal ganglia (B). C–D: T2-weighted MRI, axial slices at the level of midbrain (C) and at the level of basal ganglia (D). These MRI do not show any macroscopic abnormalities. The pictures have been acquired in the radiology department of our hospital (CHU of Liège, Belgium), on a 3T-MRI scanner.

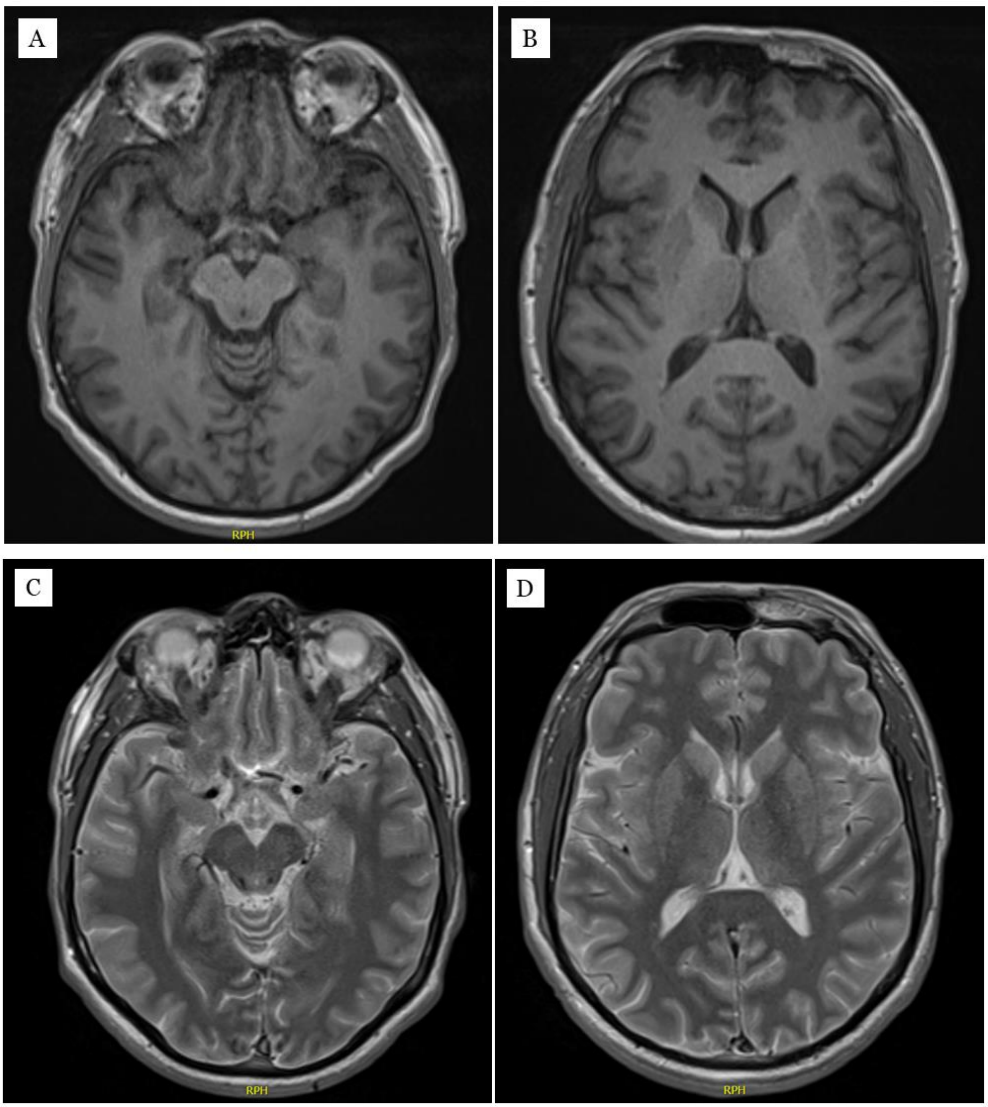

1.2 NUCLEAR IMAGING

1.2.1 OVERVIEW

As PD is characterised by nigrostriatal dopamine dysfunction, many studies tried to develop biomarkers that could detect and quantify dopaminergic modifications in vivo. Since the first human study published in 1983 (Garnett et al., 1983; Kaasinen and Vahlberg, 2017), molecular imaging with positron emission tomography (PET) or single photon emission computed tomography (SPECT) has been widely used in PD research in order to estimate levels of nigrostriatal dopaminergic degeneration and to support PD diagnosis.

In order to understand the value of the various radiotracers currently available, dopamine synthesis, transport and metabolism must be kept in mind **(see Figure 8)**. Dopamine is a neurotransmitter synthesised in catecholaminergic neurons through serial enzymatic steps. First, L-tyrosine is hydroxylated to L-DOPA by the tyrosine hydroxylase (TH), followed by the decarboxylation of L-DOPA to dopamine by the aromatic L-amino-acid decarboxylase (AADC, or simply DOPA decarboxylase). Dopamine is then transported to storage vesicles by the vesicular monoamine transporter type 2 (VMAT2). After excitation of dopaminergic neurons, the vesicles are finally emptied into the synaptic cleft, and the synaptic dopamine then interacts with postsynaptic dopamine receptors. After dopamine has been released in the synaptic cleft, dopamine neurotransmission has to be terminated. Dopamine is degraded through catecholamine-O-methyltransferase (COMT) and monoamine-oxydase A and B (MAO). Presynaptic reuptake occurs via the dopamine transporter (DAT), which removes extracellular dopamine from the synapse. DAT is the most important component regarding the end of dopamine neurotransmission cycle (Kaasinen and Vahlberg, 2017). DAT, AADC and VMAT2 are important targets in dopaminergic neuroimaging as DAT matches dopaminergic synapse density, AADC activity is a reflect of dopamine synthesis, whereas VMAT2 reflects dopamine storage. AADC is not specific to dopaminergic neurons as

it can be found in all monoaminergic neurons, and some studies have used [^{18}F]DOPA PET (marker of AADC activity, as developed below) in order to characterise extra-striatal monoamine neuronal dysfunction in Parkinson's disease (Moore et al., 2008). However, it is predominantly present in dopaminergic neurons of certain regions, such as the striatum (Kilbourn, 2021).

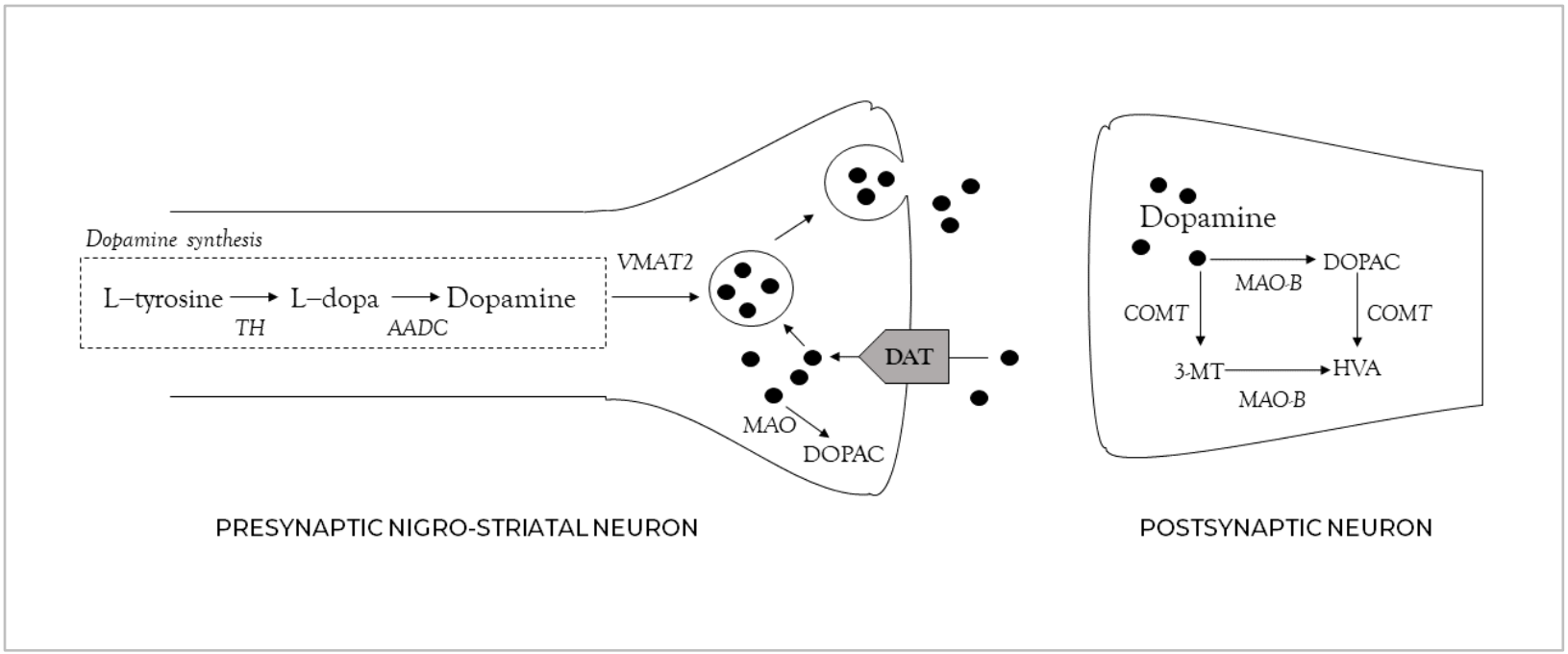

FIGURE 8 – Metabolism of dopamine and its neurotransmission

Legend: ● : dopamine, TH: tyrosine hydroxylase, AADC: L-amino acid decarboxylase, VMAT2: vesicular monoamine transporter 2, MAO: monoamine oxydase, DOPAC: 3,4-dihydroxyphenylacetic acid, COMT: catechol-O-methyltransferase, 3-MT: 3-methoxytyramine, HVA: homovanillic acid, DAT: dopamine transporter. (Fahn et al., 2011)

6-[^{18}F]fluoro-L-dopa (abbreviated here in [^{18}F]DOPA) is frequently employed as a tracer for PET. It enters in the second stage of dopamine biosynthesis where it is decarboxylated by AADC to [^{18}F]fluorodopamine, and is then considered as a marker of AADC activity. The [^{18}F]fluorodopamine is then transported by VMAT2 and irreversibly trapped into intraneuronal storage vesicles (at least over short scan times, generally inferior to 90 minutes). An alternative to [^{18}F]DOPA is β-[^{11}C]-L-dopa (Ito *et al.*, 2011). However, some disadvantages have been raised with the use of these two radiotracers, as some radiolabelled metabolites can be released as a consequence of the catabolism by catechol O-methyltransferase (COMT) in the peripheral vascular compartment. These metabolites, such as 3-*O*-methyl-[^{18}F] FDOPA (3OM-[^{18}F]FD), are able to cross the blood brain barrier and are characterised by a large volume of distribution in the brain, thus reducing signal to background ratios. Therefore, an alternative has been developed using a non-catecholic radiotracer, which is not a substrate of COMT, the 6-[^{18}F]fluoro-L-meta-tyrosine ([^{18}F]-FMT) (DeJesus *et al.*, 1997; Becker *et al.*, 2017; Kilbourn, 2021). The latter is decarboxylated by AADC and therefore represents another marker of AADC activity. However, until now, [^{18}F]DOPA remains the most widely used radiotracer for the study of dopamine synthesis process with PET imaging.

^{11}C- and ^{18}F-dihydrotetrabenazine (DTBZ) are both markers of VMAT binding. Additionally, there are numerous DAT tracers for PET and SPECT, such as [^{18}F]-(E)-*N*-(3-iodoprop-2-enyl)-2β-carbofluoroethoxy-3β-(4′-methyl-phenyl)nortropane ([^{18}F]FE-PE2I) (Jakobson Mo *et al.*, 2018) or [^{11}C]-PE2I, but the most frequently used are [^{123}I]FP-CIT (N-ω-fluoropropyl-2β-carbomethoxy-3β-(4-iodophenyl)nortropane abbreviated in FP-CIT) or [^{123}I]β-CIT (2β-carbomethoxy-3β(4-iodo-phenyl)tropane abbreviated in β-CIT).

These data are summarised in **Table 4.**

TABLE 4 – Nigro-striatal pathways tracers

TARGET		AADC	VMAT2	DAT	D2/D3 dopaminergic receptors
Process studied		AADC is responsible for decarboxylation of L-DOPA to dopamine. AADC activity is a reflect of dopamine synthesis	VMAT2 transports newly synthesised or recovered monoamines (dopamine, serotonin, norepinephrine, and histamine) from cytosol to intraneuronal storage vesicles	DAT is a transporter responsible for the reuptake of dopamine from the synaptic cleft, specific to the dopaminergic neurons	Putaminal dopamine post-synaptic D2/3 receptor availability
Radiotracers	SPECT			[^{123}I]β-CIT [^{123}I]FP-CIT	[^{123}I]-IBZM
	PET	6-[^{18}F]fluoro-L-dopa (=[^{18}F]DOPA) [β-^{11}C]-L-dopa [^{18}F]-FMT	[^{11}C]- and [^{18}F]-dihydrotetrabenazine (DTBZ)	[^{11}C]β-CIT [^{18}F]FP-CIT [^{18}F]FE-PE2I [^{11}C]-PE2I [^{11}C]Methylphenidate	[^{11}C]-raclopride [^{18}F]-fallypride N[^{11}C]Methylspiperone
Type of tracer		Pre-synaptic			Post-synaptic

1.2.2 RADIOTRACERS AND NUCLEAR IMAGING IN PARKINSON'S DISEASE

Positron emission tomography is able to detect presynaptic nigrostriatal dopamine deficiency shared by various degenerative parkinsonisms, including PD. Striatal uptake of [^{18}F]DOPA (and [^{123}I]tropanes in SPECT studies) is markedly decreased in PD, more so in the posterior putamen than in the caudate nucleus, more severely contralaterally to motor signs and in inverse proportion to disease duration and severity (Thobois *et al.*, 2001) **(see Figure 9)**.

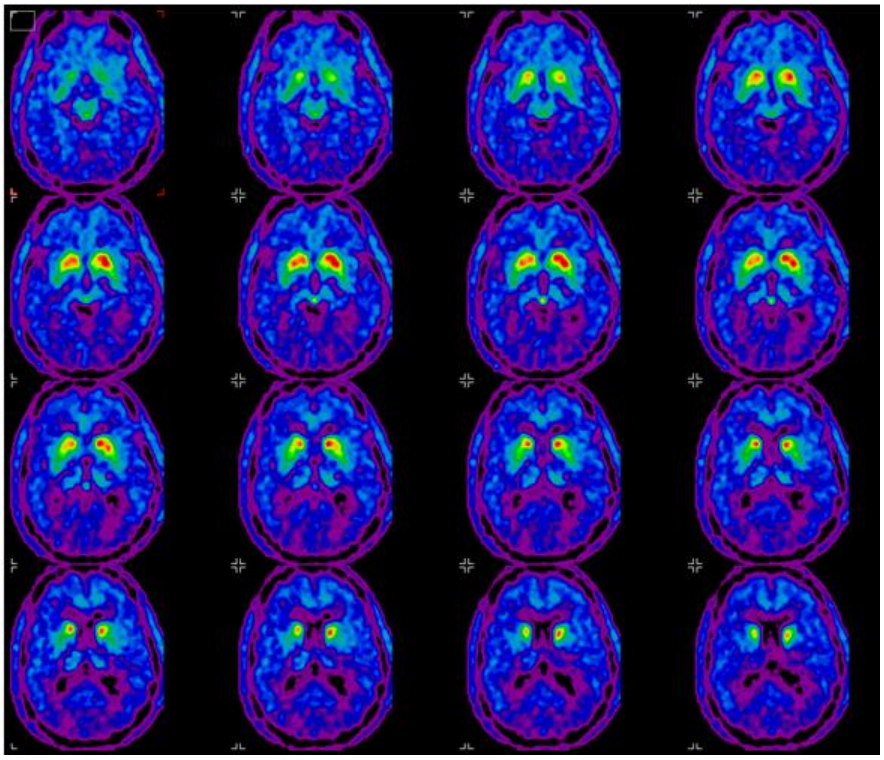

FIGURE 9 – Example of [^{18}F]DOPA PET in a Parkinson's Disease patient, with most clinical affected side on the left. 16 consecutive slices are shown, illustrating the asymmetrical reduction of [^{18}F]DOPA uptake in the posterior putamen of the patient, predominant on the right (radiological convention). These pictures have been acquired at the GIGA-CRC In Vivo Imaging, University of Liege, Belgium. Personal contribution.

Striatal dopamine deficiency can also be detected by PET imaging in atypical parkinsonisms, as MSA, PSP, and CBD, and usefully differentiates these conditions from essential and dystonic tremors, drug-induced and functional (psychogenic) parkinsonism (Berardelli *et al.*, 2013).

As mentioned above, many tracers have been proposed for this purpose, all reflecting the density of nigro-striatal dopaminergic nerve terminals. These tracers include [^{18}F]DOPA, [^{11}C]- and [^{18}F]-DTBZ, [^{123}I]FP-CIT. For example, in a study using [^{18}F]DOPA PET, it has been demonstrated that a characteristic reduction of the [^{18}F]DOPA uptake in the putamen **(see Figure 10)** can be observed in virtually all patients with PD, even in the early stage of the disease (Morrish *et al.*, 1995). These tracers all have high sensitivity for detecting **presynaptic** striatal dopamine deficiency [in the study by Jokinen and colleagues, [^{18}F]DOPA uptake was within the control range for only 5.6% of patients with a clinical diagnosis of PD (Jokinen *et al.*, 2009)], but they are not really specific for the differential diagnosis of parkinsonian syndromes. However, PD is characterised by a caudo-rostral gradient of dopamine dysfunction in putamen (Brooks *et al.*, 1990), with relative preservation of the dopaminergic function in the anterior putamen and caudate, at least in the early stages, whereas other atypical parkinsonisms (such as MSA, PSP and cortico-basal degeneration) present a more uniform dysfunction. Overall, PET imaging cannot directly diagnose PD or atypical parkinsonisms. Nevertheless, the patterns of dysfunction revealed can help supporting or refuting clinical impressions.

On the other hand, PET benzamide tracers such as [^{11}C]-raclopride, or less frequently [^{18}F]-fallypride, and [^{18}F]-desmethoxyfallypride (Segovia *et al.*, 2017), have also been proposed to study putamen dopamine **post-synaptic** D2 receptor availability. In PD, the latter is preserved as demonstrated by Brooks and colleagues in 1992, or even increased as a compensatory mechanism as shown in parkin-linked Parkinsonism (Scherfler *et al.*, 2006). By contrast, patients affected by

atypical parkinsonism show a decrease in the binding potential (BP) of dopamine receptors (Brooks *et al.*, 1992; Antonini *et al.*, 1997).

In a meta-analysis comparing dopaminergic striatal presynaptic PET and SPECT with AADC, DAT, and VMAT2 tracers in PD, Kaasinen and Vahlberg found that AADC deficiency appears to be consistently smaller than the DAT and VMAT2 defects, which likely suggests a process of upregulation of AADC function in PD (Kaasinen and Vahlberg, 2017). This hypothesis was already mentioned in Morrish and colleagues works in the nineties (Morrish *et al.*, 1995), and was also supported by studies in asymptomatic carriers of genetic mutations (LRRK2) (Nandhagopal *et al.*, 2008). Other authors have incriminated a DAT downregulation (Lee *et al.*, 2000), that can also explain this difference, or even possible compensatory changes in VMAT2 expression, as it was demonstrated in dopa-responsive dystonia (De La Fuente-Fernández *et al.*, 2003). It has to be kept in mind that these tracers do not provide a measure of nigrostriatal cell count [even if a correlation has been established between [^{18}F]DOPA uptake in the striatum and the *post-mortem* nigral cell count (Snow *et al.*, 1993)], but rather a measure of presynaptic dopaminergic terminal function, and that a depleted cell pool is able to compensate with various mechanisms.

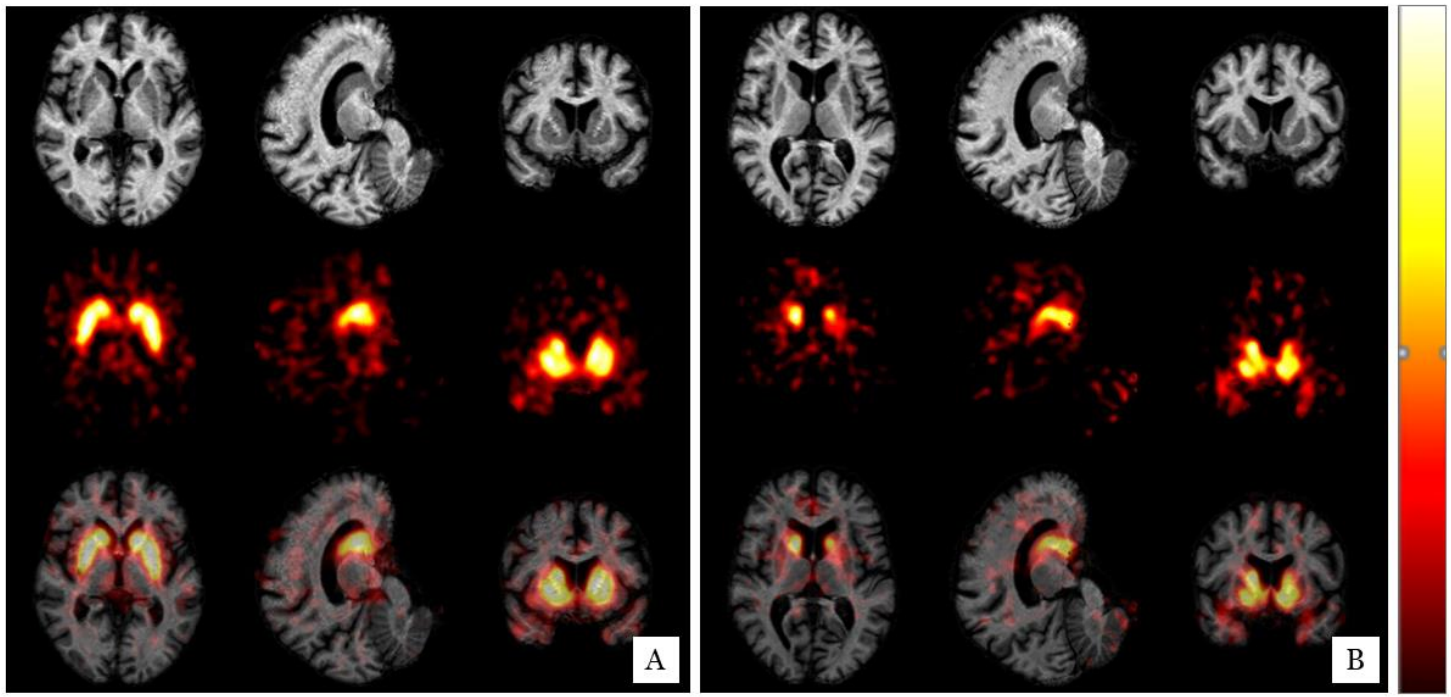

FIGURE 10 – **[^{18}F]DOPA PET in a healthy control (A) and in a Parkinson's Disease patient (B).** From left to right, images are displayed in axial, sagittal and frontal slices. The first row depicts a structural MRI (with extracranial structures removed). The second row depicts Ki maps. The third row consists of a fusion of the two imaging modalities. This comparison illustrates the visible reduction of [^{18}F]DOPA uptake predominant in the posterior putamen of the patient. The colour scale is proportional to [^{18}F]DOPA uptake (yellow indicating high [^{18}F]DOPA uptake). Images are displayed in radiological convention. These pictures have been acquired at the GIGA-CRC In Vivo Imaging, University of Liege, Belgium. Personal contribution.

Regarding the relationship between clinical severity and dopaminergic striatal presynaptic PET, Morrish and colleagues demonstrated in 1990 an inverse correlation between putamen uptake using [^{18}F]DOPA and clinical rating as assessed by both total and motor UPDRS score (Morrish *et al.*, 1995). Eshuis and colleagues found a correlation between caudate and putaminal uptake of [^{18}F]DOPA and Hoehn and Yahr stage, but also with UPDRS III score (Eshuis *et al.*, 2006). In the same study, significant but moderate correlations were demonstrated between disease duration and striatal [^{18}F]DOPA uptake. In the meta-analysis by Kaasinen and colleagues, correlations between tracer binding and disease severity in PD are particularly observed in the caudate nucleus, rather than the putamen. This could reflect a "floor effect" of putaminal dopamine function in PD, particularly in more advanced stages: as caudate nucleus function should be better preserved, the correlations with clinical parameters are still observed, whereas they might have been lost in the putamen due to earlier and more severe dopaminergic defect (Kaasinen and Vahlberg, 2017).

A few studies have investigated the rate of progression of PD using [^{18}F]DOPA PET. Nurmi and colleagues scanned PD patients and healthy controls twice at five years interval and demonstrated that PD first affects the posterior putamen, followed by the anterior putamen and the caudate nucleus, whereas in healthy controls, no significant decline in [^{18}F]DOPA uptake was observed (Nurmi *et al.*, 2001). Kaasinen and Valberg included in their meta-analysis three longitudinal studies using [^{18}F]DOPA PET with at least three time points (Brück *et al.*, 2009; Gallagher *et al.*, 2011; Nandhagopal *et al.*, 2011), and found they all showed a negative exponential decline of AADC function with time (Kaasinen and Vahlberg, 2017).

1.2.3 SINGLE PHOTON EMISSION TOMOGRAPHY

Single photon emission tomography with specific radiotracers can also offer an objective and reproducible measurement of the activity of the nigrostriatal dopaminergic system, and is able to demonstrate a loss of striatal dopaminergic terminals in PD (Innis *et al.*, 1993) **(see Figure 11).**

Current presynaptic radiotracers for SPECT studies selectively target the dopamine transporter (DAT) (see above). As for presynaptic PET radiotracers, dopamine transporter-SPECT cannot differentiate PD from atypical parkinsonisms, as nigrostriatal pathways are similarly impaired in these conditions. In clinical practice, DaTscan SPECT is rather used for the differential diagnosis between degenerative parkinsonisms and drug-induced parkinsonism (drug-induced cases being characterised by normal uptake) or essential tremor. In some countries, it is also recommended for the differential diagnosis between Alzheimer's disease and Lewy Body dementia. Similarly, as PET, D2 dopamine receptor SPECT tracers have been developed, such as [^{123}I]-Iodobenzamide ([^{123}I] IBZM), but for the same reasons as described before, cannot confirm the diagnosis of PD. It rather can help in the differential diagnosis between PD and atypical parkinsonisms, even if a meta-analysis of IBZM-SPECT studies showed that this technique has quite a low negative predictive value (Vlaar *et al.*, 2007).

In an interesting study by Eshuis and colleagues comparing directly [^{18}F]DOPA PET and [^{123}I]FP-CIT SPECT in a population of PD patients separated in two groups, *de novo* and advanced PD, the authors found a significant and strong correlation between the two tracers corresponding striatal uptake. Both scanning methods correlate moderately with motor scores, disease duration and the two tracers are equally able to distinguish *de novo* from advanced PD patients (Eshuis *et al.*, 2006). Similar results were found by Ishikawa and colleagues, who showed that [^{123}I]FP-CIT SPECT and [^{18}F]DOPA

PET were able to discriminate early stage PD patients from healthy controls with comparable sensitivity (Ishikawa *et al.*, 1996), even if according many studies, striatal [^{123}I]FP-CIT uptake should be reduced in an earlier phase of disease than [^{18}F]DOPA uptake (Ito *et al.*, 1999). These considerations are particularly important in clinical practice: widespread use of [^{18}F]DOPA PET has been limited by high costs, restricted availability of PET instruments and the difficult synthesis of [^{18}F]DOPA. In comparison, SPECT scans using radiotracers such as [^{123}I]FP-CIT ("DaTscan") are less expensive and much more widely available, but present limitations too, including lower spatial resolution when compared with PET scans. Besides, as emphasised by Ishikawa et al., despite the comparability of whole striatal values obtained with PET and SPECT techniques, critical regional changes within the striatum may not be reliably ascertained with SPECT.

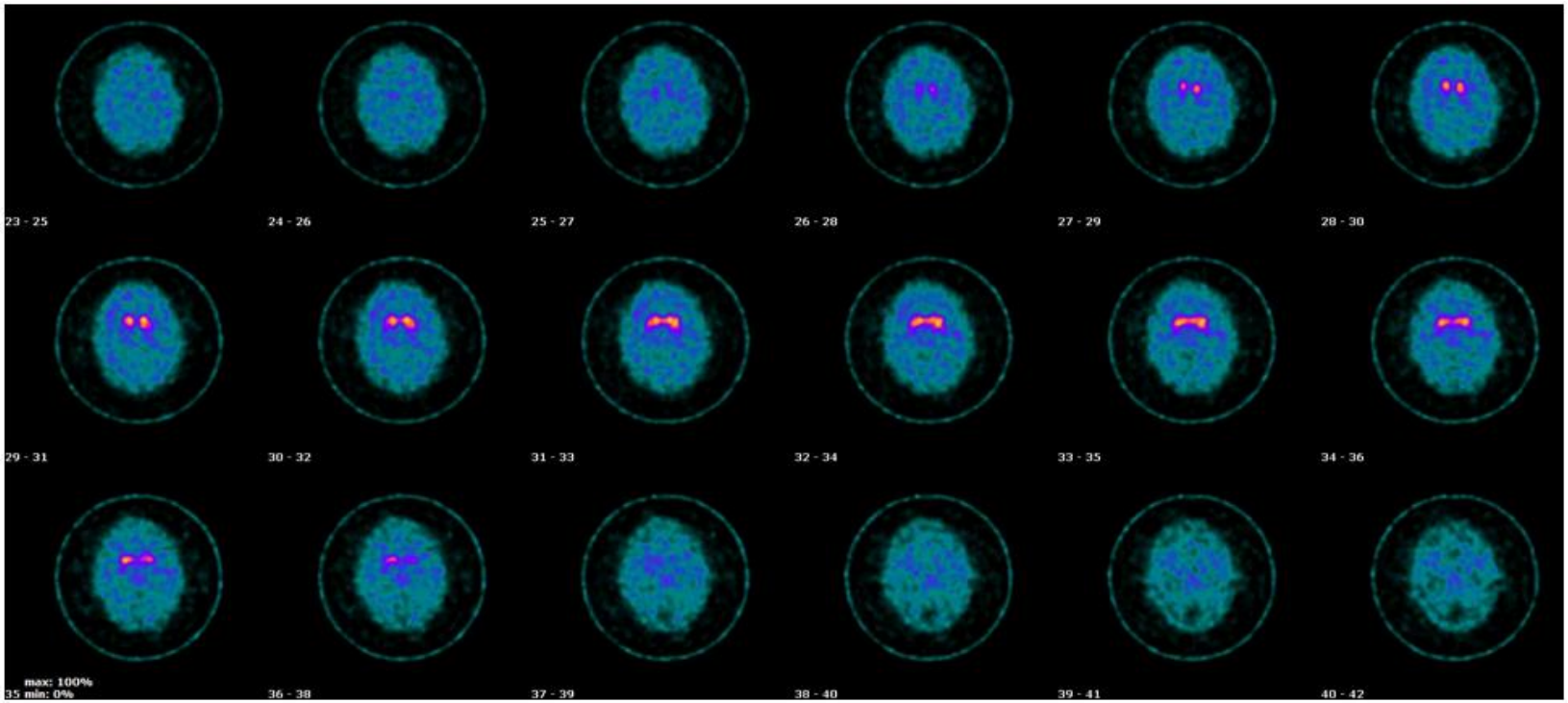

FIGURE 11 – **Example of routine DaTscan ([^{123}I]-Ioflupane SPECT)**, axial slices at the level of basal ganglia, slices 21 to 41, showing bilateral hypofixation of both putamen in a Parkinson's disease patient. Images are displayed in radiological convention. The pictures have been acquired in the nuclear medicine department of our hospital (University Hospital of Liège, Belgium).

1.2.4 CORRELATIONS BETWEEN NUCLEAR IMAGING AND NEUROPATHOLOGICAL FINDINGS

1.2.4.1 SPECT IMAGING

Even if [^{123}I]FP-CIT SPECT imaging can be a useful alternative to [^{18}F]DOPA in a number of relevant clinical or research situations, no solid cross-validation with neuropathological data has been provided until now. Saari and colleagues did not find any correlation between *ante mortem* striatal DAT binding (specific binding ratios or "SBRs", corresponding to [caudate nucleus or putamen – occipital cortex]/occipital cortex) as measured with SPECT imaging, and *post-mortem* dopaminergic neuronal counts in the SNpc of PD patients (neither TH-positive nor neuromelanin-containing neurons) (Saari *et al.*, 2017). In comparison with previous similar studies, this one employed the largest population, with 18 patients included, of which 11 with neuropathologically confirmed PD, and 7 suffering from atypical parkinsonisms.

A few years before, Kraemmer and colleagues tried to explore the same relationship, and found that averaged (left and right) striatal uptake was highly correlated with averaged cell counts in both substantia nigra. However, only nine patients were included in the study, and among them was only one PD patient. The others were suffering from various neurodegenerative diseases, such as Lewy Body dementia, Alzheimer's disease, corticobasal degeneration, Creutzfeldt-Jakob disease or even from 'atypical parkinsonism with multiple pathological conditions' (Kraemmer *et al.*, 2014). Colloby and colleagues also investigated the neuropathological correlates of dopaminergic imaging, but they focused on cognitive aspects as they used a cohort of autopsy-confirmed Alzheimer's disease, dementia with Lewy bodies, and Parkinson's disease dementia cases (Colloby *et al.*, 2012). Positive correlations were reported for Alzheimer's disease patients but not in patients with PD in whom they did not appear

significant in the scatterplots. On the other hand, in these two studies, the heterogeneous samples of patients reflected different diagnoses and their findings cannot be systematically generalised to PD.

Overall, these results question the validity of [^{123}I]FP-CIT SPECT imaging as a suitable surrogate marker for nigral neuronal viability in PD. This technique mainly reflects axonal dysfunction and DAT expression rather than the number of residual SN neurons (Saari *et al.*, 2017).

1.2.4.2 PET IMAGING

Regarding PET, Snow and colleagues found in 1993 a strong correlation between striatal [^{18}F]DOPA uptake and dopamine cell counts and densities (significant correlation with zero intercept), but again, the sample was small and heterogeneous (Snow *et al.*, 1993). Only five patients were included, among them one PD patient, three PSP patients, one Alzheimer's disease and one amyotrophic lateral sclerosis who had been scanned with [^{18}F]DOPA during life. Later, additional cases of patients who had undergone [^{18}F]DOPA PET at the University of British Columbia, and for whom autopsy data were available, have been added to this study, confirming the previous findings. Among them were two patients suffering from Alzheimer's disease (with higher [^{18}F]DOPA uptake) and one patient suffering from PSP (with lower [^{18}F]DOPA uptake) (Brooks *et al.*, 2003).

On the other hand, PET studies with 1-methyl-4-phenyl-1,2,3,6-tetrahydropyridine(MPTP)–treated monkeys have demonstrated that the striatal uptake of various dopaminergic radiotracers [[^{18}F]DOPA, [^{11}C]DTBZ, [^{11}C]CFT (dopamine transporter tracer)] does not correlate with nigral neuronal counts once the loss of dopaminergic cells exceeds 50% (Karimi *et al.*, 2013).

Again, the discrepancy between these results indicate that further studies are needed, if possible with more homogeneous populations regarding the disease considered.

1.2.5 α–SYNUCLEIN AS A NEW TARGET

As mentioned earlier (**see Chapter 2, Section 2**), α-synuclein accumulation in intraneuronal inclusions (Lewy bodies) and neuronal processes (Lewy neurites) is a key feature of PD pathology, beside neuronal loss in SNpc. We focused on the latter as the MRI techniques investigated in our study were not directly related to α-synuclein. However, in the recent years, the development of new PET tracers has progressed towards the imaging of aggregated α-synuclein in Lewy bodies and Lewy neurites, especially in order to find an early biomarker of the disease. Indeed, it is established by pathological studies that the formation of Lewy bodies precedes dopaminergic loss, resulting in the clinical premotor stage of PD (Braak and Del Tredici, 2009).

The development of such radiotracers could also provide precious tools for the diagnosis of other degenerative diseases, such as DLB and MSA, which are characterised by α-synuclein aggregates too, but with different specificities (e.g. glial cytoplasmic inclusions in MSA) or different brain distributions (Spillantini and Goedert, 2000).

A few α-synuclein PET tracers have been proposed in the past decades, such as [^{18}F]-BF227 (Kudo *et al.*, 2007), [^{125}I]-SIL23, a phenothiazine derivative (Yu *et al.*, 2012), [^{18}F]WC-58a (Chu *et al.*, 2015), and [^{125}I]IDP-4 (Uzuegbunam *et al.*, 2020) but most of them lack selectivity for α-synuclein detection versus β-amyloid and tau fibrils, have low binding affinity for the fibrillar form of α-synuclein in vivo, or show inappropriate pharmacokinetics (Shah *et al.*, 2014; Kotzbauer *et al.*, 2017; Mathis *et al.*, 2017). Investigations are still progressing presently to find a suitable α-synuclein PET tracer in vivo.

2 NEW DEVELOPMENTS IN PARKINSON'S DISEASE NEUROIMAGING

As mentioned before, routine anatomical brain imaging using T1-weighted MRI (1,5 T – 3 T) is considered as normal in PD, even in advanced cases. Substantia nigra (and the subsequent nigro-striatal dysfunction) is at the heart of the neurodegenerative process that characterises Parkinson's disease, but its study by neuroimaging has been challenging as this structure has a small size and offer poor contrasts with T1-weighted MRI. Nevertheless, spatial resolution and specificity of structural imaging have been improved recently, thanks to high field MRI (from 3 T to 7 T) or, inspired by neuropathological processes underlying PD, new MRI sequences sensitive to substantia nigra pigmentation (neuromelanin) or iron content.

This work will particularly focus on structural MR imaging advances in PD, but it has to be mentioned that other sophisticated techniques such as tractography and resting state functional connectivity have also been developed in Parkinson's disease in the past decade (Pyatigorskaya *et al.*, 2014).

2.1 SUBSTANTIA NIGRA DIVISIONS IN NEUROIMAGING STUDIES

There is no general consensus about how the SN should be segmented for specific analysis in the context of neuroimaging studies.

As a preamble to this discussion, reference frames of brain anatomy are recalled in **Figure 12**.

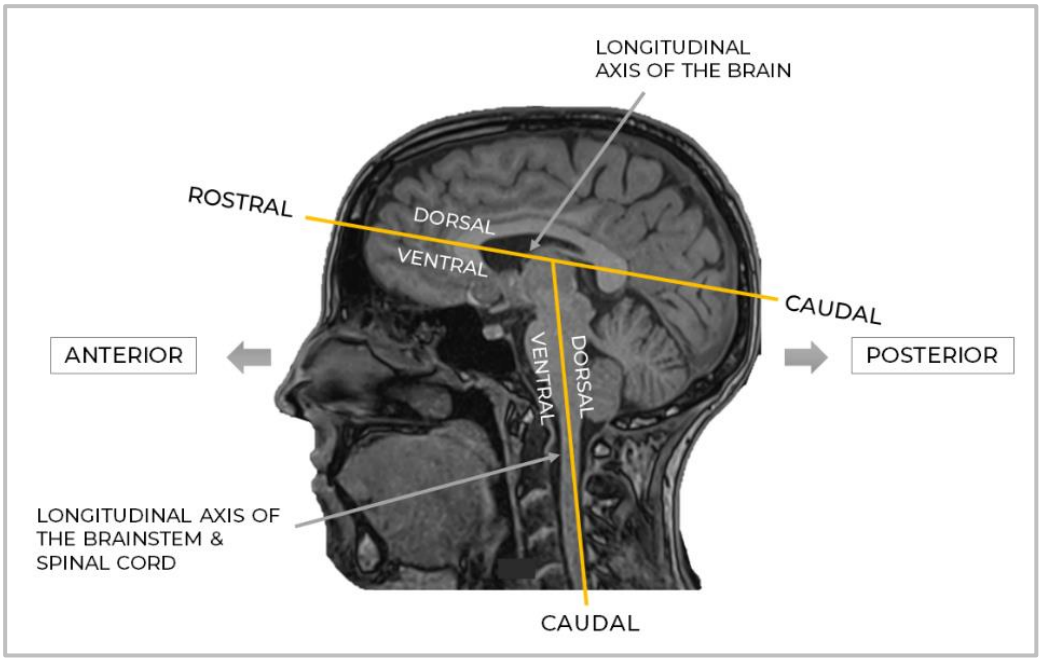

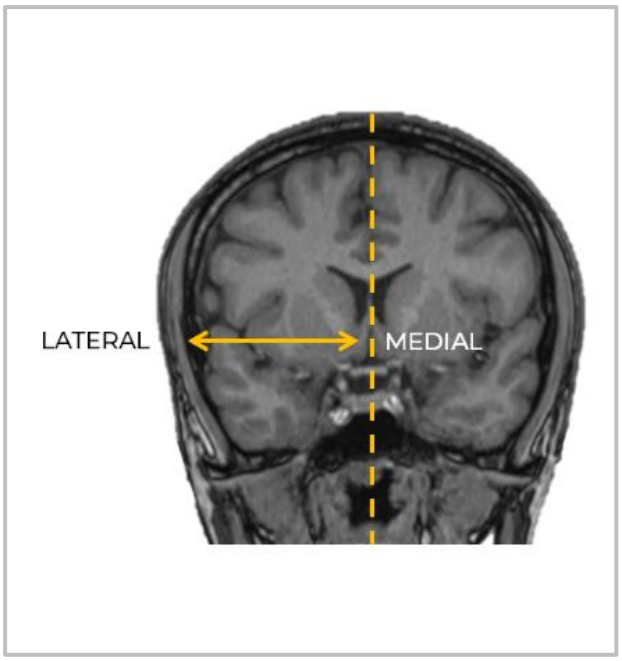

FIGURE 12 –
Reference frames of brain anatomy.
A – brain axis representation on a T1-weighted MRI (sagittal slice) of a healthy subject.
B – brain axis representation on a T1-weighted MRI (frontal slice). Personal contribution.

As demonstrated in the study by Fearnley and Lees (Fearnley and Lees, 1991), the most severe loss of dopaminergic neurons occurs in the ventrolateral part of the substantia nigra pars compacta, which is consistent with the findings of Hassler's study, published in 1937 (Hassler, 1937) **(see Chapter 2, Section 4.1, and Figure 6)**. However, the delineation of such a small and precise region is not possible with MRI, and many authors have chosen different methods to define SN subregions.

The importance of the distinction between the ventral and dorsal part of SN, based on histological observations, is highlighted in the study by Haber and colleagues, which explores the numerous connections of the midbrain dopaminergic cells (Haber, 2014). These limits are well defined in transverse sections of the midbrain **(see Figure 13)**.

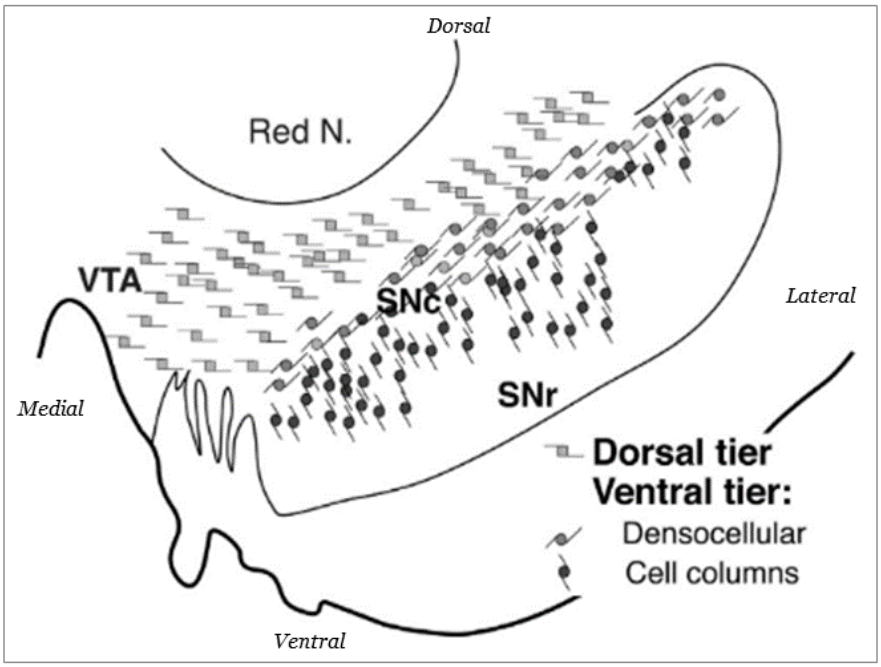

FIGURE 13 – **Illustration of dopaminergic neurons distribution within the midbrain**, showing dorsal and ventral tiers limits based on histological findings. Red N., red nucleus; SNc, substantia nigra, pars compacta; SNr, substantia nigra, pars reticulata; VTA, ventral tegmental area. Picture reproduced from Haber's publication (Haber, 2014).

Unfortunately, the terminology used in MRI studies does not always overlap the histological delineation defined by the studies mentioned above.

As an example, in their study published in 2019, Martin-Bastida and colleagues defined the anterior-medial region of SN as the '**dorsal SN**' and the posterior-lateral region as the '**ventral SN**' (**Figure 14 – A**), on an axial slice of a neuromelanin-sensitive T1-weighted template at the level of the substantia nigra (Martín-Bastida *et al.*, 2019). Schwarz and colleagues decided to use different terms, '**anterior**' and '**posterior**' SN, in a study designed to investigate the pattern of neuromelanin signal intensity loss within the SNpc, LC, and VTA in Parkinson's disease (Schwarz *et al.*, 2017).

These regions can be found in the supplementary materials of the publication, with marks cutting SN in two halves on an axial slice (**Figure 14 – B**). They found a preferential volume loss in the region of the posterior SN, which is compared to histologic findings of PD - induced cell loss of in the lateral ventral tier described by Fearnley and Lees (1991).

In a study assessing the ability of neuromelanin-sensitive MRI techniques to discriminate essential tremor from early-stage tremor-dominant PD, Reimao and colleagues chose another type of subdivision (Reimão *et al.*, 2015). SN was divided into three equal segments defining the **lateral**, **central**, and **medial** SN parts (**Figure 14 – C**) on an axial slice of a NM-sensitive MRI. Kitao and colleagues, in their study of the correlation between *post-mortem* NM-sensitive MRI and neuropathological findings (Kitao *et al.*, 2013), selected a division of SN in two parts similar to Schwarz et al as mentioned above, but decided to call them differently, namely '**lateral**' SN and '**medial**' SN (**Figure 14 –D**).

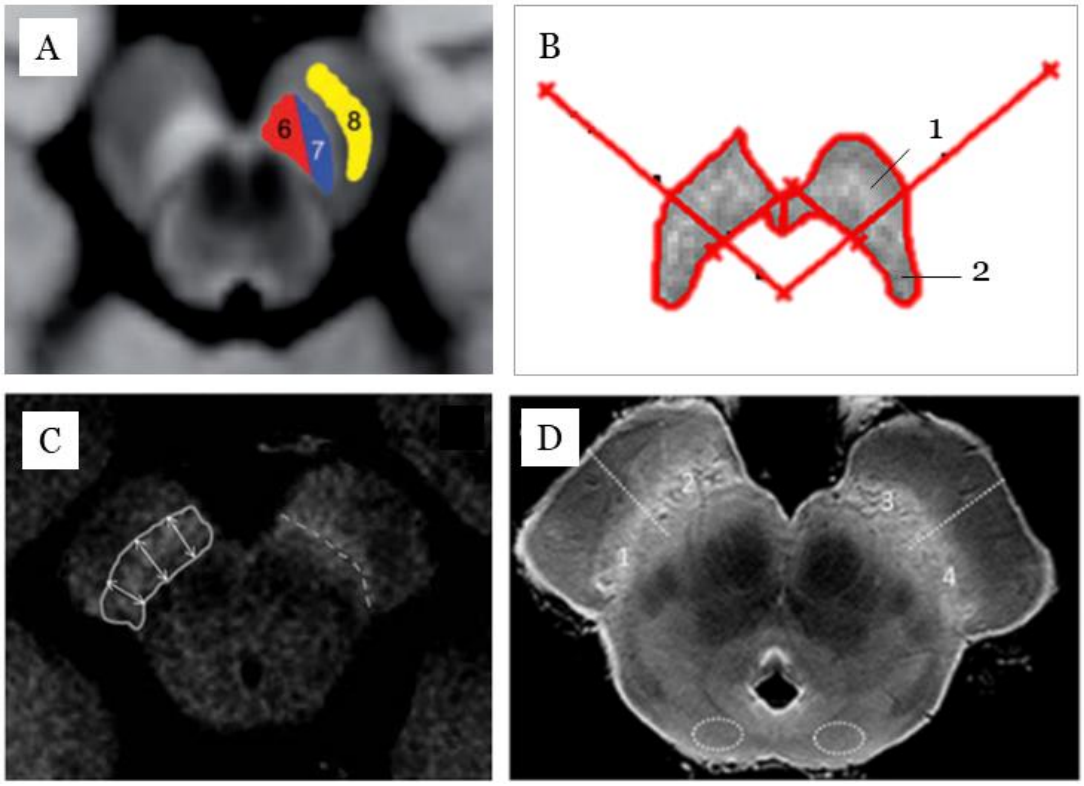

FIGURE 14 – **Subdivisions of substantia nigra in various MRI studies.** A – Divisions into "dorsal SN" (6, red on the picture) and "ventral SN" (7, blue on the picture) of the SN on an axial slice of a neuromelanin-sensitive MRI. Picture reproduced from (Martín-Bastida *et al.*, 2019). B – Divisions into "anterior SN" (1) and "posterior SN" (2) of the SN, on an axial slice. Picture reproduced from (Schwarz *et al.*, 2017). The line dividing the SN in these two studies are drawn in orthogonal directions. C – Divisions of SN into "medial", "central" and "lateral SN", on an axial slice. Picture reproduced from (Reimão *et al.*, 2015). D- Divisions of SN into "medial SN" (2,3 on the picture) and "lateral SN" (1,4 on the picture) on a *post-mortem* NM-sensitive MRI of the midbrain. Picture reproduced from (Kitao *et al.*, 2013).

The plethora of terms employed to described the various subregions of SN (lateral/medial/central, anterior/posterior, dorsal/ventral) makes difficult the comparison between results of different studies. In addition, the methods of these publications do not always warrant the division that is drawn which, most of the time, appears to be defined by the experimenter.

2.2 NEUROMELANIN-SENSITIVE MRI

2.2.1 GENERAL CONSIDERATIONS

Neuromelanin-sensitive MRI is typically based on a high-resolution T1-weighted turbo spin echo sequence, and offers a noticeable contrast between substantia nigra, locus coeruleus and surrounding midbrain tissues (Trujillo *et al.*, 2017). These first structures are particularly rich in neuromelanin pigmented neurons. The contrast obtained with the NM-sensitive MRI seems to be related to the T1 shortening associated with the presence of melanin compounds (Sasaki et al., 2006). With this technique, NM containing structures typically appear as areas of hyperintensity (**see Figure 15**). Later, Schwarz and colleagues added for the first time a spectral pre-saturation inversion-recovery pulse to the T1w fast spin-echo protocol, a manipulation which confers a magnetisation transfer effect and improves resolution contrast between the NM-rich structures and the surrounding areas (Schwarz et al., 2011).

The presence of iron, especially the fraction bound to ferritin located in the SN, has been suggested as a cause of T1- shortening effects in neuromelanin-sensitive MRI (Sasaki *et al.*, 2006). However, other structures particularly rich in iron in the brain, such as red nucleus, or basal ganglia, do not show any particular hyperintensity in neuromelanin-MRI (Trujillo *et al.*, 2017).

.

FIGURE 15 – Example of neuromelanin-sensitive MRI.

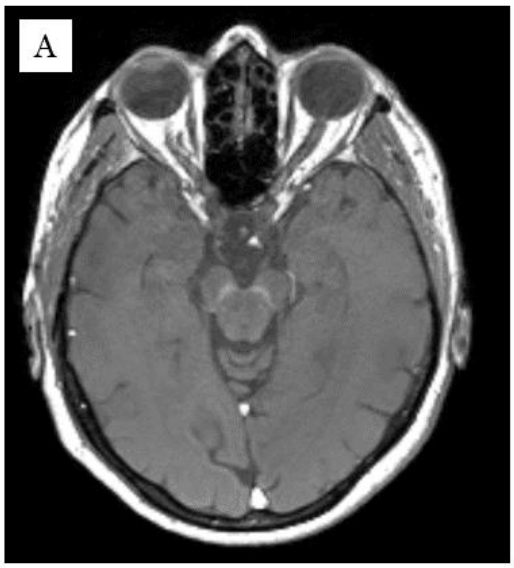

A – Axial slice at the level of the midbrain in a healthy subject.
B – Substantia nigra appears as a hyperintense structure (arrow).
C – NM-sensitive MRI acquired in a PD patient, showing a reduction of the size of the hyperintensity area corresponding to the substantia nigra. These MRI have been acquired with a 3T scanner, at the GIGA – Cyclotron Research Centre, University of Liege. Personal contribution.

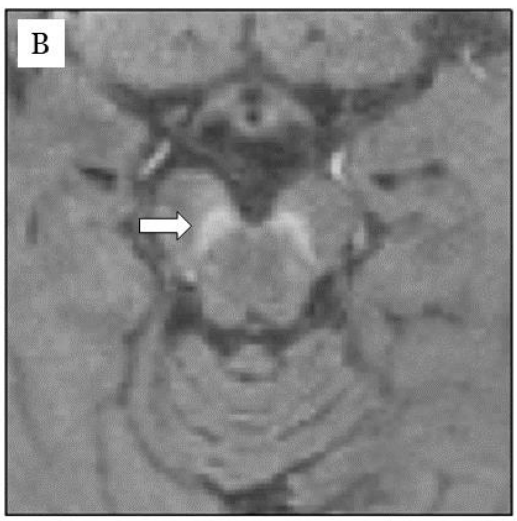

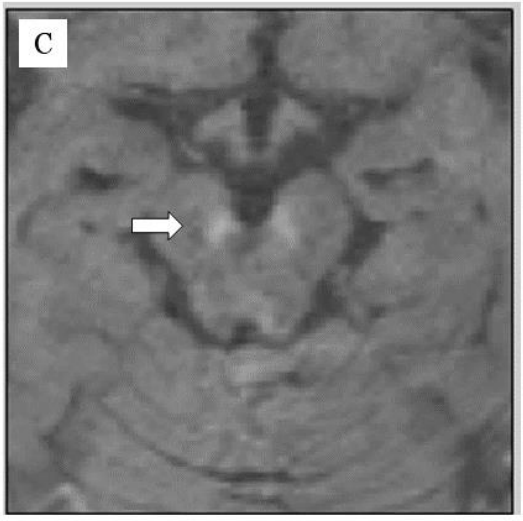

2.2.2 NEUROMELANIN-SENSITIVE MRI AND ITS RELATIONSHIP WITH PARKINSON'S DISEASE

In a direct comparison between *post-mortem* NM-sensitive MRI and neuropathological analysis, Kitao and colleagues have shown a correlation between signal intensity in the SN and the number of NM-containing neurons, supporting the link between NM-MRI hyperintensity and the presence of NM (Kitao *et al.*, 2013). Importantly, the signal intensity of the SN did not appear to be influenced by local iron content.

Several studies showed a specific reduction of NM-MRI contrast in the SN of PD patients, beyond age-dependent SN depigmentation, as it has to be taken into account that neuromelanin also declines with age in healthy individuals, both in anterior and posterior SN (Xing *et al.*, 2018).

However, up to now NM-sensitive MRI remains a qualitative technique and structural damage can be appreciated as a reduction in size, volume or signal intensity of the SN. Many techniques of signal extraction have been proposed by various authors over the years. SN signal, extracted manually or semi-automatically (e.g. circular regions of interest, manual delineation of SN, or mask of SN extracted from a reference atlas), has to be corrected for background signal. The latter is taken from either crus cerebri (Chen *et al.*, 2014; Langley *et al.*, 2015; Isaias *et al.*, 2016; Cassidy *et al.*, 2019) , pontine tegmentum (Sasaki *et al.*, 2006; Schwarz *et al.*, 2011) or superior cerebellar peduncles (Sasaki *et al.*, 2006; Martín-Bastida *et al.*, 2019). The ensuing dependent variable is either a contrast to noise ratio (CNR) (Ohtsuka *et al.*, 2013; Isaias *et al.*, 2016), or the number of voxels above an experimenter-defined threshold value (Schwarz *et al.*, 2011, 2017; Langley *et al.*, 2015). Other authors have proposed to calculate the area (Reimão *et al.*, 2015) or the volume of SN: hyperintense areas of SN are manually traced bilaterally and the volume is calculated by

multiplying the area by slice thickness (Kashihara *et al.*, 2011*b*). As accurate manual segmentation of brainstem nuclei is difficult due to their irregular morphology and low size relative to the spatial resolution of MRI, Castellano and colleagues proposed a fully automated segmentation and quantification method of the SN and LC volumes using multi-image atlas (Castellanos *et al.*, 2015).

These various studies have consistently demonstrated that SN hyperintensity or SN volume, depending on the technique used, was significantly reduced in PD patients when compared to the healthy controls.

The neuropathological pattern of the SN damage related to the disease was also assessed with NM-sensitive MRI. Ohtsuka and colleagues studied the regional differences of NM contrast within the SN, using early-stage PD patients, besides controls. Significant reduction in the lateral and central SN contrast ratios were found in the PD patients group, illustrating the rostral–caudal gradient of neuronal loss in PD as demonstrated by pathological studies (Ohtsuka *et al.*, 2013).

2.2.3 NEUROMELANIN-SENSITIVE MRI AND ITS RELATIONSHIP WITH CLINICAL PARAMETERS

Results are rather contradictory regarding correlations between imaging data and PD-related impairment as measured by various clinical scores. Schwarz and colleagues did not show any significant correlation between disease duration or H&Y stage and 'normalised neuromelanin-related volumes' of the SNpc, whereas a correlation with UPDRS was found (Schwarz *et al.*, 2017). On the other hand, Taniguchi and colleagues demonstrated that NM-SNpc area was inversely correlated with disease duration and motor deficits, estimated with the UPDRS part III score (Taniguchi *et al.*, 2018).

Other publications report an absence of consistent regression between imaging data and clinical scores (Castellanos *et al.*, 2015; Martín-Bastida *et al.*, 2019).

However, greater signal alteration was observed in the SN contralateral to the most clinically affected side (Prasad *et al.*, 2018).

Regarding progression of PD over time, a reduction of SNpc area of 17,5% a year in a population of PD patients was reported by a study focusing on NM-MRI longitudinal changes over two to three years of follow-up (Matsuura *et al.*, 2016), but only 14 PD patients were included. However, in a very recent study, Gaurav and colleagues enrolled 140 PD patients and 64 healthy subjects for a prospective longitudinal assessment of NM-MRI (again, over two to three years of follow-up) and found a significant progressive and measurable reduction of SN volume based on neuromelanin signal analysis in PD (Gaurav *et al.*, 2021).

Some authors suggested that NM-sensitive MRI could also be used to identify prodromal premotor symptoms of PD. Beside hyposmia, REM sleep behaviour disorder (RBD) is a well-known premotor symptom of PD, implicating specifically locus coeruleus structures (Arnulf *et al.*, 2000). Garcia-Lorenzo and colleagues studied a group of PD patients presenting with and without RBD, using video-polysomnography and multimodal MRI including the NM-sensitive sequences, and found significant reduction of NM signal in the locus coeruleus (LC) in the group of PD patients with RBD (García-Lorenzo *et al.*, 2013). However, many studies have shown a great discrepancy between the absolute degree of LC cell loss found in *post-mortem* brains and the LC signal intensity loss in PD (Sasaki *et al.*, 2006; Castellanos *et al.*, 2015; Schwarz *et al.*, 2017). The place of NM-sensitive MRI in prodromal PD assessment is yet to be determined.

2.2.4 NEUROMELANIN-SENSITIVE MRI AND ITS USE IN THE DIFFERENTIAL DIAGNOSIS OF PARKINSONISMS

Only a few NM-sensitive MRI studies have considered the usefulness of this approach for the differential diagnosis of atypical parkinsonisms. Kashikara and colleagues studied with NM-sensitive MRI a large group of patients suffering from PD, MSA, PSP, DCB and spinocerebellar atrophy (SCA), and compared them to controls. They showed that the volumes of the neuromelanin-positive SN regions in patients with PD, MSA, PSP and CBD, but not SCA, were reduced compared with healthy controls (Kashihara *et al.*, 2011*a*). However, in a similar study, Ohtsuka and colleagues found that the signal intensity of the lateral SNpc and LC, as measured with contrast ratio, was lower in the PD and MSA-P groups than in the PSP and control groups (Ohtsuka *et al.*, 2014). In a study comparing PD, MSA patients and healthy controls, Matsuura and colleagues also showed a reduction of LC and SNpc contrast ratios in the MSA and PD patients groups, but not in healthy controls (Matsuura *et al.*, 2013). Recently, Simoes and colleagues studied a group of patients with the parkinsonian variant of multiple system atrophy (MSA–p) and compared them with PD patients and healthy subjects. Simple visual MRI analysis showing normal neuromelanin SN and LC, combined with nigrosome 1 loss **(see Chapter 2, Section 4.1)** in susceptibility-weighted sequences, allowed the distinction of the MSA-p group from PD and controls (Simões *et al.*, 2020).

2.3 IRON-SENSITIVE MRI

2.3.1 GENERAL CONSIDERATIONS

As mentioned earlier **(see Chapter 2, Section 4.3)**, numerous neuropathological studies have demonstrated that Parkinson's disease is typically characterised by an increase of total iron concentration in the brain of affected individuals, particularly in the substantia nigra, beyond what is observed with age.

Many recent imaging studies concentrated on the development of MRI modalities that could be sensitive to iron-signal. Indeed, iron is a paramagnetic element that induces magnetic field inhomogeneities, corresponding to differences in the local magnetic field, causing faster signal decay in T2 and T2*- weighted MR and increased transverse relaxation rates R2 and R2* (1/T2*; apparent transverse relaxation rates). Overall, the T2 shortening effects of iron provide enhanced contrast, thus improving the delineation of structures containing this element (Pyatigorskaya *et al.*, 2014).

This specific feature can be used to estimate iron content with MRI based on a reduction in T2∗ relaxation time or an increase in R2∗ **(see Figure 16)**, phase changes in susceptibility-weighted imaging (SWI), or increased susceptibility values on quantitative susceptibility mapping (QSM) (Pyatigorskaya *et al.*, 2020). SWI utilises the magnetic susceptibility differences between brain tissues: with long echo times, the signal from structures with different magnetic susceptibilities compared to the background tissues will become out of phase with these tissues, a process enhancing contrast in MRI (Haacke *et al.*, 2004). QSM is a post-acquisition processing technique allowing the calculation of the bulk magnetic susceptibility distribution of tissue in vivo from gradient echo magnetic resonance phase images (Li and Leigh, 2004; Langkammer *et al.*, 2012). For the sake of clarity, quantitative MRI is developed further in the next section.

These MRI modalities, gathered under the term "iron-sensitive MRI", provide a non-invasive estimation of iron content in various structures of the brain. Langkammer and colleagues demonstrated in 2012 the relation between tissue magnetic susceptibility using QSM and brain iron concentration in unfixed (*in situ*) *post-mortem* brains of 13 subjects determined by using inductively coupled plasma mass spectrometry (Langkammer *et al.*, 2012).

Limitations of R2* imaging have been emphasised in a few studies: although R2* signal is primarily modulated by local iron content, it is also influenced by calcium, myelin and lipid content, fibre orientation relative to the magnetic field, and macroscopic geometry (He and Yablonskiy, 2009; Bagnato *et al.*, 2018). In addition, R2* value of each voxel is a weighted summation of magnetic properties from both local and surrounding tissue (Du *et al.*, 2016; Wang *et al.*, 2016). In comparison, QSM removes the effects of susceptibility of the surrounding tissue through deconvolution, thus providing a direct measure of local tissue magnetic properties (Wang and Liu, 2015; Du *et al.*, 2016).

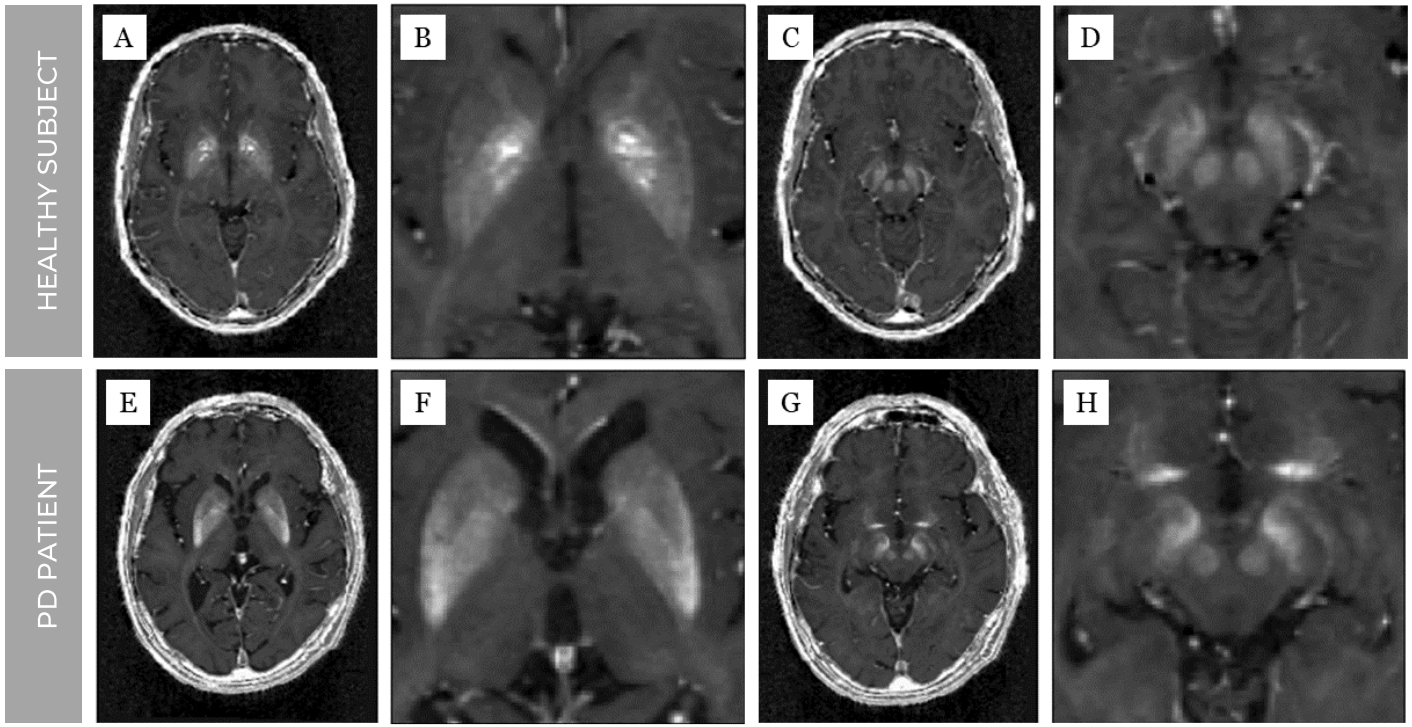

FIGURE 16 – **Example of iron-sensitive MRI** (R2* map obtained with a multiparameter protocol). First row. A–D: Iron-sensitive MRI of a healthy subject (A, full volume, axial slice at the level of the basal ganglia; B, enlarged view of an 80mm by 80mm area around the basal ganglia; C, full volume, axial slice at the level of the midbrain; D, enlarged view of an 80mm by 80mm area at the level of midbrain). Second row. E–H: R2*-sensitive MRI of a Parkinson's disease patient (E, full volume, axial slice at the level of the basal ganglia; F, enlarged view of an 80mm by 80mm area around the basal ganglia; G, full volume, axial slice at the level of the midbrain; H, enlarged view of an 80mm by 80mm area at the level of midbrain). Iron deposits appears as hyperintense structures. These pictures illustrate the distinct distribution of hyperintensities in PD (e.g. posterior putamen) when compared to healthy subjects. Images are displayed in radiological convention. These MRI have been acquired on a T3 MRI scanner, at the GIGA-CRC In Vivo Imaging, University of Liege, Belgium. Personal contribution.

2.3.2 QUANTITATIVE MRI

Conventional structural MRI mainly provides morphological measures of the brain. Typically, morphometry based on structural MRI estimates the volume and thickness of the cortex or sub-cortical grey matter structures (Ashburner and Friston, 2000; Ashburner *et al.*, 2003). These measures are then compared between groups, or tracked longitudinally.

However, morphometric measures are not specific to a particular MRI parameter, and lack specificity. Moreover, the interpretation of morphometric changes may be difficult because they can be influenced by spatial smoothing, image contrast, tissue segmentation (Helms *et al.*, 2009), artefacts, etc.

By contrast, quantitative MRI (qMRI) estimates specific MRI brain properties at the voxel level (e.g., relaxation times, magnetic susceptibility, proton density, diffusion, cerebral blood flow, etc.). These physical parameters depend on local factors, such as iron and macromolecular concentrations (Stüber *et al.*, 2014), thereby assessing local tissue microstructure (Callaghan *et al.*, 2014; Weiskopf *et al.*, 2015). For instance, magnetization transfer correlate with myelin content, measured histologically on *post-mortem* brains (Schmierer *et al.*, 2004).

Moreover, the quantitation of physical tissue properties ensures its reproducibility across laboratories and across times, as long as the magnetic field is identical: Deoni and colleagues showed the reliability of quantitative T1 and T2 imaging derived from data acquired on various MRI scanners of different manufacturers in different imaging centres (Deoni *et al.*, 2008).

In the next sections, we will particularly focus on various MRI techniques sensitive to iron content; QSM and quantitative R2 maps being two examples of quantitative MRI approaches.

2.3.3 IRON-SENSITIVE MRI AND ITS RELATIONSHIP WITH PARKINSON'S DISEASE

Considering the role of iron in PD pathology, many studies investigated the role of iron-sensitive MRI in PD and its relevance as a biomarker in PD diagnosis. Most of them (Gorell *et al.*, 1995; Martin *et al.*, 2008; Baudrexel *et al.*, 2010; Pyatigorskaya *et al.*, 2015; Reimão *et al.*, 2016; Langley *et al.*, 2017) including two meta-analysis (Wang *et al.*, 2016; Pyatigorskaya *et al.*, 2020) found an increase in iron content in the substantia nigra of PD patients in comparison with matched healthy controls, using either R2*, SWI or QSM. Negative findings were also published (Mondino *et al.*, 2002; Isaias *et al.*, 2016). Others showed that iron overload affects the whole nigrostriatal system, but predominantly the SN, by measurements of R2* values (Wallis *et al.*, 2008; Hopes *et al.*, 2016). Increased iron levels were also found in red nucleus of PD patients (Wang *et al.*, 2016), or in the subthalamic nucleus (Kosta *et al.*, 2006).

Particularly, the topography of iron deposition in SN is still a matter of debate: some authors found increased iron content (as estimated by iron-sensitive MRI signal) over the whole SN (Graham *et al.*, 2000; Pyatigorskaya *et al.*, 2015; Hopes *et al.*, 2016), while others report increased R2* in posterior (Azuma *et al.*, 2016), medial (Baudrexel *et al.*, 2010), lateral (Martin *et al.*, 2008; Wieler *et al.*, 2015; Du *et al.*, 2016) or anterior SN (Arribarat *et al.*, 2019). Some authors divided the SN into SNpc and SNr and found that mean R2* in the SNpc was significantly increased in PD as compared with healthy controls (Langley *et al.*, 2019).

In the meta-analysis comparing iron-sensitive MRI techniques between them, SWI measurements were the most variable across studies. Indeed, as mentioned above, SWI is purely a qualitative method. Besides, recent studies comparing R2∗ and QSM values in the same group of PD patients (as compared with healthy controls)

showed the greater sensitivity of QSM to map the spatially heterogeneous iron deposition in the SN, suggesting that QSM might be a more robust marker than R2∗ (Du *et al.*, 2016; Li *et al.*, 2019; Prange *et al.*, 2019; Pyatigorskaya *et al.*, 2020).

2.3.4 IRON-SENSITIVE MRI AND ITS RELATIONSHIP WITH CLINICAL PARAMETERS

The role of iron-sensitive MRI for monitoring disease progression in PD and its correlation with clinical symptoms is still unclear. Du and colleagues demonstrated that susceptibility values in the SN, obtained by QSM, were correlated significantly with disease duration, UPDRS II, and LEDD (Du *et al.*, 2016). However, in the same study, R2* was not significantly correlated with disease severity measures. Wieler and colleagues also demonstrated a correlation between R2* in the lateral SNpc and motor symptomatology assessed with UPDRS III score, but also with PDQ-39 mobility sub-scores **(see Appendix 2, Table 2)** (Wieler *et al.*, 2015). In a longitudinal study by Ulla and colleagues, a positive correlation between R2* variation and the worsening of motor symptoms of PD, determined with UPDRS III score, was demonstrated (Ulla *et al.*, 2013). However, Isaias and colleagues did not find any correlation between neither R2* nor susceptibility values and any clinical parameter (Isaias *et al.*, 2016). In most studies, no significant relationship was shown between iron deposition and disease duration (Martin *et al.*, 2008; Ulla *et al.*, 2013).

A few longitudinal studies have reported contradictory results about how R2* is modified with PD progression. According to Hopes and colleagues (Hopes *et al.*, 2016), early-stage patients displayed significantly higher R2* values in the substantia nigra, in comparison with *de novo* patients. They also observed that disease progression and iron overload were not linearly correlated, as iron accumulation worsened rapidly over the first 3 to 5 years but was slower in advanced

disease. Ulla and colleagues also found a significant variation of R2* in the SN and caudal putamen of PD patients evolving over a three-year period (Ulla *et al.*, 2013). Notwithstanding, Wieler and colleagues found different results, as R2* tended to increase in the PD patients with more advanced disease and to decrease in those with milder disease (Wieler *et al.*, 2015). The absence of linear relation between iron accumulation and disease progression over time might explain the lack of correlation between motor severity and iron content found in some cross-sectional studies (Hopes *et al.*, 2016).

Regarding QSM and disease progression, Du and colleagues compared QSM and R2* in another study in 2018 and found that susceptibility MRI revealed distinct patterns of PD progression in the SNpc and SNr. The different patterns were particularly obvious in later stage patients (Du *et al.*, 2018). In this study, R2*increase in SNpc correlated with changes in non-motor symptoms, whereas SNr QSM correlated with changes in motor signs.

2.3.5 IRON-SENSITIVE MRI AND ITS POTENTIAL USE AS A BIOMARKER FOR PARKINSON'S DISEASE

Overall, even if they differed in iron measurement techniques, most of the studies using iron-sensitive MRI detected iron overload in the SN of PD patients compared to healthy controls even in the early stage of disease, which is in agreement with the abnormal iron metabolism found in neuropathology studies of PD. The consistent increase in MRI measures of iron content confirms that these imaging tools provide reliable markers of iron accumulation in PD, but QSM and R2∗ are preferable to SWI because they offer quantitative values unlike SWI (Wang *et al.*, 2016; Pyatigorskaya *et al.*, 2020).

2.4 RECENT ADVANCES IN SUBSTANTIA NIGRA STRUCTURAL IMAGING

2.4.1 SWALLOW-TAIL SIGN IN MRI

Besides its use as described above, iron-sensitive MRI has also been studied to find a typical pattern that could be identified in PD by visual assessment, similarly as the hummingbird sign in PSP, or the hot cross bun sign in MSA. As the loss of substantia nigra dopaminergic neurons is prominent in sub-regions called nigrosomes **(see Chapter 2, Section 4.1)**, some research teams have focused on the delineation of these areas by advanced MRI sequences. Blazejewska and colleagues demonstrated that high-resolution, iron-sensitive MRI (T2*-weighted) at ultra-high magnetic field strengths of 7T allows direct nigrosome-1 visualisation in healthy people (as hyperintense, ovoid area within the dorsolateral border of the otherwise hypointense SNpc) but not in PD (Blazejewska *et al.*, 2013). The same team demonstrated a correlation between *post-mortem* MRI data using these particular sequences and the histological analysis of three brains. Schwarz and colleagues have studied the potential of

nigrosome-1 detection by high-resolution 3T SWI MRI and demonstrated that in healthy subjects, nigrosome-1 can be readily outlined, giving rise to a 'swallow tail' appearance of the dorsolateral substantia nigra, whereas this feature is lost in PD (Schwarz *et al.*, 2014). In the same study, visual radiological assessment provided a high diagnostic accuracy for PD by comparison with healthy controls. Schmidt et al. confirmed in 2017 the high inter-rater reliability of the detection of the swallow-tail sign, using high-resolution 7T SWI (Schmidt *et al.*, 2017). Nevertheless, some authors have shown that the occurrence of the swallow tail sign is not always consistent or symmetric in some healthy subjects, reducing the reliability of this sign (Gramsch *et al.*, 2017; Schmidt *et al.*, 2017).

2.4.2 VOXEL-BASED MORPHOMETRY

As mentioned previously, PD pathological changes are not limited to the SN and extend to subcortical and cortical structures, including in the early stages of the disease. As a result, dopaminergic projections to the basal ganglia are functionally impaired, which can be explored using PET or SPECT (**see Chapter 3, Section 1.2**). However, some studies have also investigated the structural alterations in this network and found a negative correlation between striatum grey matter density (at voxel level) and UPDRS III score, using high resolution structural MRI T1 in PD patients (Li *et al.*, 2018). In another study using voxel-based morphometry to assess cortical grey matter changes, and automated volumetry and shape analysis for volume changes estimation of subcortical grey matter structures, Lee and colleagues showed that compared to controls, PD patients had significant reductions in adjusted volumes of putamen, nucleus accumbens, and hippocampus (Lee *et al.*, 2014). These results are consistent with a previous study using shape analysis in T1- and T2-weighted brain 3T MRI in order to characterise spatial distribution of striatal atrophy. Compared to controls, lower putamen and caudate volumes were

found in PD patients, affecting particularly caudal putamen, as well as head and dorsal body of the caudate (Sterling *et al.*, 2013).

The impact of the disease on cortical structures have also been investigated. In early stage non-demented PD patients, reduced DAT uptake was associated with longitudinal cortical grey matter thinning in frontal and posterior cortical brain regions. Rather than being entirely due to cholinergic degeneration occurring in later stages of the disease, this suggests that dopamine loss promotes posterior cortical atrophy quite early (Sampedro *et al.*, 2019).

2.4.3 TRANSCRANIAL SONOGRAPHY IN PARKINSON'S DISEASE

During the two last decades, transcranial sonography (TCS) has been established as a valuable tool in the diagnosis of PD and the differential diagnosis of extrapyramidal disorders (Berg *et al.*, 2006). Indeed, many studies using TCS of the midbrain demonstrated that hyperechogenicity of the substantia nigra was found in about 90% of patients with Parkinson's disease (Gröger and Berg, 2012).

High-end ultrasound systems with standardised published settings allow planimetric measurement of the area of hyperechogenicity at the anatomical site of the SN (Berg *et al.*, 2006; Berardelli *et al.*, 2013) **(see Figure 17)**. Nevertheless, some limitations do exist (Berg, 2011), and among them, the quality of the temporal bone window (transtemporal bone window is inadequate in about 10% of the Caucasian population), availability of the ultrasound machines and probes, and the experience of the investigator. Besides, it has been demonstrated that substantia nigra hyperechogenicity is observed in about 10% of the healthy population.

In a study comparing TCS and [^{18}F]DOPA PET, Berg and colleagues showed that increased echogenicity of the SN, characteristically seen in Parkinson disease, correlates with functional impairment of the

nigrostriatal system as revealed by [^{18}F]DOPA PET exams (Berg *et al.*, 2002). In another study, they also demonstrated that SN hyperechogenicity is related to a higher tissue iron level (Berg, 2006). Ultrasound investigation of 60 *post-mortem* brains from healthy subjects showed a positive correlation between the echogenic area of the substantia nigra and the concentration of iron and heavy and light chain ferritin (Berg, 2006; Ward *et al.*, 2014). There is also a significant negative correlation between SN echogenicity and neuromelanin content of the SN as determined by histological examination of *post-mortem* brains (Zecca *et al.*, 2005).

Beyond the diagnosis of degenerative PD, current evidence suggests that TCS is also useful in the differential diagnosis between PD and other parkinsonian syndromes, especially MSA. According various studies, only 9% of patients with atypical parkinsonism show hyperechogenicity of SN (Bouwmans *et al.*, 2010). According to Walter and colleagues, the finding of marked SN hyperechogenicity in combination with normal lenticular-nucleus echogenicity discriminates idiopathic Parkinson's disease from MSA and PSP with a positive predictive value of more than 90% (Walter *et al.*, 2007). Other studies revealed the usefulness of TCS in the differentiation of secondary parkinsonian syndromes, e.g. vascular parkinsonism (Venegas-Francke, 2010), and in the detection of subjects with preclinical PD, including asymptomatic mutation carriers of monogenic forms of PD (Walter *et al.*, 2004; Hagenah *et al.*, 2007).

Beside the limitations mentioned above, TCS has numerous advantages, such as the fact it is a quick and non-invasive method, applicable even in agitated patients, and it is less expensive than brain MRI (Walter *et al.*, 2007). Even if this technique is not yet widely used, current guidelines for PD diagnosis consider that TCS is recommended (Level A) for differential diagnosis of PD from atypical parkinsonisms and secondary parkinsonian syndromes, but also for early diagnosis of PD and detection of subjects at risk for PD. However, TCS should be combined with other screening procedures

as SN hyperechogenicity is not entirely specific to PD (Berardelli *et al.*, 2013).

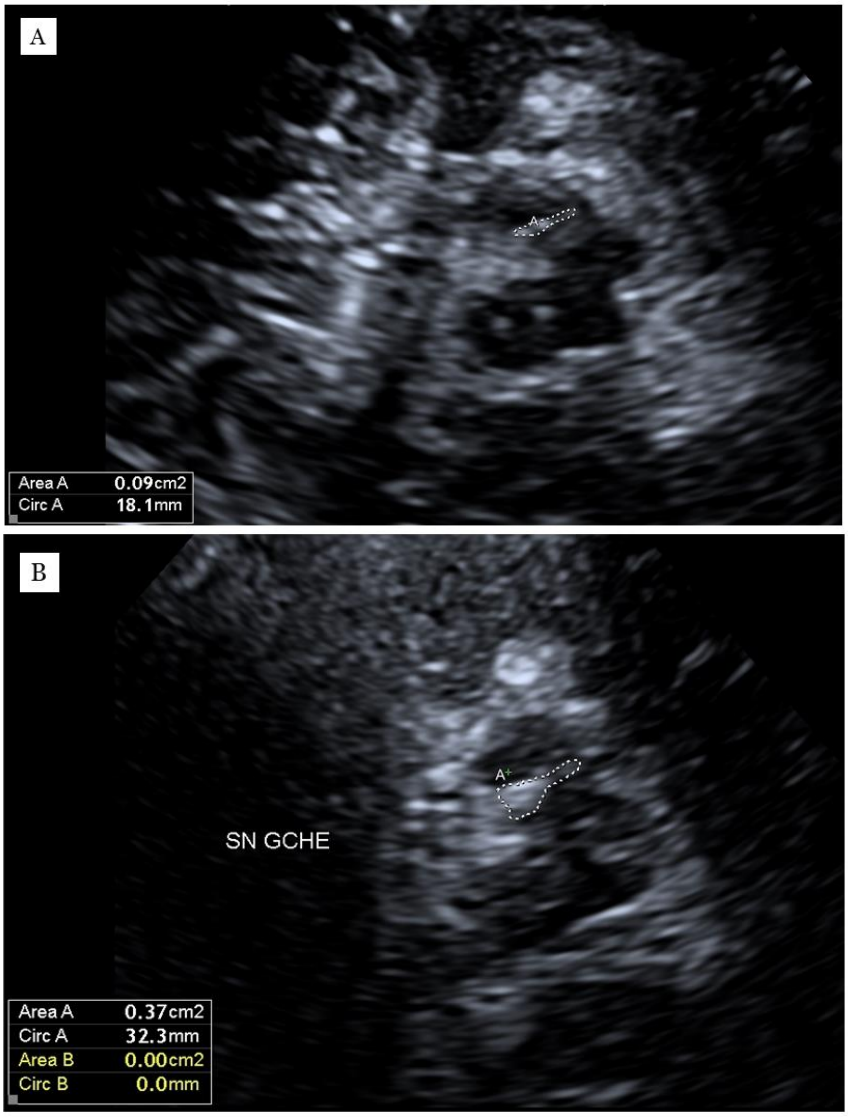

FIGURE 17 – **Transcranial sonography of the midbrain.** Picture A: Midbrain (visible as a butterfly-shaped structure) of a healthy control with normal echogenicity of the substantia nigra (delineated ipsilaterally with a dotted line). Picture B: In a patient with Parkinson's disease, the area of hyperechogenicity at the anatomical site of the SN is enlarged (encircled ipsilaterally with a dotted line). These pictures have been acquired in our movement disorder clinic, with kind contribution of Dr E. Parmentier and Dr E. Drion.

PART 2

Personal Contribution

4 CHAPTER 4

STUDY OBJECTIVES

As the clinical diagnosis of PD remains challenging, particularly in early stages where symptoms may overlap with other parkinsonian disorders, there is a crucial need for *in vivo* biomarkers, guiding clinicians in their differential diagnosis.

Neuroimaging biomarkers derived from images are expected to reliably reflect the presence of diseases, their severity, progression, etc. In PD, such biomarker should detect early neuropathological features and mechanisms underlying neurodegeneration (Pyatigorskaya *et al.*, 2014).

Of course, in vivo biomarkers of PD with potential quantification have already been developed in nuclear imaging, allowing measurement of dopaminergic dysfunction using positron emission tomography and single photon emission computed tomography. However, these techniques are not always widely available, may be expensive and expose the subject to irradiation, limiting their clinical application.

MRI is an attractive alternative to radiotracers methods but, as detailed above, conventional MRI is of little use in clinical practice. Nevertheless, in the past decade, advances in structural and functional MR imaging have improved the ability of MRI to detect changes in PD. In particular, the delineation of the SN and other small brainstem

nuclei have been possible with new MR contrasts and image analysis technique (Pyatigorskaya *et al.*, 2014; Prange *et al.*, 2019). As described above, NM-sensitive MRI and iron-sensitive imaging appear as promising candidates as biomarkers of PD. Indeed, they provide information about different processes implicated in SN degeneration.

As described in **Chapter 3, Sections 2.2 and 2.3**, many recent MRI studies using NM-sensitive imaging demonstrated a reduction of NM in SN, and others showed a consistent increase in iron load in the SN using various iron-sensitive MRI modalities. However, the association between NM distribution and iron accumulation in SN is yet to be ascertained (Martin-Bastida *et al.*, 2017). Very few studies explored that particular relationship. Reimao and colleagues did not find any significant correlation between SN neuromelanin signal and iron content in early-stage PD patients or controls (Reimão *et al.*, 2016), but the number of patients included and the range of disease severity were limited. Besides, some studies suggested there could be a limitation using NM-sensitive MRI as it is unclear if paramagnetic effects of local iron deposits in the SN influence NM signal. This specific relationship between iron signal and NM-sensitive MRI deserves to be clarified as these two techniques could provide precious information about particular pathophysiological pathways that might not be parallel in PD neurodegeneration.

On the other hand, these new MRI modalities provide a static picture of SN pathology and local alterations, but little is known about their relationship with nigro-striatal functioning. A few studies proposed striatal DAT SPECT imaging as a tool to investigate nigro-striatal pathway integrity in combination with MRI. Isaias and colleagues found that nigral contrast ratios and volumes determined by NM-sensitive MRI positively correlated with striatal DAT uptake values; however, no other association with nigral–iron accumulation were demonstrated (Isaias *et al.*, 2016; Martin-Bastida *et al.*, 2017). In the study conducted by Martin-Bastida and colleagues, no significant association between nigral pigmentation assessed with NM-MRI and

nigral dopamine transporter density was found. However, a significant relationship was observed between these parameters when the authors considered the clinically-defined most affected side and subdivided the regions implicated according neuropathology data (SN into ventral and dorsal tier, and striatum into pre-commissural and post-commissural striatal subregions) (Martín-Bastida *et al.*, 2019). To date, no such association has been established between iron- and neuromelanin- sensitive MRI and [^{18}F]DOPA PET.

In the present work, we aim to investigate the correlation between iron content in the different subregions of the SN and the neuromelanin signal changes in PD, and to study their individual relationships with dopaminergic function. Besides, it has to be highlighted that the objective of our study is neither focused on the validation of these techniques, nor on the establishment of their diagnostic performances.

We have decided to focus on SN degeneration – admittedly a late event in the time course of PD pathology, as demonstrated by Braak and colleagues (Braak *et al.*, 2003). Based on their findings about the location of Lewy neurites, they proposed that PD begins in the olfactory tract, lower brainstem (locus coeruleus, dorsal vagal nucleus, etc.) and peripheral tissues, with a caudal to rostral spread of Lewy neurites. Our work is rather centred on biomarkers that could be useful for diagnosis purposes, in clinical settings, not on biomarkers sensitive to prodromal PD and premotor stages. Clinical motor features emerge when nigral dopaminergic neurons are affected by the disease, which corresponds to the moment when the neurologist is consulted by the patient, and thus the question that must be answered is: "are these signs related to nigral impairment?" or "is it Parkinson's disease, or something else?".

CHAPTER 5

5 PARKINSON'S DISEASE MULTIMODAL IMAGING:

F-DOPA PET, NEUROMELANIN-SENSITIVE AND QUANTITATIVE IRON-SENSITIVE MRI

Section based upon the following publication:

Depierreux F., Parmentier E., Mackels L., Baquero K., Degueldre C., Balteau E., Salmon E., Phillips C., Bahri M. A., Maquet P., Garraux G. Parkinson's disease multimodal imaging: F-DOPA PET, neuromelanin-sensitive and quantitative iron-sensitive MRI. Published in NPJ Parkinson's Disease, July 2021 (DOI: 10.1038/s41531-021-00199-2).

1 INTRODUCTION

Parkinson's disease (PD) is the second most frequent neurodegenerative disorder worldwide and a growing public health issue given population aging (Erkkinen *et al.*, 2018). Yet, our understanding of PD remains fragmentary. Although the neuropathological hallmark of PD brain consists of the accumulation of insoluble synuclein deposits in both the peripheral and central nervous systems (Braak *et al.*, 1999; Dickson *et al.*, 2009; Halliday *et al.*, 2011), a strong clinical emphasis has been put on the neuronal loss in dopaminergic neuromelanin (NM) -pigmented neurons of the substantia nigra *compacta* (SN) (Hirsch *et al.*, 1988). Indeed, the decline of dopaminergic nigro-striatal neurotransmission is

considered as the core mechanism explaining most motor symptoms of PD and the diagnosis of PD still mainly relies on the clinical observation of motor signs (Postuma *et al.*, 2015). The latter only appear when 50 to 60 % of dopaminergic neurons of SN are already lost (Cheng *et al.*, 2010). Unfortunately, even in typical PD cases, the accurate diagnosis of PD remains challenging: only 74 to 84% diagnostic accuracy is achieved, depending on the practitioner's expertise in movement disorders (Hughes *et al.*, 1992, Rizzo *et al.*, 2016*b*). Therefore, there is a need for reliable *in vivo* diagnostic biomarkers. Measurement of striatal [^{18}F]DOPA uptake by positron emission tomography (PET) is still regarded as one of the most reliable tool for the *in vivo* diagnosis of PD because it directly probes the nigro-striate synthesis of dopamine (Snow *et al.*, 1993; Morrish *et al.*, 1995, 1996), and as such considered as a measure of dopamine terminal loss. [^{18}F]DOPA uptake is decreased in the putamen in virtually all patients with PD, even in the early stage of the disease (Morrish *et al.*, 1995). Nevertheless, the access to [^{18}F]DOPA PET is limited and the technique exposes patients to radiation hazards. More recently, MRI sequences allowed for the estimation of SN content in NM (Sasaki *et al.*, 2006; Kitao *et al.*, 2013; Martin-Bastida *et al.*, 2017; Cassidy *et al.*, 2019) as well as brain iron levels which induce an increase in apparent transverse relaxation rates (R2$*$) (Pyatigorskaya *et al.*, 2020). In PD, it is expected that R2* would increase in SN due to iron accumulation, whereas the signal of NM-sensitive MRI would decrease in SN, due to dopaminergic neuron loss and depigmentation.

FDOPA PET, NM- and iron-sensitive MRI then probe three different molecular aspects of PD pathophysiology, and although changes in each of these parameters were consistently observed in PD (decreased striatal DA synthesis, NM reduction and iron accumulation in SN), their joint modifications remain hardly known (Martin-Bastida *et al.*, 2017). This knowledge gap is important to fill in because these molecular markers of PD provide critical and complementary information on PD pathophysiology. In particular, the specific association between iron deposits and NM loss deserve to be

investigated as it could provide precious information about pathological processes that might not be parallel in PD neurodegeneration. These relations might be obscured by the heterogeneous subnuclear distribution of dopaminergic neurons in the SN: nearly half of them are packed in discrete zones. The larger of these packs is located in the dorsal and lateral regions of SN (Damier *et al.*, 1999*a*), where neuronal loss predominates (Damier *et al.*, 1999*b*). Likewise, the depletion of dopamine fibres within the putamen is most pronounced in its posterior portions (Kish *et al.*, 1988). The main goal of this study was precisely to compare, between PD patients and healthy control participants (HC), the relationships linking the dopaminergic function as measured in putamen by [^{18}F]DOPA PET to NM content and iron load in the SN, using respectively NM- and iron-sensitive MRI, taking into account the predominant pattern of disappearance of dopaminergic neurons and fibres, respectively in lateral SN and posterior putamen. We systematically probed the effect of disease on R2*, NM-sensitive and [^{18}F]DOPA signal, then the voxel wise relationships between (1) NM and R2* in SN , (2) R2* in SN and whole brain [^{18}F]DOPA influx rate constant (Ki) and (3) NM in SN and whole brain Ki **(see Figure 18)**.

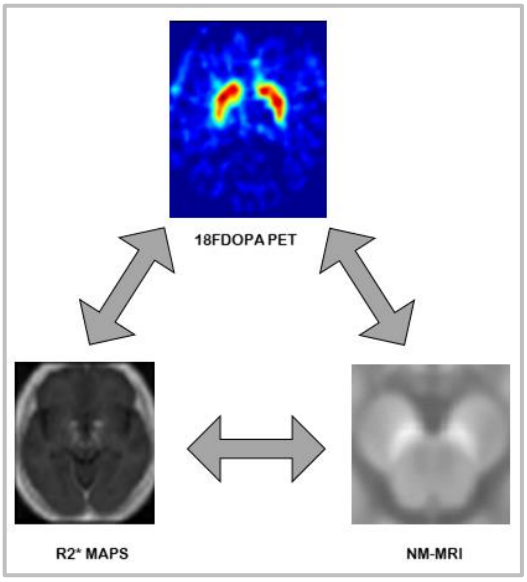

FIGURE 18 – **Analyses design.**
This diagram shows the three types of relationship explored in this study, between NM-MRI, R2* maps and FDOPA PETscan. This diagram will be recalled beside every correlation studied.

2 MATERIALS AND METHODS

2.1 PATIENTS

Forty-six participants took part in this study, which was approved by the local ethic committee (Belgian approval number 2012/79), and was performed in accordance with the ethical standards described in the Declaration of Helsinki (1964). Written informed consent was obtained from all participants. Twenty-three patients were recruited at the movement disorder clinic of the CHU Liège, Belgium, with a diagnosis of PD according to UK Brain Bank Criteria (Hughes *et al.*, 1992) and Movement Disorders Society guidelines (Postuma *et al.*, 2015), excluding atypical parkinsonism, vascular and other secondary parkinsonisms. Six patients had early parkinsonism (disease duration ≤ two years) and the diagnosis was confirmed four years later, using the same criteria (UK Brain Bank and MDS guidelines). All patients had a positive response to dopaminergic drugs/agents. The inclusion criteria were (1) age between 40 and 90 y., (2) Hoehn and Yahr scale<4, (3) compatibility with MRI, (4) no pregnancy. Twenty-three healthy control (HC) participants individually matched for age and gender, free from neurological or psychiatric disease, followed the exact same experimental protocol (**see Appendix 3, Table 3**).

2.2 DESIGN OVERVIEW

Participants were invited on a single day to MRI and [^{18}F]DOPA-PET imaging sessions. MRI and PET sessions was respectively scheduled in the morning and the afternoon. Clinical assessments were interleaved between imaging sessions.

Parkinson's disease patients were assessed with Unified Parkinson's Disease Rating Scale part III (UPDRS III) (Goetz et al., 2008), by two experienced raters to determine motor severity in OFF state (which was defined as absence of any treatment (N = 3) or treatment discontinuation for at least 24 hours for all the others). Clinical

laterality was established based on medical history and examination at the Movement Disorder Unit. The disease stage was determined using the Hoehn and Yahr scale (H&Y). Disease duration was estimated as the period since first recalled motor symptoms (Herb et al., 2016). Levodopa equivalent daily dose (LEDD) was calculated for each patient (Tomlinson et al., 2010).

2.3 MR IMAGE ACQUISITION, PRE-PROCESSING AND PET ACQUISITIONS

All scans were conducted at the GIGA Cyclotron Research Centre-*in vivo* imaging laboratory of the University of Liège, Belgium. MRI data were acquired on a 3T whole-body MRI-scanner (Magnetom Prisma, Siemens Medical Solutions, Erlangen, Germany) **(see Appendix 4, Table 4).** Chart flow of image analysis appear on **Figure 19.**

FIGURE 19 – **Chartflow of data processing and analyses (see text).**

1. Preprocessing ensures that MRI and PET data are registered in a common space.
2. Neuromelanin data consist of ESNV across all SN voxels, corrected for baseline values taken from bilateral cruces.
3. ESNV skewness act as regressor for R2* and Ki maps.
4. R2* maps serve in a group comparison
5. R2* values in SN serve as regressor for Ki maps.
6. Ki map are used to show the voxelwise group effect.

The grey diagrams illustrate design matrices.

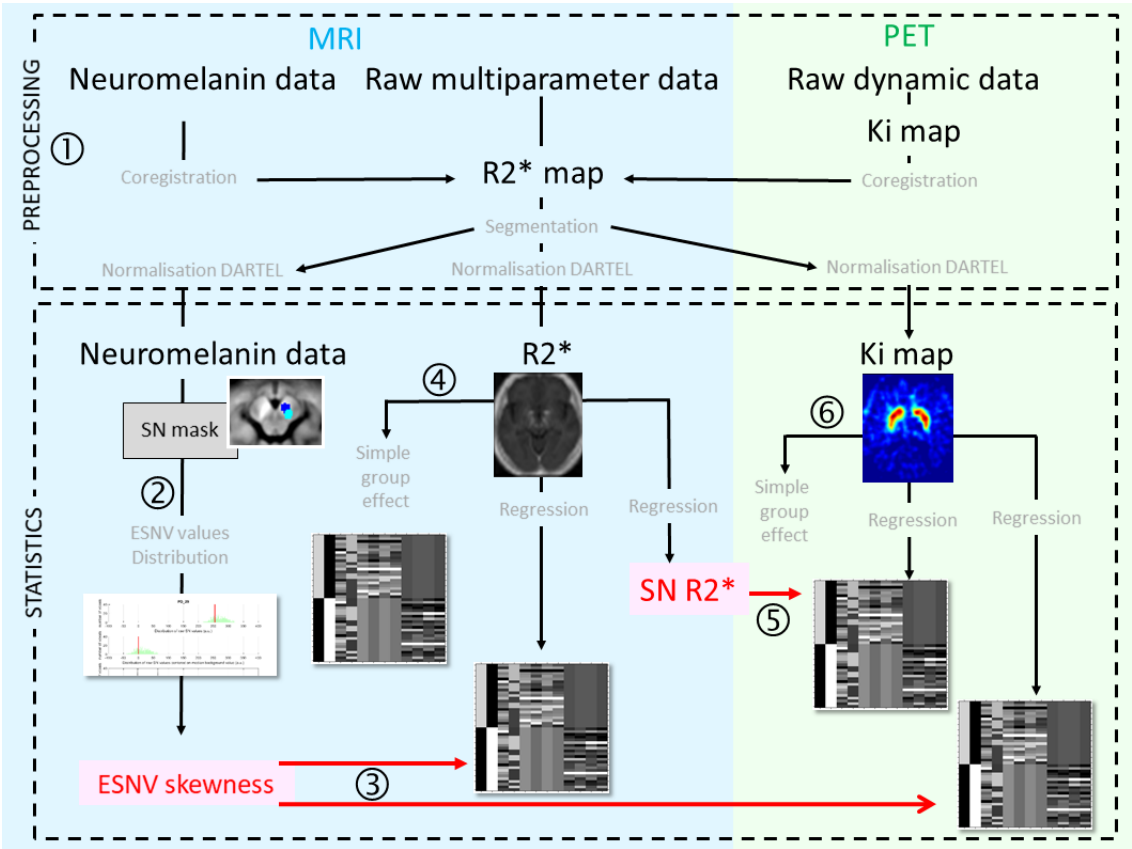

2.3.1 APPARENT TRANSVERSE RELAXATION TIME (R2*)

The whole-brain MRI acquisitions included a multiparameter mapping (MPM) protocol, that allows voxelwise R2* quantification (as well as MT saturation, R1 and PD estimation). developed in the framework of an international collaborative effort (Weiskopf *et al.*, 2013; Tabelow *et al.*, 2019). This protocol consists of three co-localised 3D multi-echo fast low angle shot (FLASH) acquisitions at 1 x 1 x 1 mm^3 resolution and two additional calibration sequences to correct for inhomogeneities in the RF transmit field (Lutti *et al.*, 2010, 2012). The FLASH data sets were acquired with predominantly proton density (PD), T1 and magnetisation transfer (MT) weighting, referred to in the following as PDw, T1w and MTw, acquired at different echo times **(see Figure 20)**. All three had high bandwidth to minimise off-resonance and chemical shift artefacts. Volumes were acquired in 176 sagittal slices using a 256 x 224 voxel matrix. GRAPPA parallel imaging was combined with partial Fourier acquisition to speed up acquisition time to approximately 20 minutes.

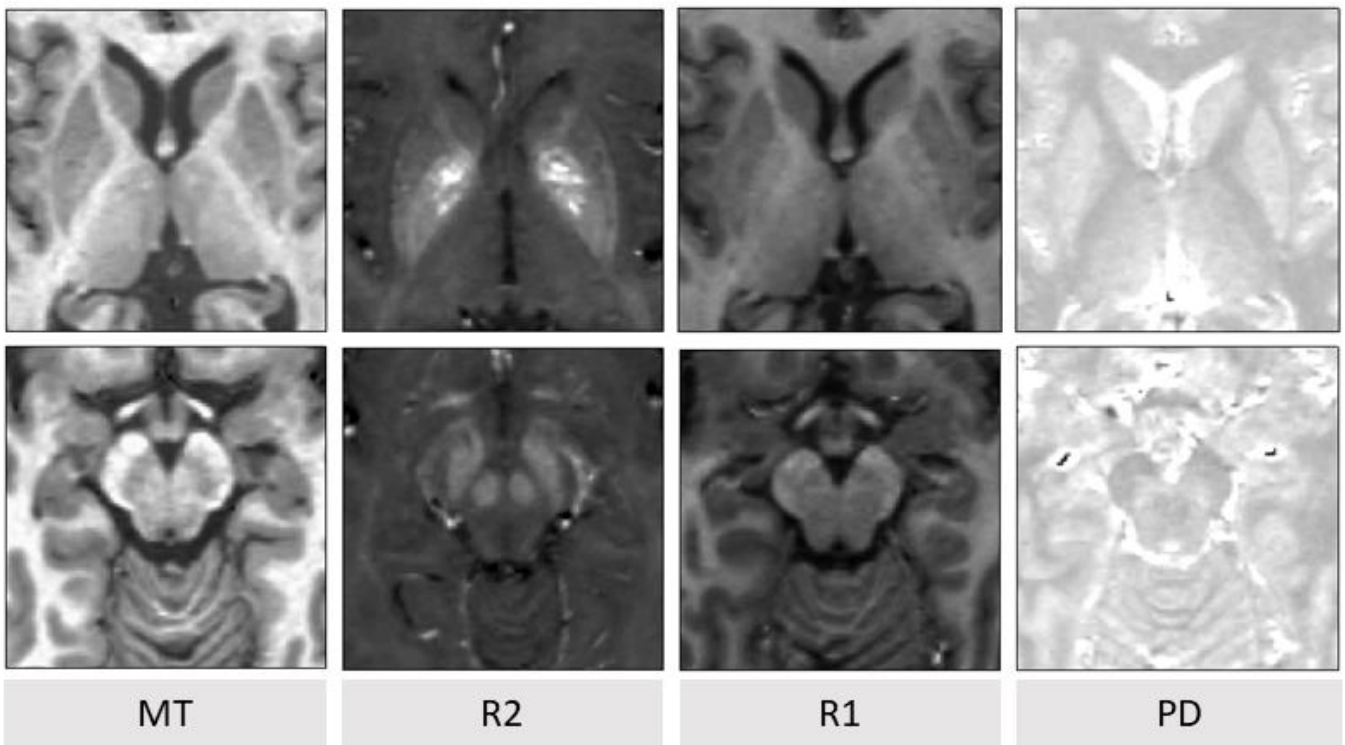

FIGURE 20 – **Example of data acquired with MPM protocol in a healthy subject.**
First row: example of MT, R2, R1 and PD maps, axial slice centred on basal ganglia. Second row: example of MT, R2, R1 and PD maps, axial slice centred on midbrain. MT: magnetisation transfer, PD: proton density. MPM: multiparameter mapping. These data have been acquired on a T3 MRI scanner, at the GIGA-CRC In Vivo Imaging, University of Liege, Belgium. Personal contribution.

2.3.2 NM-SENSITIVE MRI

Neuromelanin-sensitive (NM-MRI) images of the brainstem were recorded (**see Figure 15, Chapter 3, Section 2.2**), using high resolution 3D-FLASH sequence including an MT preparation pulse for NM-sensitization (Priovoulos *et al.*, 2018). The following acquisition parameters were used: FoV = 256 x 232 mm^2, 52 slices (+23% oversampling), matrix size = 256 x 232 x 52, 1 mm isotropic resolution, TR = 30 ms, TE = 2.61 ms, flip angle = 23°, GRAPPA acceleration factor 2, 6/8 partial Fourier in through-plane direction, 3 averages, bandwidth = 450 Hz/pixel, acquisition time = 9'10". The TR was made longer (30-35 ms) to fulfil SAR limitations when needed (normal SAR operating mode for all patients). A T1-weighted anatomical image [3D magnetization-prepared rapid gradient echo (MPRAGE) sequence] acquired in the same session was used to position the slices accurately.

2.3.3 PET ACQUISITIONS

All participants received 100 mg of oral Carbidopa (Lodosyn® 25 mg) one hour before tracer injection and 50 mg at injection time. Patients were asked to interrupt their treatment at least 12h before the experiment (withdrawal of L-dopa, rasagiline, entacapone, amantadine, dopamine agonist and 48h discontinuation for prolonged duration formulations).

PET imaging was conducted on an ECAT EXACT HR+ scanner (Siemens CTI, Knoxville, TN). Head movements were minimised using a thermoplastic mask moulded on the subject's head. After a 10-minute transmission scan for attenuation correction, participants received a single dose of [^{18}F]DOPA administered as a one-minute bolus in an antecubital vein (injected dose 313.78 ± 20.25SD MBq). The dynamic image acquisition started immediately after injection and consisted of 34 frames of 6 x 10, 8 x 30, 5 x 120, and 15 x 300

seconds (total = 90 min). All PET images were reconstructed using filtered back-projection (Hann filter, 4.9 mm FWHM) including corrections for attenuation, dead time, random and scatter events using standard software (ECAT 7.1, Siemens/CTI, Knoxville, TN). With these acquisition and reconstruction settings, the transaxial resolution in water is 6.5 mm in the brain volume (voxel size 2.57 x 2.57 x 2.43 mm3).

2.4 IMAGE PROCESSING

2.4.1 MASKS

We had strong predictions about where significant changes would be observed: the SN and the striatum. Based on the literature and neuropathological data (Fearnley and Lees, 1991), we further split SN into lateral and medial tiers on each side (**see Figure 21**, regions 1 and 2; with volumes of left medial, right medial, left lateral, right lateral SN of 164, 130, 137, 100 mm^3). Likewise, striatum was divided into pre-, post-commissural, left and right striatum (**see Figure 21**, regions 4 and 5 (Kish *et al.*, 1988; Kordower *et al.*, 2013); with volumes of left anterior putamen, right anterior putamen, left posterior putamen and right posterior putamen of 5356, 3787, 5322, 3203 mm^3). ATAG atlas of elderly population striatum and SN (freely available on https://www.nitrc.org/projects/atag) has been non linearly registered to DARTEL study space (Ashburner and Friston, 2005). Binary masks were derived from the probabilistic images, using an experimenter-defined threshold [corresponding to 4 a.u. (according to ATAG metrics)] that ensures optimal anatomical coverage of SN and striatum. To *generate regressors* for statistical analyses, SN masks were used to extract values of SN voxels. Data from NM- and iron-sensitive sequences were extracted separately on each side from medial and lateral SN, keeping in mind that NM signal loss is known to predominate in lateral SN (Ohtsuka *et al.*, 2013; Martin-Bastida *et al.*, 2017). By contrast, for statistical *inferences*, we used either bilateral

masks of medial and lateral SN (for the regression between R2* maps and NM signal) or pre- and post-commissural striatum (for regression with Ki maps).

Masks for bilateral *cruces cerebri* consisted of two 14-mm³ spheres positioned by the experimenter on the mean study structural image (**see Figure 21**, region 3). These masks were used to compute the background signal for SN values (see below). Finally, for voxelwise statistics, an explicit GM mask was used as previously proposed (Callaghan *et al.*, 2014): the smooth modulated warped individual GM and WM maps were averaged across all subjects and the GM mask only included voxels for which the mean GM probability was (1) larger than that of WM, and (2) above 20%. This ensures that the GM mask includes voxels (on average over the population) with a sufficient amount of GM and more than of WM.

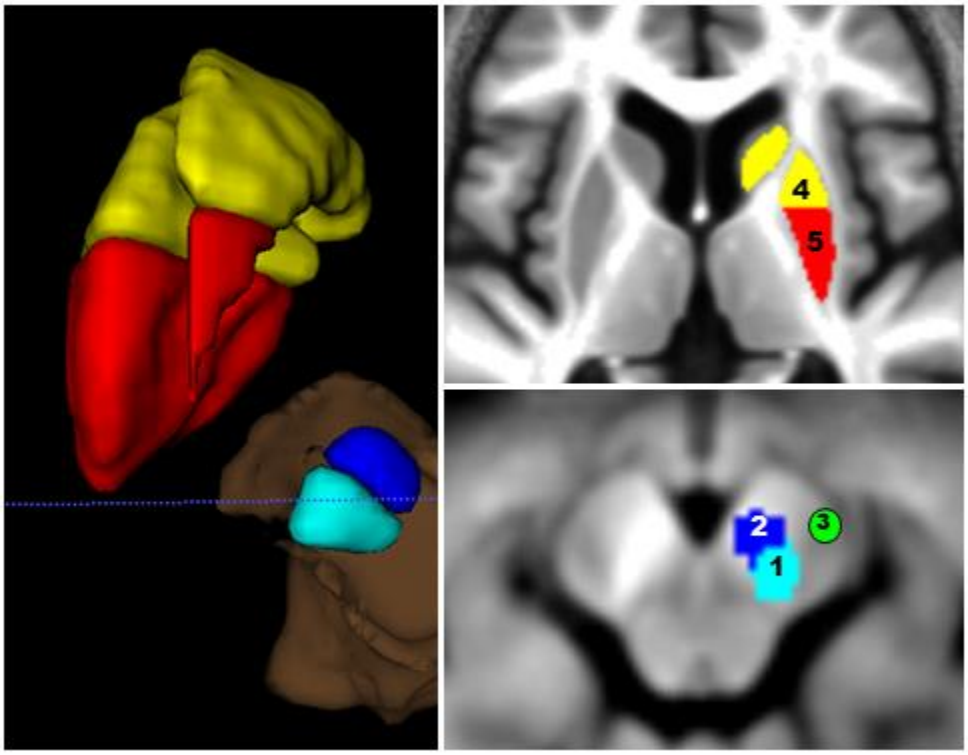

FIGURE 21 – **Definition of substantia nigra and striatum masks.**
Left panel – tridimensional view of left SN and striatum with their divisions. Right upper panel – Axial slice at the level of basal ganglia on the mean structural image of the whole population sample (PD+HC), showing striatum delineation. Precommissural striatum is depicted in yellow (4) and postcommissural striatum in red (5) This division is supported by anatomical and functional data (Kish et al., 1988; Haber, 2014). Right lower panel – Axial slices at the level of midbrain on a NM-MRI, showing substantia nigra delineation, with division in lateral tiers (1, light blue) and medial tiers (2, dark blue), according to neuropathological data (Fearnley and Lees, 1991). Cerebral peduncle is also delineated (3, green).

2.4.2 MRI PROCESSING

R2* maps were processed using Matlab R2015b (The MathWorks Inc., Natick, MA, USA) , SPM12 (Wellcome Centre for Human Neuroimaging, London, UK; www.fil.ion.ucl.ac.uk/spm) and a dedicated SPM toolbox for quantitative MRI [*hMRI toolbox,* http://hmri.info, (Tabelow *et al.*, 2019)]. R2* quantitative maps of PD patients and controls were segmented using the 'unified segmentation' scheme (Ashburner and Friston, 2005). GM (grey matter) and WM (white matter) probability maps from all subjects were then warped together into a study-specific reference space, based on diffeomorphic transformations (DARTEL) , and aligned with the MNI space, providing a subject-specific deformation field (Ashburner, 2007). For voxel-based analyses, R2* maps were normalised using the subject-specific deformation field without modulation. A tissue-weighted smoothing (4 mm FWHM isotropic) yielded a smoothed tissue-specific multiparameter map which optimally preserved quantitative parameter values within each tissue class (Draganski *et al.*, 2011). Parametric maps of seven PD patients were flipped according to the clinically most impaired side (the latter was identified following clinical examination by two experienced movement disorder specialists, taking into account the highest UDPRS score of each side), in order to gather the most affected sides of all patients on the left side of the images. However, it must be kept in mind that many of our patients had already bilateral symptoms and signs.

For NM-sensitive MRI, voxel values included in the SN and crus masks were extracted for each participant. NM content was parametrised simply as the difference between any given SN voxel and background values estimated as the median signal in *crus cerebri* and will be referred to as 'effective SN values' [ESNV = $S_{i,SN}$−mean (S_{crus}) , with $S_{i,SN}$, the value of the i^{th} voxel; median (S_{crus}) , the median value of crus]. The difference between SN and crus values, a linear operator, was preferred to their ratio, a nonlinear operator which can yield spurious results in case of small background levels. Because individual

ESNV distributions were not normal (Kolmogorov-Smirnov; p =0.0157), we derived their skewness, which ultimately served as the dependent variable because it was shown sensitive to SN depigmentation (see results). As opposed to previous studies focusing on NM–sensitive MRI, the mean or median of the values of the SN voxels could not be used as the distribution was not normal. By contrast, skewness captures in a single parameter the shape of ESNV distribution, which was suspected to be modified by pathological PD processes.

2.4.3 PET PROCESSING

PET data were preprocessed using SPM12. For each participant, an average PET image was created using the data acquired between 8 and 20 minutes corresponding to frames 15 to 19. The count statistics in this average image makes it a better source image for co-registration of PET data to structural MRI. The average PET image was co-registered to the individual structural MRI and normalised in the common standard space using the flow-field deformation parameters obtained during the spatial normalization of structural MRI. Two regions of interest (putamen and occipital cortex), with and without specific uptake respectively, were identified using the Automated Anatomical Labelling (AAL) atlas (Tzourio-Mazoyer *et al.*, 2002). These two regions were transferred to the space of individual dynamic PET series, after applying the inverse normalization transformations, then used to extract time activity curves needed to compute parametric maps of [^{18}F]DOPA influx rate constant (Ki). In order to avoid any additional partial volume effect which might be introduced during the preprocessing of the data, we preferred to send the AAL ROIs back into the subject space, extract the time series directly from the raw data, and then create the Ki maps in the subject space. Kinetic modeling using dynamic PET data and time activity curves for reference region (occipital cortex and putamen) was conducted in PMOD software (Version 3.7, PMOD Technologies, Zurich, Switzerland). Patlak linear graphical analysis was used to compute

brain parametric images of Ki map (Patlak and Blasberg, 1985). The time-activity curve in putamen was used to determine the start time of the linear segment (t*) of the graph (estimated to 30 min) and used to compute voxel-wise Ki. The Ki map, generated in the subject space, was then normalised into the MNI space by applying individual normalization parameters computed on the average PET image. Finally, images were smoothed with an isotropic Gaussian kernel of 4 mm **(see Figure 9 and 10 in Chapter 3, Section 1.2).**

2.5 STATISTICAL ANALYSES

2.5.1 STATISTICS ON FDOPA Ki MAPS

Voxelwise one-tailed 'two-sample *t*-test' assessed the group effect by comparing Ki between healthy subjects and PD patients.

A multiple regression tested for the interaction between the group effect and SN R2*. Median R2* was derived from lateral, medial, left and right SN, centred and included as group specific regressors in an analysis, which also included age and sex as regressors of no interest. Inferences were conducted as above. Contrasts tested the regression of bilateral, lateral and medial, ESNV on Ki maps **(see Table 5)**.

TABLE 5 – Definition of regressor used in the analysis.

ESNV (resp. R2*) were extracted from different SN or putamen sub-regions and used as regressors in multiple regression analyses. Contrasts always involved both sides of each subregion and masks used for inference were also bilateral.

MAP	REGRESSOR
Left medial SN R2*	Bilateral lateral ESNV
Left anterior putamen Ki	Bilateral lateral ESNV
Bilateral posterior putamen Ki	Bilateral lateral R2*

A last multiple regression tested for the interaction between the group effect and ESNV skewness, as described above for R2* analyses. Contrasts tested the regression of bilateral, lateral and medial, R2* on Ki maps **(see Table 5)**. Inferences were conducted as above.

2.5.2 STATISTICS ON R2*

Whole-brain voxel-based quantification (VBQ) analyses relied on multiple linear regression models embedded in the general linear model framework of SPM12.

Statistics on R2* differences between PD patients and HC in GM were estimated by separate 'two-sample one-tailed *t* tests'. Age and sex were included as regressors of no interest.

Within the patient population, multiple regressions looked for significant voxel-wise regression between R2* in GM and clinical scores (UPDRS III in OFF-state, Hoehn and Yahr scale, LEDD, disease duration).

Finally, a multiple regression tested voxelwise for the interaction between group effect and ESNV skewness on R2*. As described above, individual ESNV skewnesses were derived from lateral and medial, left and right SN **(see Section 'Masks')**, centred and included as group specific regressors in the analysis, which also included age and sex as regressors of no interest. Contrasts tested the regression of bilateral, lateral and medial, ESNV on R2*maps **(see Table 5)**. In all cases, inferences were conducted at the voxel level at $p < 0.05$ FWE, after small volume correction using the bilateral masks described above. We controlled for the potential type I error over the 2 masks used for inferences, respectively for SN (medial and lateral) or striatum (pre and post-commissural).

2.5.3 STATISTICS ON NM-SENSITIVE MRI DATA

After checking for the normality of ESNV skewness distribution, a generalised linear mixed model (GLMM) tested the effects of group (PD versus HC), SN ROIs (4 sub-ROIs), and their interaction on ESNV skewness, using patient intercept as a random variable and SAS software, version 9.4 (SAS Institute Inc., 2013). The regression between ESNV skewness and UPDRS III, disease duration, Hoehn and Yahr score or LEDD was also tested.

2.5.4 OTHER STATISTICS

Statistical analyses on demographic data were computed using SAS software, version 9.4 (SAS Institute Inc., 2013).

3 RESULTS

3.1 DEMOGRAPHY

Demographic data appear in **Table 6**. There were no significant differences between HC and PD patients, in terms of age (two-sample *t* test; *t* (44) = -0.12, p = 0.90) and gender (p= 1).

	PD PATIENTS	HC	STATISTIC
Total number (n)	23	23	
Gender (male:female)	13:10	11:12	Chi-Square: df = 1; value = 0.3485; p = 0.5550
Age (years)	67.3 ± 9.9	67.7 ± 9.7	Two-sample t test; t (44) = 0.12, p = 0.90
Most affected side (right:left)	16:7	NA	
Disease Duration (years)	5.6 ± 3.8 [1-15]	NA	
Hoehn and Yahr score	1.9 ± 0.6 [1-3]	NA	
UPDRS III (motor)	28.2 ± 11.8 [10-54]	NA	
LEDD (mg)	448.2 ± 286.8 [0-937]	NA	

TABLE 6 – **Demographic data.** Values represent the mean ± standard deviation [range] for disease duration, UPDRS III [Unified Parkinson's Disease Rating Score (Goetz *et al.*, 2008)], Hoehn and Yahr score and LEDD [Levodopa equivalent daily dose (Tomlinson *et al.*, 2010)].

3.2 NM-SENSITIVE DATA

ESNV skewness was normally distributed across participants (Kolmogorov-Smirnoff, p = 0.124). We observed a significant effect of group (F(1) = 7.10; p = 0.011) and SN ROIs (F(3) = 9.76; p < 0.001). ESNV skewness was more negative in PD than in HC (least square estimates: -0.138 in PD, -0.02 in HC; t(44)= 2.66, p = 0.011, Tukey adjustment for multiple comparison; **see Figure 22**). By contrast, there was not any significant group by ROI interaction (F(3) = 1.95 p = 0.125).

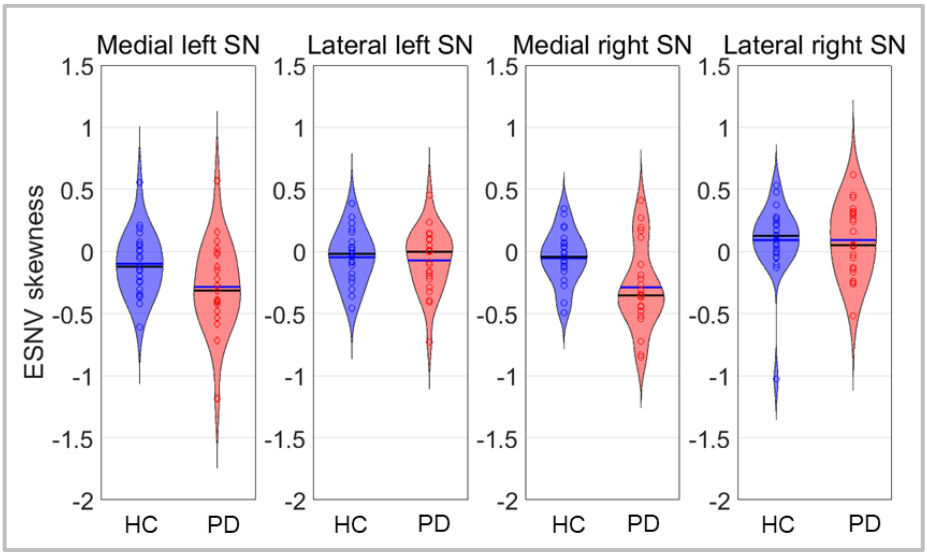

FIGURE 22 – **Effective substantia nigra values (ESNV) skewness violin plot.** ESNV skewness distribution in HC and PD patients in the 4 SN subregions (PD patients are depicted in red, and HC in blue).

We considered that the decrease in ESNV skewness quantitates SN depigmentation. These results confirm the depopulation of NM-containing neurons in PD, as PD individuals have more voxels with low NM signal than voxels with high NM signal **(see Figure 23)**. They also suggest that the depigmentation evenly involves all SN subdivisions. Finally, no correlation was found between ESNV skewness and UPDRS III, disease duration, Hoehn and Yahr score or LEDD.

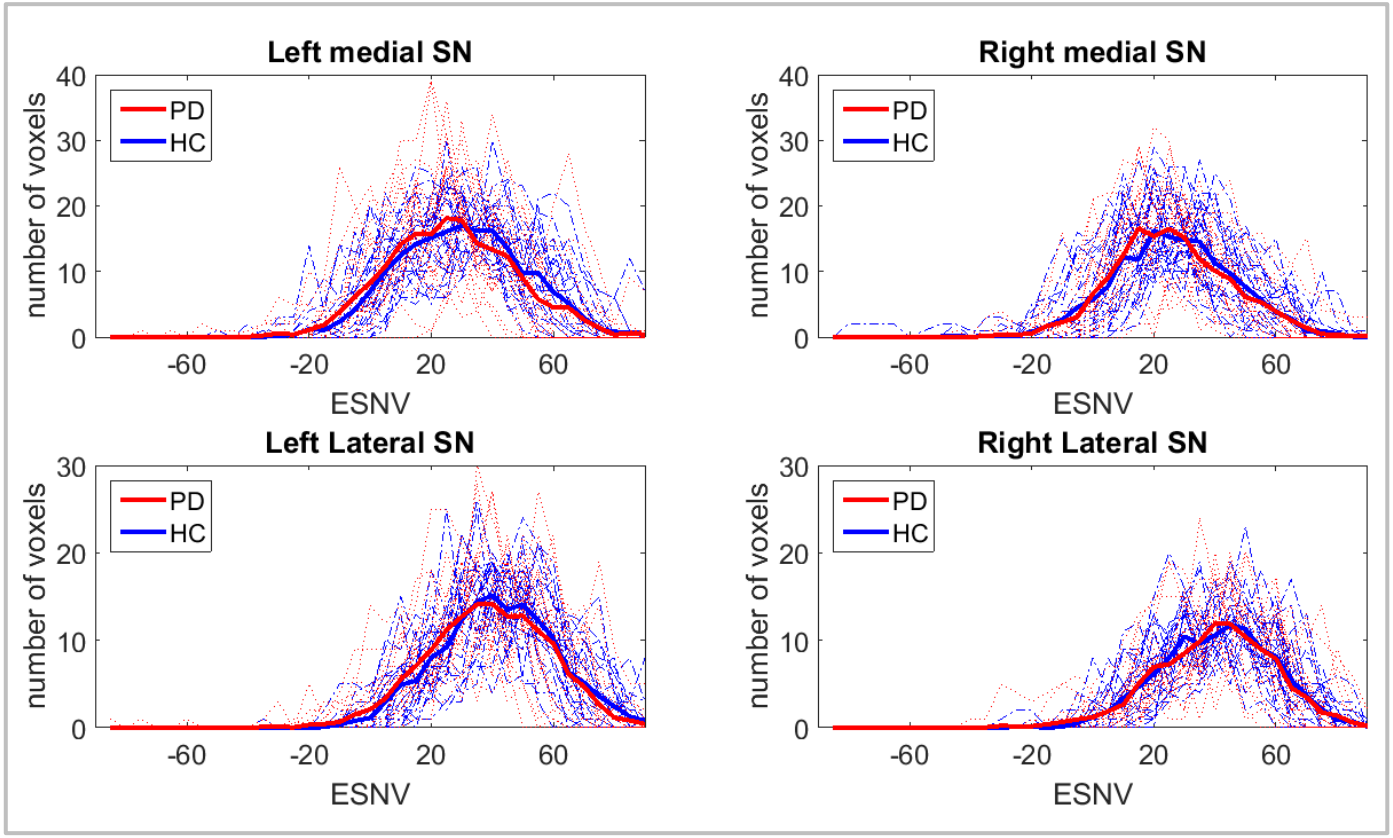

FIGURE 23 – **ESNV distribution.** Diagrams show ESNV distribution across PD and HC populations, in all four subregions of SN (PD patients are depicted in red, and HC in blue). ESNV in PD are characterised by a larger tail of small ESNV (i.e., a more negative skewness than in HC, particularly visible on the left side).

3.3 R2* CHANGES IN PD AND THEIR RELATIONSHIPS WITH NM-SENSITIVE MRI

We first confirmed that R2* values were related to regional brain iron content extracted from non-PD *post-mortem* material published in the landmark study by Hallgren and Sourander (Hallgren and Sourander, 1958), a quality control suggested by Martin and colleagues (Martin *et al.*, 2008) **(see Figure 24)**.

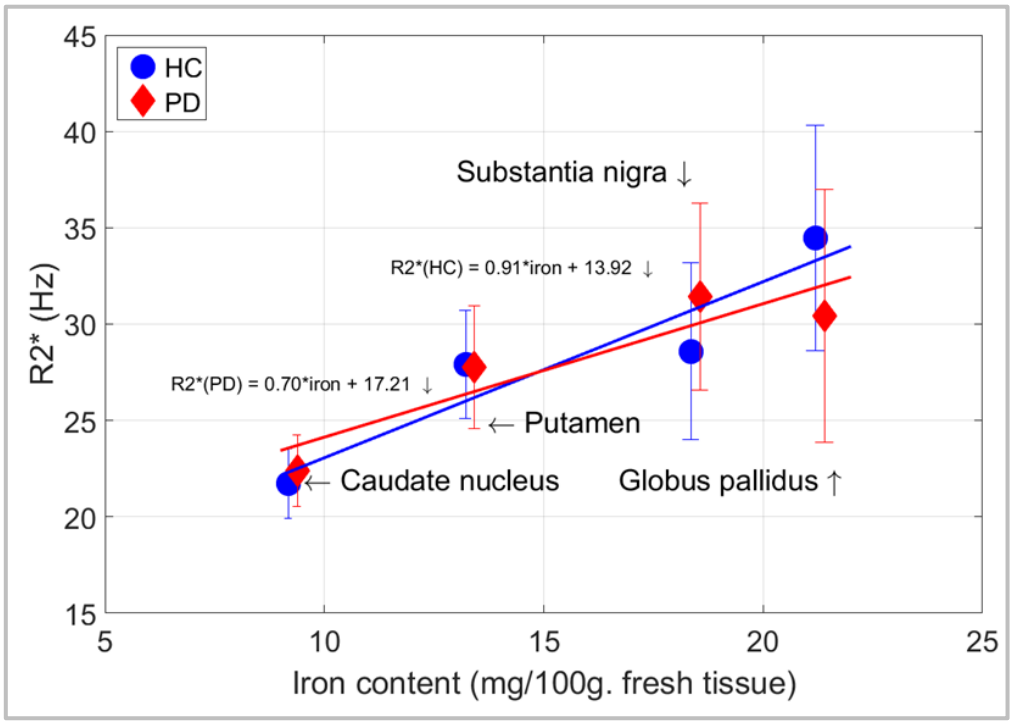

FIGURE 24 – **Correlation between published regional brain iron content and regional R2* values of the present study.**

We then looked for the voxelwise main effect of disease on brain R2*. Two-sample *t* tests revealed that R2* in the left SN lateral tier was significantly higher in PD patients than in controls ([-10 -21 -11] mm; Z =3.12; p_{SVC}= 0.041; the result does not survive correction for multiple comparisons across 2 ROIs – medial and lateral SN) suggesting a higher iron content in that area. The lateralization of R2* increase is consistent with the clinically most affected side, as data were all positioned according to the latter **(see Figure 25, a–c)**.

By contrast, we did not find any significant variation of R2* according to clinical parameters (UPDRS III, H&Y scale, disease duration or LEDD).

We then wondered whether brain R2* would covary with lateral SN ESNV skewness, looking for a relationship between iron accumulation and SN pigmented neurons loss. In a dorsal part of left medial SN, we observed a significant difference between PD patients and HC in the regression between R2* and SN ESNV skewness (group by ESNV skewness interaction; [-12 -15 -9 mm]; Z = 3.50; $p_{SVC\ (medSN)}$ =0.011). However, as shown on **Figure 5, d–f**, ESNV skewness in lateral SN unexpectedly *increases* significantly as R2* *increases* in left medial SN in PD patients, a behaviour which is not observed in HC. This result suggests that lateral SN ESNV skewness becomes more *positive*, as iron accumulation progresses in the medial SN or, alternatively that lateral ESNV skewness decrease (i.e., depigmentation) is associated with decreased iron content in medial SN.

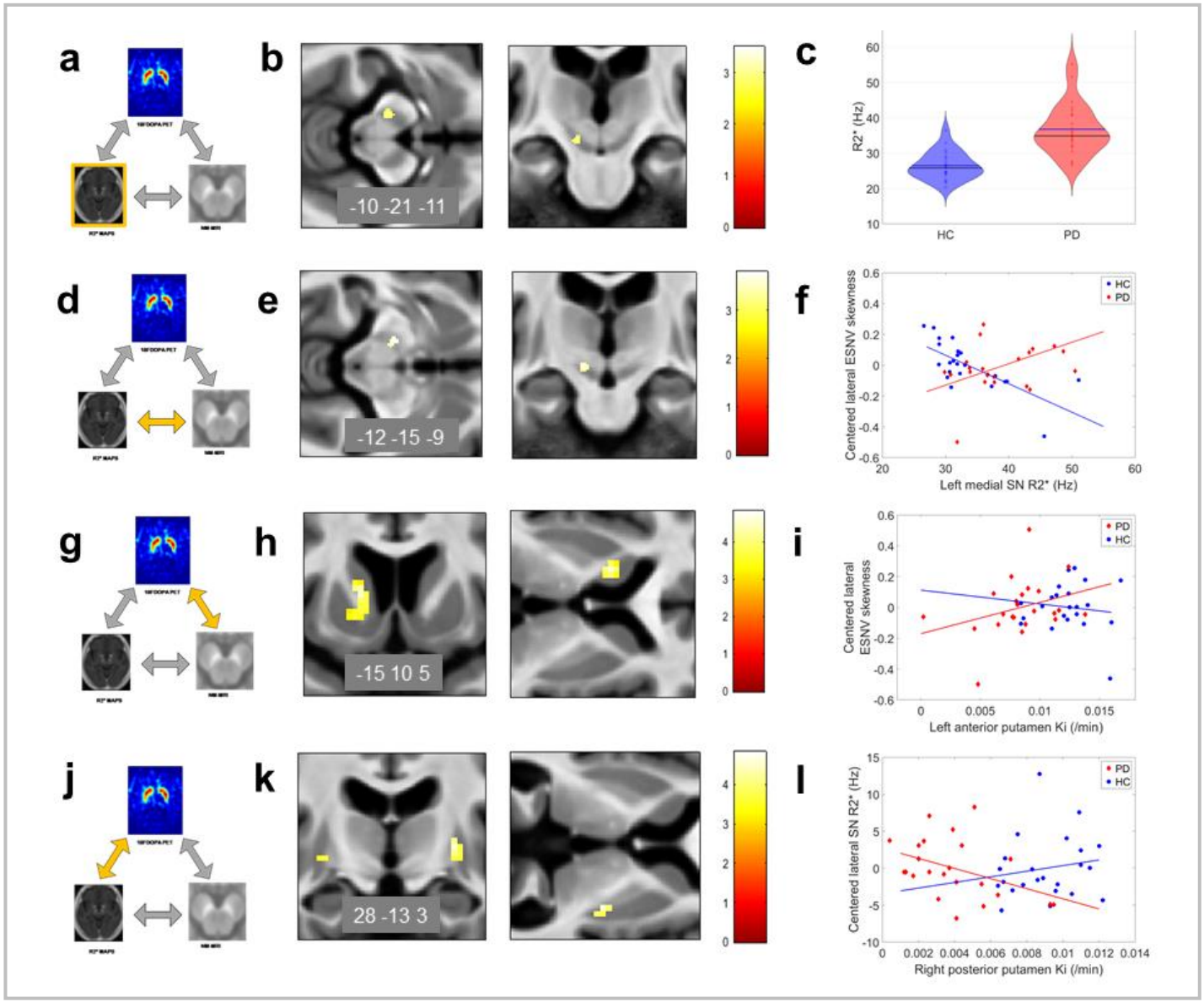
a
b
-10 -21 -11
c
R2* (Hz)
HC
PD
d
e
-12 -15 -9
f
Centered lateral ESNV skewness
Left medial SN R2* (Hz)
HC
PD
g
h
-15 10 5
i
Centered lateral ESNV skewness
Left anterior putamen Ki (/min)
PD
HC
j
k
28 -13 3
l
Centered lateral SN R2* (Hz)
Right posterior putamen Ki (/min)
PD
HC

FIGURE 25 – **Relationships between NM-sensitive MRI, R2* and [^{18}F]DOPA-PET changes in Parkinson's disease.**

Figure 25. a–c: R2* changes in Parkinson's disease. Main effect of disease on brain iron, as assessed by R2*, displayed at $p<0.001$ uncorrected over the mean structural image of the whole population. Colour scales are proportional to t-values.

Figure 25. d–f: Relationship between R2* and NM-sensitive MRI data. Diagram f shows that peak voxel ESNV skewness in both SN increases as R2* increases in left SN, significantly more in PD patients than HC.

Figure 25. g–i: Relationship between dopaminergic neurotransmission ([^{18}F]DOPA-PET) and NM-sensitive MRI data. Regression between peak voxel in left anterior putamen Ki and bilateral SN ESNV skewness.

Figure 25. j–l: Relationship between dopaminergic neurotransmission ([^{18}F]DOPA-PET) and R2*. Peak voxel Ki values in posterior putamen regressed differentially in PD and HC with lateral SN R2*.

All results are displayed at $p<0.001$ uncorrected over the mean structural image of the whole population. Colour scales are proportional to t-values.

3.4 [^{18}F]DOPA-PET AND ITS RELATIONSHIPS WITH SN R2* AND NM DATA

We first checked the effect of disease on the function of nigro-striate neurons, as assessed by *in vivo* measure of dopamine synthesis (Ki). As expected, putamen Ki values were significantly lower in PD patients than in healthy controls on both sides ([-25 3 5] mm, Z = 6.46, p_{FWE}< 0.001; [30 0 3], Z= 5.54; p_{FWE}<0.001) **(see Figure 26)**, thus representing the loss of dopaminergic terminals.

We further assessed whether there was any relationship between dopaminergic function and NM-sensitive MRI data. We found a significant between-group difference in the regression between Ki and bilateral SN ESNV skewness in the left anterior putamen (group by ESNV skewness interaction; [-15 10 5] mm, Z = 4.57, p_{SVC}=0.002; **see Figure 25, g–i**). In PD, left anterior putamen, oddly enough not the most denervated part of the striatum (Kish *et al.*, 1988), Ki significantly decreased as individual lateral SN ESNV skewness decreased, whereas no significant regression was found in HC. This result suggests that, in PD, dopamine synthesis is increasingly impaired as SN depigmentation, labelled by a more negative skewness of ESNV distribution, progresses **(see Figure 23)**.

Eventually, we wondered whether dopaminergic function varies in proportion to SN iron accumulation, as indicated by R2* measures. [^{18}F]DOPA Ki values of bilateral posterior putamina regressed more tightly in PD than HC with SN R2* of lateral SN, significantly only in the right side ([28 -13 3] mm, Z = 4.14, p_{SVC}= 0.005), indicating that putamen denervation progresses as iron accumulation (R2*) increases in lateral SN **(see Figure 25, j–l)**. This regression was significant in PD ([28 -13 3] mm, Z = 3.76, p_{FWE} = 0.024) but not in HC. In addition, these differences differed between posterior and anterior putamen, although the triple interaction (group x R2* x ROI) did not survive correction for multiple comparisons.

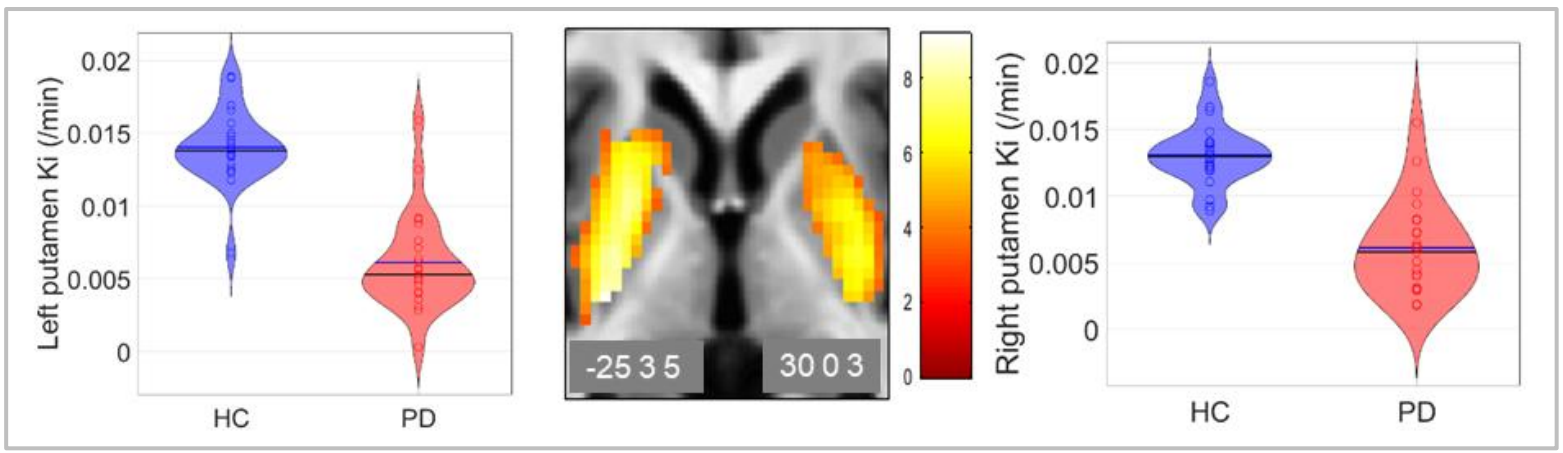

FIGURE 26 – Changes in dopaminergic neurotransmission.
Effect of disease on dopaminergic function measured by [^{18}F]DOPA PET.
Results are displayed at $p<0.001$ uncorrected over the mean structural image of the whole population. Colour scales are proportional to t-values.
As seen on the violin plots representing PD patients, putaminal Ki values substantially vary across patients, an interindividual variability which is, in part, due to the disease duration as we have included early stage (and even *de novo*) patients. The clinical most impaired side must also be considered, as Ki values of the opposite side should be substantially different, at least at the beginning of the disease.

4 DISCUSSION

In this study, three separate imaging biomarkers were, for the first time, jointly used to characterise basal ganglia structure and function in PD patients, as compared to HC: R2* iron-sensitive and NM-sensitive MRI, and [^{18}F]DOPA PET. The key results are fivefold: As compared to HC, (1) Dopamine accumulation in presynaptic terminals is decreased in PD striatum; (2) NM depigmentation does not progress differently across SN subdivisions and it results in an augmented amount of low NM signal voxels, i.e. a more negatively skewed distribution; (3) By contrast, iron selectively tends to accumulate in the lateral SN of PD patients, as shown by the hint of a larger R2* in left lateral SN in PD than HC; (4) Dopaminergic function decreases in anterior putamen as the distribution of NM-sensitive signal is negatively skewed by PD, indicating that the impairment of dopaminergic neurons progresses with lateral SN depigmentation and (5) Dopaminergic function negatively relates to lateral SN R2* in PD, suggesting that dopaminergic function deteriorates as iron accumulates in lateral SN. Unexpectedly, R2* in *medial* SN differs significantly between PD and HC as lateral SN ESNV skewness *increases*. This suggests that although both signals in the lateral SN covary with dopaminergic function, their mutual interactions are not straightforward. Indeed, this finding suggests that iron accumulates in the medial SN as high NM signal voxels are over-represented therein.

4.1 NM-SENSITIVE MRI DATA

In a neuropathological study of three brains (one PD) , the signal of NM-sensitive MRI was found to correspond to the density of residual NM-containing neurons (Kitao *et al.*, 2013). Importantly, the signal was not influenced by iron deposition. Likewise, iron complexed in NM does not profoundly modify NM-sensitive MRI signal (Trujillo *et al.*, 2017). Several studies showed a reduction of NM-MRI contrast in

the SN of PD patients [(Lehéricy *et al.*, 2012; Martin-Bastida *et al.*, 2017; Biondetti *et al.*, 2020) but see (Langley *et al.*, 2019) for negative results], over and above an age-dependent SN depigmentation(Xing *et al.*, 2018). However, current NM-sensitive MRI is, at best, semi-quantitative. Neuromelanin SN signal, extracted manually or semi-automatically, has to be corrected for background signal. The latter is taken from either crus cerebri (Chen *et al.*, 2014; Langley *et al.*, 2015; Isaias *et al.*, 2016; Cassidy *et al.*, 2019), pontine tegmentum (Schwarz *et al.*, 2011) or superior cerebellar peduncles (Martín-Bastida *et al.*, 2019). The ensuing dependent variable is either a contrast-to-noise ratio (Ohtsuka *et al.*, 2013; Isaias *et al.*, 2016), or the number of voxels above an experimenter-defined threshold value (Schwarz *et al.*, 2011, 2017; Langley *et al.*, 2015). Here, we resorted to a data-based, reproducible, and fully automatic extraction of SN values from SN voxels identified on an independent probabilistic atlas of basal ganglia. Voxel values in SN were generated simply as the difference between SN and background signal. Individual ESNV were not distributed normally, we thus derived their third moment which allowed us to depict their distribution by a single quantitative value. ESNV skewness differed between groups, with PD distribution being more negatively skewed than in HC. However, the effect of PD did not predominate in any SN subregion. These results suggest that depigmentation increases the abundance of voxels with low NM density, explaining a decrease in ESNV skewness.

4.2 IRON-SENSITIVE MRI DATA

Neuropathological studies observed an increase in iron within the SN of PD [(Lhermitte *et al.*, 1924, Sofic *et al.*, 1988*a*; Hirsch *et al.*, 1991)but see(Uitti *et al.*, 1989) for negative findings]. Human local brain iron content can be assessed *in vivo* by qualitative (susceptibility-weighted imaging, SWI) (Rossi *et al.*, 2010; Langley *et al.*, 2015) or quantitative MRI techniques [R2*, R2 (Langkammer *et al.*, 2010),

susceptibility mapping (Langkammer *et al.*, 2012)]. Accordingly, a number of studies (Martin *et al.*, 2008; Baudrexel *et al.*, 2010; Pyatigorskaya *et al.*, 2015; Reimão *et al.*, 2016; Langley *et al.*, 2017) and two meta-analysis (Wang *et al.*, 2016; Pyatigorskaya *et al.*, 2020) report an increase in iron in the SN of PD patients, although negative findings were also reported (Isaias *et al.*, 2016). Our results concord with the former results and detect an increase of R2* in PD left lateral SN.

R2* signal is primarily modulated by local iron content, although myelin and calcium content, fibre orientation relative to the magnetic field, and macroscopic geometry also participate in T2* signal decay (Bagnato *et al.*, 2018). Nevertheless, we confirmed that R2* predicts regional brain iron content, as measured by biochemical methods on non-PD human brain samples (Hallgren and Sourander, 1958) **(see Figure 24)**. The effect size (R^2= 0.82) indicates that iron explains a major part of R2* signal in basal ganglia. Most of brain iron is bound to ferritin (Galazka-Friedman *et al.*, 1996), which is more abundant in glial cells than in neurons (Hare and Double, 2016). Within SN dopaminergic neurons, iron is primarily stored within NM, which boasts antioxidant and radical scavenging properties contributing to buffer cellular oxidative stress by binding free iron (Zecca *et al.*, 2004*b*; Ward *et al.*, 2014). Dopaminergic neurons would selectively degenerate (Hirsch *et al.*, 1988) when NM antioxidant properties are exceeded (Zucca *et al.*, 2014). At neuronal death, NM is released in the extracellular space where it stimulates inflammation. As a consequence, in PD SN, iron is observed mainly in reactive microglia rather than in dopaminergic NM-positive neurons (Jellinger *et al.*, 1990; Morrish *et al.*, 1996).

The topography of iron deposition in SN is still a matter of debate: some authors found R2* increase in lateral (Pyatigorskaya *et al.*, 2020), or posterior SN (Azuma *et al.*, 2016), while others report an augmented R2* in medial (Baudrexel *et al.*, 2010) or anterior SN (Arribarat *et al.*, 2019). We here observed the increase in R2* in the

lateral SN of PD patients and postulate that it mainly reflects the accumulation of iron in microglia, as a result of the neuro-inflammation accompanying the neuronal loss.

4.3 RELATIONS BETWEEN [^{18}F]DOPA PET, IRON- AND NM-SENSITIVE MRI DATA

[^{18}F]DOPA uptake rate constants correlate with dopamine cells counts (Snow *et al.*, 1993). However, [^{18}F]DOPA PET being a functional biomarker, it possibly underestimates the loss in dopaminergic neuron because of a compensatory upregulation of amino-acid decarboxylase activity in remaining cells (Stoessl *et al.*, 2014; Isaias *et al.*, 2016; Kaasinen and Vahlberg, 2017). Nonetheless, we found that [^{18}F]DOPA PET signal is related to microstructural information conveyed by iron- and NM-sensitive MRI data.

An original finding consisted of the relationship between putamen Ki and NM-sensitive data in SN. It illustrates the deterioration of dopaminergic function as depigmentation progresses in the SN of PD patients. This result is supported by similar studies, which resorted to dopamine transporter (DAT) imaging to validate NM-sensitive MRI (Isaias et al., 2016; Kuya et al., 2016; Martín-Bastida et al., 2019; Okuzumi et al., 2019). In consequence, NM-sensitive MRI is often presented as a useful tool to assess Parkinson's disease pathology as it can predict dopaminergic dysfunction. Unexpectedly, the alteration of dopaminergic function related to SN depigmentation predominates in the anterior putamen, where dopamine levels decrease less than in the posterior putamen (Kish et al., 1988). This finding suggests that depigmentation is an early event, which results in a proportional decrease in dopamine secretion. By contrast, this relationship is lost with more advanced deterioration of nigro-striate function.

We found that in PD, SN R2* increases as Ki decreases in posterior putamen. This result suggests that iron accumulation in lateral SN is a late process which follows and concurs to (Hirsch and Hunot, 2009) the deterioration of dopaminergic function in posterior putamen, the area where dopamine depletion predominates.

[^{18}F]DOPA PET and DAT SPECT reflect two different aspects of dopaminergic neurotransmission. The former is directly representative of dopamine synthesis which is the core molecular defect of PD (Kaasinen and Vahlberg, 2017). [^{18}F]DOPA PET still represents a robust validated (Snow et al., 1993) biomarker for its ability to detect and monitor dopamine deficiency, disease progression (Morrish et al., 1996), and for its correlation with clinical rating (Morrish et al., 1995, 1998; Eshuis et al., 2006). By contrast, DAT imaging probes the re-uptake sites of dopaminergic synapses. It does not predict the number of nigral neurons in Parkinson disease (Saari et al., 2017) but would be less prone to underestimate dopaminergic dysfunction, as compared to [^{18}F]DOPA PET (Kaasinen and Vahlberg, 2017).

4.4 RELATIONS BETWEEN IRON- AND NM-SENSITIVE MRI DATA

We found that medial SN R2* is proportional to lateral SN ESNV skewness, significantly more in PD than in HC. A first explanation would posit that iron accumulation in medial SN decreases as low NM signal voxels accumulate in PD, suggesting that neuroinflammation decreases in medial SN as depigmentation progresses in lateral SN. This interpretation is counterintuitive but might emphasise a regionally-specific time course of iron accumulation within SN in PD. Alternatively, this result would arise fortuitously from our limited sample of PD patients. Indeed, relationships between R2* and NM signal are known to be weak (Reimão *et al.*, 2016).

4.5 STRENGTHS AND LIMITATIONS

This study boasts some methodological strengths. First, most studies exploring the brain correlates of PD used manually drawn regions of interest (Morrish et al., 1996; Aquino et al., 2014; Reimão et al., 2015). Such methods are prone to observer bias and cannot be easily compared between laboratories. By contrast, we extracted regions of interest from an independent atlas, freely available to the community. Second, in order to observe the effect of disease processes properly, we strictly matched for age PD patients with HC, on an individual basis. Indeed, brain iron levels increase as a function of age in deep grey matter structure (Hallgren and Sourander, 1958; Killilea et al., 2004; Ward et al., 2014) and age-dependent changes were to be accounted for.

The study also presents some limitations, the first one being the small number of participants. Considering the duration of MRI and PET acquisitions, we could not include patients with advanced PD (Hoehn and Yahr scale >3) given the discomfort of the experiment. In consequence, the results only show effects predominant in stages H&Y 1 to 3, or effects stable over for a long period of time. We did not recruit patients with atypical parkinsonism, which did not allow us to study the specificity of the results for the identification of PD and its differentiation from other akinetic-rigid syndromes. Another limitation comes from the methodological sophistication of a group analysis which is not available in most hospitals, thereby of little help for individual PD diagnosis in clinical practice.

We did not find any correlation between imaging data and clinical scores, in concordance with previous reports (Castellanos et al., 2015; Martín-Bastida et al., 2019). Most of the time, results are mixed. In Schwarz et al. 2017 study for example, there was no significant correlation between disease duration or H&Y and neuromelanin signal intensity, whereas a correlation with UPDRS was found (Schwarz et al., 2017).

We have explored the role of these neuro-imaging techniques as diagnostic biomarkers. Such biomarkers ideally quantify the presence of the disease, and can be used to provide new insights into pathogenic pathways (Antoniades and Barker, 2009). [^{18}F]DOPA PET does not measure the number of dopaminergic neurons, but rather measure a biologic process. NM-MRI offers the opportunity to measure the amount of surviving pigmented neurons. Iron-sensitive MRI shows another aspect of the neuropathological process through iron deposits measurements. The specificity of these two neuroimaging biomarkers regarding PD diagnosis remains to be investigated as our population did not include patients suffering from atypical parkinsonism. While it was proven there is a progressive regional decline in striatal [^{18}F]DOPA uptake with PD evolution (Whone et al., 2003; Brück et al., 2006), we cannot make any statement about the use of NM-MRI and iron-sensitive MRI as biomarkers of disease progression as we did not study the alteration of the signal over time.

Finally, this cross-sectional study cannot characterise the evolution of these MRI biomarkers along time, nor specify the differential course of iron, NM and [^{18}F]DOPA signals, as they might label different pathological processes.

5 CONCLUSION

Our results show that (1) Iron selectively increases in lateral SN; (2) Iron in lateral SN increases as dopaminergic function fails in posterior putamen; (3) Depigmentation of SN does not show any regional specificity within SN and correlates with dopaminergic failure in anterior putamen; (4) Despite their respective association with dopaminergic function, iron and NM signals show regionally complex interactions. These metrics convey information about separate processes, respectively inflammation and loss of NM-containing neurons, which might unfold following different time courses. Our study speaks for (1) the need to develop MRI sequences quantifying NM and (2) longitudinal studies of iron- and NM-sensitive imaging to assess their respective sensitivity and specificity to the natural individual evolution of PD across time.

6 CHAPTER 6

DISCUSSION

1 CONCLUSIONS

1.1 METHODOLOGICAL STRENGTHS AND LIMITATIONS…

While the results of the present work confirm the relevance of NM-sensitive and iron-sensitive MRI in the study of Parkinson's disease, our study suffers from limitations that highlight various methodological issues in this particular field of neuroimaging.

1.1.1 … REGARDING THE POPULATION SELECTED IN THE STUDY

As stated in the introduction, a few clinico-pathological correlation studies have demonstrated that PD was misdiagnosed in about 20% of cases, depending on various factors. This emphasises the importance of an accurate clinical diagnosis in the population chosen for a study focusing on PD. We have selected our PD patients very carefully, and the diagnosis was based both on UK Brain Bank Criteria (Hughes *et al.*, 1992) and Movement Disorders Society guidelines (Postuma *et al.*, 2015). These were patients followed in our clinic for at least five years, and patients were systematically re-

assessed, the same diagnosis criteria being applied. We have discarded patients with the least symptom suggesting atypical parkinsonism or even poor response to Levodopa. This longitudinal clinical assessment naturally reduced the size of the PD population we could study.

We did not select patients with premotor phase of PD, which would have been interesting to explore these neuro-imaging biomarkers at early stages of the disease. However, a few *de novo* patients were included in the study.

We also decided to scan all the PD patients in OFF-state, which represents another difficulty as many subjects presented with tremor, or could not tolerate long acquisition time. The symptoms associated with OFF-state led to the occurrence of movement artefacts, especially during MRI scans, and we had to restart acquisitions for a great number of subjects. Despite a very tiring day for older subjects, MRI, PET and clinical acquisitions have always been realised on the same day. MDS-UPDRS certification was required for the two experienced neurologists who performed the rating scales.

Non-motor scores were not assessed and included in the clinical correlations part of the study. Indeed, we decided to focus on the motor aspects of PD as the neuro-imaging biomarkers we investigated were centred on the SN and the degeneration of nigro-striatal pathways, which are at the heart of the pathological process characterising PD and closely related to its motor impairment.

1.1.2 … REGARDING NEUROIMAGING ASPECTS

As developed in the introduction, anatomical definitions of SN subregions are different from one study to another, making the results hardly comparable. As our work tries to establish a link between neuroimaging and pathological biomarkers of the nigrostriatal pathway, we decided to define our SN subregions according to Fearnley and Lees divisions (Fearnley and Lees, 1991), without being

able to accomplish the same level of precision given the small size of the nuclei studied. Indeed, the structure targeted is quite small [the mean overall volume of SN in healthy subjects has been estimated in *post-mortem* histological studies as 188.3 $mm^3 \pm 34.1$ (Di Lorenzo Alho et al., 2016; Schwarz et al., 2017)] in comparison with the spatial resolution of the MRI sequences employed, and SN is a very complex three-dimensional structure, making these divisions difficult to delineate manually.

In addition, the extraction of SN signal from NM-sensitive MRI is still not codified and a different technique is found in most publications on the subject. Automatic segmentation of brainstem nuclei is still difficult due to their irregular morphology, and most of the authors propose a manual or semi-automatic extraction of the signal, which makes the technique less reproducible. Besides, SN signal has then to be corrected for background signal, which is taken from variable regions of the brain **(see Chapter 3, Section 2.1)**. Finally, the value obtained is also different from one study to another, including areas, volumes or contrast to noise ratio. Until now, it appears that none of these approaches proved to be superior to the others. This plethora of analysis techniques and the absence of consensus in the literature represented a particularly difficult part of the processing stage of our study. Besides, the absence of unified approach does not make NM-sensitive MRI a practical tool in routine clinical practice. A fully automated voxelwise method of NM-MRI analysis should be available in the near future, making it an easier screening tool for daily hospital practice.

In our study, we decided to adopt a semi-automatic approach regarding NM extraction technique. As claimed by Sulzer and colleagues, 'there is a fundamental problem when the NM-MRI signal is measured on the same scan used to define the SNpc regions of interest' (Sulzer et al., 2018). Indeed, in PD patients, the loss of NM-containing neurons tends to reduce the contrast between SN and its background, making the delineation of this structure particularly difficult if the reference region is traced manually. Moreover, in most

studies, the regions of interest are defined on a single axial slice from each individual's MRI. To avoid this, we used three-dimensional SN masks from an independent atlas, common for the whole population, which were applied in a second time onto the NM-sensitive MRI of all the subjects.

Beside these considerations, an automatic voxel-based approach for the analysis of the NM-MRI signal would ensure higher accuracy especially regarding underlying neuropathological process as our current approach ignores sub-regional variations of the signal. Indeed, we have mentioned many times in this work that the degeneration process characterising PD is not homogeneous throughout SN (**see Chapter 2, Section 4**). This observation should be considered with the use of a voxel-wise approach (Sulzer et al., 2018).

In comparison, iron-sensitive MRI appears as a more reliable technique as quantitative analysis is possible. Indeed, quantitative measures hold the promise to achieve better sensitivity and may represent a reproductive mean to follow the progression of PD degenerative processes (Prange et al., 2019). Our results were consistent with previous studies, as we showed that iron selectively tends to accumulate in the lateral SN of PD patients, as shown by the hint of a larger R2* in most affected lateral SN in PD when compared to healthy controls. However, SWI and relaxometry are progressively supplanted by quantitative susceptibility mapping (QSM) as this technique seems to offer increased reliability and to be more sensitive with respect to magnetic tissue properties than conventional magnitude-based techniques such as mapping transverse relaxation rates, which is possibly influenced by local cellular structural properties (Langkammer et al., 2012). QSM has the ability to map the spatially heterogeneous iron deposition across the SN, even in early-stage PD patients (Azuma et al., 2016; Li et al., 2019). Moreover, greater susceptibility values in the SN have been correlated with motor impairment severity (Du et al., 2018). Eventually, Lewis et al. confirmed that in vivo QSM correlates better with iron content in *post-mortem* brain tissue than R2* (Lewis et al., 2018). QSM was

unfortunately not available when we started our research, but should be preferred in future studies for a better accuracy.

1.2 THE NEUROPATHOLOGICAL PROCESS AND ITS TIME COURSE

Finally, our study established a link between [^{18}F]DOPA PET signal and microstructural information conveyed by iron- and NM-sensitive MRI data. Indeed, dopaminergic function decreases in anterior putamen as the distribution of NM-sensitive signal is negatively skewed by PD, illustrating the relationship between the impairment of dopaminergic neurons with lateral SN depigmentation. Besides, dopaminergic function in bilateral posterior putamina negatively relates to lateral SN R2* in PD, suggesting that dopaminergic function deteriorates as iron accumulates in lateral SN. Lateral SN seems to be predominantly affected in the different relationships investigated, whereas putaminal subregions vary. These discrepancies regarding the topography of signal alteration suggest different temporal dynamics of two events, namely dopaminergic cell loss and iron accumulation. This may explain why changes in NM signal, for example, may correlate with a change in FDOPA Ki in a region that does not represent the highest magnitude of change in PD at this point, but may be on the verge of degeneration. This suggests that NM signal alteration, reflecting dopaminergic neurons loss in SN, may be an early event, whereas iron accumulation may represent a later stage of the disease. By the time the first symptoms of the disease appear, it is known that 30 to 50% of dopaminergic SN neurons have already died (Riederer and Wuketich, 1976; Cheng et al., 2010). However, depletion of dopaminergic terminals markers in the striatum is estimated between 50 to 80% as compared to healthy subjects when the symptoms of the disease are identified (Bernheimer et al., 1973; Kish et al., 1988; Lee et al., 2000). As highlighted by Martin-Bastida and colleagues, the discrepancy between these estimations raises questions regarding the relationship (particularly in terms of kinetic)

between SN degeneration and its consequences on the function of nigrostriatal terminals (Martín-Bastida et al., 2019). As pointed out in many studies, a measurable loss of neuromelanin is likely to precede the clinical phase of PD as it should represent a precocious event (Zecca et al., 2005). Then, neuronal loss may continue to progress over the next five years, but some radioligand studies following PD progression suggested the existence of a "plateau" after that period of time (Morrish et al., 1996; Nurmi et al., 2001). Another recent study proposed another explanation, with exponential cell loss continuing beyond five years (Perlmutter and Norris, 2014). In their study comparing pathological data (number of surviving TH-positive and neuromelanin containing dopaminergic neurons in *post-mortem* brains of PD patients) and DaTscan results, Saari and colleagues did not find any correlation between nigral cell counts and 123I-FP-CIT striatal specific binding. They proposed this result might be explained by the loss of the relationship between surviving nigral cells and striatal dopamine in later stages of the disease, after a certain amount of damage has already occurred (Saari et al., 2017). In their meta-analysis including many SPECT and PET studies in PD, Kaasinen and Vahlberg found stronger correlations between clinical severity and tracer binding in the caudate nucleus than in the putamen. As an explanation, they proposed these data might reflect a 'floor effect' of putaminal dopaminergic function in PD. In order words, caudate nucleus dopaminergic function is supposed to be better preserved than posterior putamen function, thus showing correlations with clinical parameters that are already lost in the posterior putamen due to earlier and more severe dopaminergic impairment (Kaasinen and Vahlberg, 2017).

By contrast, despite its critical role demonstrated in the pathogenesis of nigro-striatal injury in PD, it is still not clear whether the increase of iron is a causal factor of neuronal death or a secondary phenomenon that comes later on. According various studies, iron tends to accumulate in the SN of PD patients particularly in the later stages (Martin et al., 2008; Lewis et al., 2018). Among them, Du and

colleagues demonstrated that R2* in all SN subregions was significantly increased in the mid-stage and late-stage, but not early-stage, of Parkinson's disease subjects (Du et al., 2012). Eventually, it has to be kept in mind that dopaminergic striatal dysfunction has also its own kinetics, as demonstrated in a few [^{18}F]DOPA PET studies and mentioned above **(see Chapter 3, Section 1.2.2)**. Dopaminergic function is indeed severely impaired in the early stage of PD, whereas the anterior part of the putamen and the caudate is relatively spared at the beginning but becomes progressively involved too as the disease progresses (Brooks et al., 1990). The three pathological processes that we have investigated through neuroimaging clearly have different time course in different brain regions, highlighting the need of longitudinal studies.

1.3 THE CONCEPT OF BIOMARKERS

What is the position of the neuroimaging tools among PD biomarkers? To answer that question, it is important to start with their current definition and subtypes. A biomarker is 'a defined characteristic that is measured as an indicator of normal biological processes, pathogenic processes or responses to an exposure or intervention' (Califf, 2018). Among various purposes, a suitable biomarker 'can quantify the presence or progression of a disease, and can be used to help define disease heterogeneity, to provide new insights into pathogenic pathways' (Antoniades and Barker, 2009). In many situations, biomarkers that predict the onset of a disease are different to those that can diagnose the disease, which in turn may be different from those that follow disease progression.

The goal of our study was not to determine the sensitivity and specificity of these new MRI techniques but to assess their ability to detect the changes related to the disease, and to cross-compare them to another established imaging approach. We decided to test as **diagnostic** biomarkers of PD three parameters (striatal FDOPA

decline, SN R2* and SN depigmentation), that were shown to correlate to neuropathologic alterations reported *post-mortem* in PD. [^{18}F]DOPA PET does not measure the number of dopaminergic neurons, but rather measure the net dopaminergic drive, resulting from the loss of dopaminergic terminals and compensatory mechanisms. NM-MRI measures the amount of surviving pigmented neurons (we postulated that the amount of extracellular NM was negligible). Iron-sensitive MRI shows another key aspect of the neuropathological process through iron deposit measurements. The specificity of these two neuroimaging biomarkers regarding PD diagnosis remains to be investigated as our population did not include patients suffering from atypical parkinsonism or other synucleinopathy. Their sensibility was not assessed either as we did not select prodromal PD patients and included only a few de novo patients.

In our current state of knowledge, these markers might help the diagnosis of PD although they do not correlate with the clinical status (at least in our sample). What our study does not show is whether this absence of correlation arises from the signal modifications preceding the clinical findings (hopefully not following them), or a floor (or ceiling) effect or whichever nonlinear relationship between the markers and clinical ratings (**see "Methodological limitations" section above**). While it was proven there is a progressive regional decline in striatal FDOPA uptake with PD evolution (Whone et al. 2003, Bruck et al. 2006), we cannot make any statement about the use of NM-MRI and iron-sensitive MRI as biomarkers of disease progression as we did not study the alteration of the signal over time.

Finally, as we lack a method to identify in-vivo accumulation of pathologic species of alpha-synuclein, the current biomarkers probably serve as in vivo proxies of the genuine initial PD processes.

2 PERSPECTIVES

2.1 MACHINE LEARNING APPLICATIONS

Over the past few years, machine learning have deeply changed the management and diagnosis of neurological diseases, and have shown great promise for imaging applications (Patel *et al.*, 2021).

Machine learning is one form of artificial intelligence, using specific algorithms developed in order to enable computers to learn from existing data without explicit programming (Zaharchuk *et al.*, 2018). In the context of differential diagnosis between PD and atypical parkinsonisms, sophisticated systems based on machine learning have been proposed for DaTscan (Prashanth *et al.*, 2014; Oliveira and Castelo-Branco, 2015), FDG PET (Garraux *et al.*, 2013; Mudali *et al.*, 2015), or even DMFP (desmethoxyfallypride) PET (Segovia *et al.*, 2017), using various approaches and methods (partial least squares, multiple kernel approach, scaled subprofile model/principal component analysis, etc.). These techniques are able to distinguish structures or patterns in biological signals or images. The results of these studies have shown that these systems based on the recognition of specific patterns (referred to as features) achieved adequate performance for the differentiation between PD and atypical parkinsonism (Raghavendra *et al.*, 2020).

Other research groups explored the potential of machine learning systems for the detection of PD using brain MRI. Banerjee and colleagues focused on diffusion MRI, using Cauchy deformation tensor (CDT) to establish a method of automated discrimination between controls and PD patients (Banerjee *et al.*, 2016), whereas Cigdem and colleagues studied structural MRI, using support vector machine (SVM) to distinguish PD patients from healthy controls (Cigdem *et al.*, 2018). The set of data we have collected could be used in the same purpose, using iron- and NM-sensitive MRI to assist the diagnosis of PD in an individual patient, rather than focusing on group comparisons as we did until now. However, a large number of

patients should be enrolled over the years, with careful clinical selection, as feature distributions are more accurately and precisely estimated as the number of observations increases.

In the future, computer-aided diagnosis systems will hopefully assist neurologists and neuroradiologists in their clinical decisions and particularly in the differential diagnosis between conditions with overlapping clinical features (Garraux *et al.*, 2013).

2.2 MRI DEVELOPMENTS IN DYSTONIA

Over the past few years, beside Parkinson's disease imaging, our team has developed a special interest for dystonia, botulinum toxin treatment and children movement disorders, which are three intertwined fields (Barrea *et al.*, 2019; Depierreux *et al.*, 2020, 2021; Barrea and Depierreux, 2021; Drion and Depierreux, 2021; Hardy *et al.*, 2021). As the diagnosis of congenital or early dystonia can be challenging, neuroimaging might be considered as an efficient diagnostic aid, particularly when genetic testing does not identify any known variant.

Although the neuroanatomical substrates for dystonia are only partly understood, many studies demonstrated that basal ganglia and related thalamo-cortical networks are intimately implicated in the pathophysiology of primary dystonia (Stoessl *et al.*, 2014). In primary sporadic dystonias in which conventional imaging is negative, PET studies, functional MRI, quantitative structural imaging and diffusion imaging techniques showed abnormalities in various regions of the brain (Black *et al.*, 1998; Eimeren and Siebner, 2006; Neychev *et al.*, 2011).

Among these techniques, voxel-based morphometry (VBM; allowing the voxelwise statistical estimation of structural differences in local volume or grey matter density according to brain tissue class) identified structural abnormalities in basal ganglia, such as increased

volume of the putamen, and/or alterations in the associated cortical areas, thalamus, and cerebellum (Garraux *et al.*, 2004; Bradley *et al.*, 2009; Draganski *et al.*, 2009).

Additionally, specific types of dystonia are inherently associated with an increased brain iron deposition. Some authors found elevated R2* values in the globus pallidus of patients suffering from cervical dystonia, providing the *in vivo* confirmation of an increased brain iron content (Aschermann *et al.*, 2015). In ten patients suffering from neuroferritinopathy (an autosomal dominant adult-onset dystonia due to mutations in the ferritin light chain gene) who underwent 3D-T1w and quantitative T2 whole brain MRI, Keogh and colleagues found a progressive iron accumulation in the caudate nucleus using voxel-based relaxometry (VBR) when compared to healthy controls (Keogh *et al.*, 2015). Moreover, VBM detected significant tissue changes within the substantia nigra, midbrain and dentate with significant cerebellar atrophy. Relaxometry then appears as promising in the neuroimaging study of dystonia. On the other hand, in a recent study by Gracien and colleagues focusing on idiopathic cervical dystonia, neither whole brain voxel-wise statistics nor regions of interest-based analyses revealed significant group differences for any quantitative MRI parameter under investigation (Gracien *et al.*, 2019).

Overall, these studies yielded conflicting results, but the sample size is generally quite small, and case mix heterogeneous [in most of the studies, there is no systematic genetic testing of dystonic patients studied by quantitative MRI (qMRI) experiment]. We contend that patients must be carefully phenotyped and genotyped in the first place, because different genetic conditions can lead to a similar dystonic phenotype, whereas the underlying pathogenic mechanisms most likely differ. Needless to say, this potentially influences the MRI signal.

From a technical point of view, qMRI uses *physical* models to calculate quantitative parameter maps (**see Chapter 3, Section 2.3.2**). Recently, *biophysical* models of qMRI signals have been developed in order to

estimate microscopic brain tissue parameters. This emerging field, called *in-vivo* histology using MRI or hMRI, provides quantitative histological measures of brain tissue, such as myelin density, iron density, axonal diameters, etc.

In the future, we would like to explore the potential usefulness of histological MRI in the diagnosis of various types of dystonia, using iron-sensitive MRI and particularly QSM which appears more robust than quantitative R2* (**see Chapter 3, Section 2.3.1**). The availability in our laboratory of ultra-high field MRI (7T) should improve the spatial accuracy of the analyses, down to the subnuclear level. As the targeted structures are similar (e.g., basal ganglia and brainstem nuclei), the various analytical methods developed in the context of the present neuroimaging study of Parkinson's disease could be usefully adapted and optimised to sub-millimetric structural data.

Of course, some limitations are expected: the patients concerned are generally not easily scanned, the main reason being the constant dystonic movement they suffer from. Severe dystonic posture of the neck, head tremor, opisthotonos, etc. are clinical features that might require sedation or general anaesthesia. In addition, some conditions typically affect younger patients, such as PKAN (panthonate kinase-associated neurodegeneration also known as NBIA1, for neurodegeneration with brain iron accumulation-1), or even small children, making MRI acquisitions and spatial processing even more difficult. Finally, these affections are not frequent and sample size is expected to be low, making necessary the use of specific statistical analyses (e.g., resampling techniques allowing for the estimation of the sample distribution).

The ultimate goal of this research would remain to better understand the pathophysiological correlates and time course of these diseases, predict their functional outcome and response to treatment, i.e. to provide the patients with the hope of a better life.

PART 3

Appendices

1

SUPPLEMENTARY MATERIALS RELATED TO CHAPTER 1, SECTION 4.1

TABLE 1: MDS - UPDRS PART III (MOTOR EXAMINATION)

GENERAL REMARKS

If the patient takes any medication for Parkinson's Disease, the current patient's state should be mentioned. ON state means that the patient is in his best motor state during the examination. OFF state means that he is performing with more difficulties than usual. Delay between examination and last levodopa intake should be noted. If dyskinesias are present, they should be mentioned. One should not decide whether the motor ability is linked to PD or another disease, but if the task is impossible (e.g., amputee), one should rate UR (unable to rate).

The scale is always a 5-point one:

0= Normal

1= Slight

2=Mild

3= Moderate

4= Severe

Reference: (Goetz *et al.*, 2008)

3.1 SPEECH /4

Instructions to examiner: Listen to the patient's free-flowing speech and engage in conversation if necessary. Evaluate volume, modulation (prosody) and clarity, including slurring, palilalia (repetition of syllables), and tachyphemia (rapid speech, running syllables together).

0: No speech problems.

1: Loss of modulation, diction, or volume, but still all words easy to understand.

2: Loss of modulation, diction, or volume, with a few words unclear, but the overall sentences easy to follow.

3: Speech is difficult to understand to the point that some, but not most, sentences are poorly understood.

4: Most speech is difficult to understand or unintelligible.

3.2 FACIAL EXPRESSION /4

Instructions to examiner: Observe the patient sitting at rest for 10 seconds, without talking and also while talking. Observe eye-blink frequency, masked facies or loss of facial expression, spontaneous smiling, and parting of lips.

0: Normal facial expression.

1: Minimal masked facies manifested only by decreased frequency of blinking.

2: In addition to decreased eye-blink frequency, masked facies present in the lower face as well, namely fewer movements around the mouth, such as less spontaneous smiling, but lips not parted.

3: Masked facies with lips parted some of the time when the mouth Is at rest.

4: Masked facies with lips parted most of the time when the mouth is at rest.

3.3 RIGIDITY /20

Instructions to examiner: Rigidity is judged on slow passive movement of major joints with the patient in a relaxed position and the examiner manipulating the limbs and neck. First, test without an activation manoeuvre. Test and rate neck and each limb separately. For arms, test the wrist and elbow joints simultaneously. For legs, test the hip and knee joints simultaneously. If no rigidity is detected, use an activation manoeuvre such as tapping fingers, fist opening/closing, or heel tapping in a limb not being tested. Explain to the patient to go as limp as possible as you test for rigidity.

0: No rigidity.

1: Rigidity only detected with activation manoeuvre.

2: Rigidity detected without the activation manoeuvre, but full range of motion is easily achieved.

3: Rigidity detected without the activation manoeuvre; full range of motion is achieved with effort.

4: Rigidity detected without the activation manoeuvre and full range of motion not achieved.

3.4 FINGER TAPPING /8

Instructions to examiner: Each hand is tested separately. Demonstrate the task, but do not continue to perform the task while the patient is being tested. Instruct the patient to tap the index finger on the thumb 10 times as quickly AND as big as possible. Rate each side separately, evaluating speed, amplitude, hesitations, halts, and decrementing amplitude.

0: No problems.

1: Any of the following: a) the regular rhythm is broken with one or two interruptions or hesitations of the tapping movement; b) slight slowing; c) the amplitude decrements near the end of the 10 taps.

2: Any of the following: a) 3 to 5 interruptions during tapping; b) mild slowing; c) the amplitude decrements midway in the 10-tap sequence.

3: Any of the following: a) more than 5 interruptions during tapping or at least one longer arrest (freeze) in ongoing movement; b) moderate slowing; c) the amplitude decrements starting after the 1st tap.

4: Cannot or can only barely perform the task because of slowing, interruptions, or decrements.

3.5 HAND MOVEMENTS /8

Instructions to examiner: cf. 3.4. Instruct the patient to make a tight fist with the arm bent at the elbow so that the palm faces the examiner. Have the patient open the hand 10 times as fully AND as quickly as possible. If the patient fails to make a tight fist or to open the hand fully, remind him/ her to do so. Rate each side as described in 3.4.

3.6 PRONATION-SUPINATION MOVEMENTS OF HANDS /8

Instructions to examiner: cf. 3.4. Instruct the patient to extend the arm out in front of his/her body with the palms down, and then to turn the palm up and down alternately 10 times as fast and as fully as possible. Rate each side as described in 3.4.

3.7 TOE TAPPING /8

Instructions to examiner: cf. 3.4. Have the patient sit in a straight-backed chair with arms, both feet on the floor. Instruct the patient to place the heel on the ground in a comfortable position and then tap the toes 10 times as big and as fast as possible. Rate each side as described in 3.4.

3.8 LEG AGILITY /8

Instructions to examiner: cf. 3.7. Instruct the patient to place the foot on the ground in a comfortable position and then raise and stomp the foot on the ground 10 times as high and as fast as possible. Rate each side as described in 3.4.

3.9 ARISING FROM A CHAIR /4

Instructions to examiner: Have the patient sit in a straight-backed chair with arms, with both feet on the floor and sitting back in the chair (if the patient is not too short). Ask the patient to cross his/her arms across the chest and then to stand up. If the patient is not successful, repeat this attempt up to a maximum of two more times. If still unsuccessful, allow the patient to move forward in the chair to arise with arms folded across the chest. Allow only one attempt in this situation. If unsuccessful, allow the patient to push off using his/her hands on the arms of the chair. Allow a maximum of three trials of pushing off. If still not successful, assist the patient to arise. After the patient stands up, observe the posture for item 3.13.

0: No problems. Able to arise quickly without hesitation.

1: Arising is slower than normal; or may need more than one attempt; or may need to move forward in the chair to arise. No need to use the arms of the chair.

2: Pushes self up from the arms of the chair without difficulty.

3: Needs to push off, but tends to fall back; or may have to try more than one time using the arms of the chair, but can get up without help.

4: Unable to arise without help.

3.10 GAIT /4

Instructions to examiner: Testing gait is best performed by having the patient walking away from and towards the examiner so that both right and left sides of the body can be easily observed simultaneously. The patient should walk at least 10 meters, then turn around and return to the examiner. This item measures multiple behaviors: stride amplitude, stride speed, height of foot lift, heel strike during walking, turning, and arm swing, but not freezing. Assess also for "freezing of gait" (next item 3.11) while patient is walking. Observe posture for item 3.13.

0: No problems.

1: Independent walking with minor gait impairment.

2: Independent walking but with substantial gait impairment.

3: Requires an assistance device for safe walking (walking stick, walker) but not a person.

4: Cannot walk at all or only with another person's assistance.

3.11 FREEZING OF GAIT /4

Instructions to examiner: While assessing gait, also assess for the presence of any gait freezing episodes. Observe for start hesitation and stuttering movements especially when turning and reaching the end of the task. To the extent that safety permits, patients may NOT use sensory tricks during the assessment.

0: No freezing.

1: Freezes on starting, turning, or walking through doorway with a single halt during any of these events, but then continues smoothly without freezing during straight walking.

2: Freezes on starting, turning, or walking through doorway with more than one halt during any of these activities, but continues smoothly without freezing during straight walking.

3: Freezes once during straight walking.

4: Freezes multiple times during straight walking.

3.12 POSTURAL STABILITY /4

Instructions to examiner: The test examines the response to sudden body displacement produced by a quick, forceful pull on the shoulders while the patient is standing erect with eyes open and feet comfortably apart and parallel to each other. Test retropulsion. Stand behind the patient and instruct the patient on what is about to happen. Explain that s/he is allowed to take a step backwards to avoid falling. There should be a solid wall behind the examiner, at least 1-2 meters away

to allow for the observation of the number of retropulsive steps. The first pull is an instructional demonstration and is purposely milder and not rated. The second time the shoulders are pulled briskly and forcefully towards the examiner with enough force to displace the center of gravity so that patient MUST take a step backwards. The examiner needs to be ready to catch the patient, but must stand sufficiently back so as to allow enough room for the patient to take several steps to recover independently. Do not allow the patient to flex the body abnormally forward in anticipation of the pull. Observe for the number of steps backwards or falling. If the patient fails to understand the test, the examiner can repeat the test so that the rating is based on an assessment that the examiner feels reflects the patient's limitations rather than misunderstanding or lack of preparedness. Observe standing posture for item 3.13.

0: No problems. Recovers with one or two steps.

1: 3-5 steps, but subject recovers unaided.

2: More than 5 steps, but subject recovers unaided.

3: Stands safely, but with absence of postural response; falls if not caught by examiner.

4: Very unstable, tends to lose balance spontaneously or with just a gentle pull on the shoulders.

3.13 POSTURE /4

Instructions to examiner: Posture is assessed with the patient standing erect after arising from a chair, during walking, and while being tested for postural reflexes. If you notice poor posture, tell the patient to stand up straight and see if the posture improves. Rate the worst posture seen in these three observation points. Observe for flexion and side-to-side leaning.

0: No problems.

1: Not quite erect, but posture could be normal for older person.

2: Definite flexion, scoliosis or leaning to one side, but patient can correct posture to normal posture when asked to do so.

3: Stooped posture, scoliosis or leaning to one side that cannot be corrected volitionally to a normal posture by the patient.

4: Flexion, scoliosis or leaning with extreme abnormality of posture.

3.14 GLOBAL SPONTANEITY OF MOVEMENT /4

Instructions to examiner: This global rating combines all observations on slowness, hesitancy, and small amplitude and poverty of movement in general, including a reduction of gesturing and of crossing the legs. This assessment is based on the examiner's global impression after observing for spontaneous gestures while sitting, and the nature of arising and walking.

0: No problems.

1: Slight global slowness and poverty of spontaneous movements.

2: Mild global slowness and poverty of spontaneous movements.

3: Moderate global slowness and poverty of spontaneous movements.

4: Severe global slowness and poverty of spontaneous movements.

3.15 POSTURAL TREMOR OF THE HANDS /8

Instructions to examiner: All tremor, including re-emergent rest tremor, that is present in this posture is to be included in this rating. Rate each hand separately. Rate the highest amplitude seen. Instruct the patient to stretch the arms out in front of the body with palms down. The wrist should be straight and the fingers comfortably separated so that they do not touch each other. Observe this posture for 10 seconds.

0: No tremor.

1: Tremor is < 1 cm in amplitude.

2: Tremor is ≥ 1 cm but < 3 cm in amplitude.

3: Tremor is ≥ 3 cm but < 10 cm in amplitude.

4: Tremor is ≥ 10cm in amplitude.

3.16 KINETIC TREMOR OF THE HANDS /8

Instructions to examiner: This is tested by the finger-to-nose maneuver. With the arm starting from the outstretched position, have the patient perform at least three finger-to-nose maneuvers with each hand reaching as far as possible to touch the examiner's finger. The finger-to-nose maneuver should be performed slowly enough not to hide any tremor that could occur with very fast arm movements. Repeat with the other hand, rating each hand separately. The tremor can be present throughout the movement or as the tremor reaches either target (nose or finger). Rate the highest amplitude seen as described in 3.15.

3.17 REST TREMOR AMPLITUDE /20

Instructions to examiner: This and the next item have been placed purposefully at the end of the examination to allow the rater to gather observations on rest tremor that may appear at any time during the exam, including when quietly sitting, during walking, and during activities when some body parts are moving but others are at rest. Score the maximum amplitude that is seen at any time as the final score. Rate only the amplitude and not the persistence or the intermittency of the tremor. As part of this rating, the patient should sit quietly in a chair with the hands placed on the arms of the chair (not in the lap) and the feet comfortably supported on the floor for 10 seconds with no other directives. Rest tremor is assessed separately for all four limbs and also for the lip/jaw. Rate only the maximum amplitude that is seen at any time as the final rating. Rate limbs' tremor as described in 3.15.

Lip/jaw ratings:

0: No tremor.

1: Tremor is < 1 cm in maximal amplitude.

2: Tremor is ≥ 1 cm but < 2 cm in maximal amplitude.

3: Tremor is ≥ 2 cm but < 3 cm in maximal amplitude.

4: Tremor is ≥ 3 cm in maximal amplitude.

3.18 CONSTANCY OF REST TREMOR /4

Instructions to examiner: This item receives one rating for all rest tremor and focuses on the constancy of rest tremor during the examination period when different body parts are variously at rest. It is rated purposefully at the end of the examination so that several minutes of information can be coalesced into the rating.

0: No tremor.

1: Tremor is present ≤25% of the entire time.

2: Tremor is present 26-50% of the entire time.

3: Tremor is present 51-75% of the entire time.

4: Tremor is present >75% of the entire time

TOTAL SCORE: /142

DYSKINESIA IMPACT ON PART III RATINGS

A. Were dyskinesias (chorea or dystonia) present during examination?

B. If yes, did these movements interfere with your ratings

2

SUPPLEMENTARY MATERIALS RELATED TO CHAPTER 1, SECTION 1.4

TABLE 2: PDQ-39 QUESTIONNAIRE

GENERAL REMARKS

PDQ-39 is a 39 items self-report questionnaire, which assesses how often patients experience difficulties across 8 quality of life dimensions, and the impact of the disease on specific dimensions of functioning and well-being (Jenkinson et al., 1997).

	Due to having Parkinson's disease, how often during the last month have you....	Never	Occasio-nally	Some-times	Often	Always Or cannot do at all
1	Had difficulty doing the leisure activities which you would like to do?					
2	Had difficulty looking after your home, e.g. DIY, housework, cooking?					
3	Had difficulty carrying bags of shopping?					
4	Had problems walking half a mile?					
5	Had problems walking 100 yards?					
6	Had problems getting around the house as easily as you would like?					
7	Had difficulty getting around in public?					
8	Needed someone else to accompany you when you went out?					
9	Felt frightened or worried about falling over in public?					
10	Been confined to the house more than you would like?					
11	Had difficulty washing yourself?					
12	Had difficulty dressing yourself?					
13	Had problems doing up your shoe laces?					
14	Had problems writing clearly?					
15	Had difficulty cutting up your food?					
16	Had difficulty holding a drink without spilling it?					
17	Felt depressed?					
18	Felt isolated and lonely?					
19	Felt weepy or tearful?					
20	Felt angry or bitter?					
21	Felt anxious?					

22	Felt worried about your future?					
23	Felt you had to conceal your Parkinson's from people?					
24	Avoided situations which involve eating or drinking in public?					
25	Felt embarrassed in public due to having Parkinson's disease?					
26	Felt worried by other people's reaction to you?					
27	Had problems with your close personal relationships?					
28	Lacked support in the ways you need from your spouse or partner? (*If you do not have a spouse or partner tick here)*					
29	Lacked support in the ways you need from your family or close friends?					
30	Unexpectedly fallen asleep during the day?					
31	Had problems with your concentration, e.g. when reading or watching TV?					
32	Felt your memory was bad?					
33	Had distressing dreams or hallucinations?					
34	Had difficulty with your speech?					
35	Felt unable to communicate with people properly?					
36	Felt ignored by people?					
37	Had painful muscle cramps or spasms?					
38	Had aches and pains in your joints or body?					
39	Felt unpleasantly hot or cold?					

The patient has to tick <u>one</u> box for each question

3

SUPPLEMENTARY MATERIALS RELATED TO CHAPTER 5, SECTION 2.1

TABLE 3: DEMOGRAPHIC DATA

HEALTHY SUBJECTS

SUBJECT ID	GENDER	AGE AT MRI
HS-1	F	70
HS-2	F	55
HS-3	F	77
HS-4	F	69
HS-5	F	73
HS-6	F	48
HS-7	M	88
HS-8	F	63
HS-9	F	74
HS-10	F	56
HS-11	M	71
HS-12	F	69
HS-13	M	78
HS-14	M	59
HS-15	F	65
HS-16	F	67
HS-17	M	51
HS-18	M	71
HS-19	M	78
HS-20	M	73
HS-21	M	68
HS-22	M	53
HS-23	M	72
	Sex ratio 11M/12F	Mean age [SD] 67,30 [9.86]

PARKINSON'S DISEASE PATIENTS

SUBJECT ID	GENDER	AGE AT MRI (YEARS)	MOST AFFECTED SIDE	UPDRS	H&Y STAGE	LED	DISEASE DURATION (YEARS)
HS-1	M	75	left	33	1,5	775	7
HS-2	M	87	left	15	1,5	300	15
HS-3	M	56	left	36	2	937,5	7
HS-4	F	71	left	28	3	550	10
HS-5	F	76	right	20	1,5	540	8
HS-6	F	76	right	15	3	105	7
HS-7	F	68	right	19	1,5	880	4
HS-8	F	61	right	10	1	0	0
HS-9	M	51	left	40	1,5	786	10
HS-10	M	71	right	14	1	555	8
HS-11	F	64	right	34	2	240	5
HS-12	F	69	left	26	2,5	300	1
HS-13	M	67	right	22	1	820	7
HS-14	M	49	right	21	2	310	2
HS-15	F	75	right	29	3	0	2
HS-16	M	80	right	54	2	400	5
HS-17	M	73	right	29	2	632	6
HS-18	M	69	right	31	2	201	1
HS-19	M	78	right	52	2	465,5	11

HS-20	F	57	right	36	2,5	632	5
HS-21	M	67	left	43	2	575	4
HS-22	F	56	right	15	1	0	1
HS-23	M	60	right	28	1,5	305	3
	Sex ratio:	Mean (SD):	L/R:	Mean (SD):	Mean [Range]:	Mean [Range]:	Mean [Range]:
	13M/10F	67,65 (9.68)	7 L/16 R	28,26 (11,8)	1,67 [1-3]	448,22 [0-937]	5,61 [1-15]

4 SUPPLEMENTARY MATERIALS RELATED TO CHAPTER 5, SECTION 2.3

TABLE 4: MRI ACQUISITION PARAMETERS

The whole-brain MRI acquisitions included a multiparameter mapping (MPM) protocol that allows voxelwise R2* quantification (as well as MT saturation, R1 and PD estimation). This MPM protocol has been developed in the framework of an international collaborative effort (Weiskopf et al., 2013; Tabelow et al., 2019) and consists of three co-localised 3D multi-echo fast low angle shot (FLASH) acquisitions at 1 x 1 x 1 mm^3 resolution and two additional calibration sequences to correct for inhomogeneities in the RF transmit field (Lutti et al., 2010, 2012). The FLASH data sets were acquired with predominantly proton density (PD), T1 and magnetization transfer (MT) weighting, referred to in the following as PDw, T1w and MTw, acquired at different echo times. All three had high bandwidth to minimise off-resonance and chemical shift artefacts. Volumes were acquired in 176 sagittal slices using a 256 x 224 voxel matrix. GRAPPA parallel imaging was combined with partial Fourier acquisition to speed up acquisition time to approximately 20 minutes.

This information is gathered in the table below.

	MULTIPARAMETER PROTOCOL			NEUROMELANIN-SENSITIVE MRI
	T1w	PDw	MTw	
TR	24.5 ms			30 ms*
FLIP ANGLE	21°	6°	6°	23°
BIPOLAR GRADIENT ECHOES/TE	8/TE 2.34 – 18,72 ms		6/TE 2.34 – 14,04 ms	2.61 ms
BANDWIDTH	465 [Hz/Px]			450 [Hz/Px]
RESOLUTION	1 x 1 x 1 mm^3			1 mm isotropic resolution

* The TR was made longer (30-35 ms) to fulfill SAR limitations when needed (normal SAR operating mode for all patients).

PART 4

Publications

1 PUBLICATIONS AS FIRST OR CO-AUTHOR

Depierreux, F., Parmentier, E., Mackels, L., Baquero Duarte, K., Degueldre, C., Balteau, E., Salmon, E., Philips, C., Bahri, M.A., Maquet, P., Garraux, G. 2021. Parkinson's disease multimodal imaging: F-DOPA PET, neuromelanin-sensitive and quantitative iron-sensitive MRI. *NPJ Park. Dis.* 2021: 1-10.

Mackels, L., **Depierreux, F.** 2021. Multimodal imaging of a patient with RAB-39 mutation. Submitted to *Neuroradiology* (in review).

Marx, B., **Depierreux, F.** 2021. Comment j'explore… un blépharospasme. Accepted in *Revue Médicale de Liège.*

Hardy, P.-Y., Hallet, C., Kirsch, M., Samalea Suarez, N., Hick, G., Petry, J., Lois, F., Jastrowicz, J., **Depierreux, F. 2021**. Anesthetic Management of a Child with Rapid-Onset Dystonia-Parkinsonism (DYT12-ATP1A3): A Case Report. *Anesthesia & Analgesia Practice*, 15(4).

Depierreux, F., Parmentier, E., Hardy, P.-Y., Leroy, P., & Maquet, P. **2021**. Successful treatment of hand dystonia with botulinum toxin in a DYT12 patient. *Toxicon*, 190S1, 16.

Drion, E., **Depierreux, F. 2021**. Botulinum toxin treatment of focal dystonia in kernicterus-related movement disorders. *Toxicon*, 190S1, 17-S18.

Barrea, C., **Depierreux, F. 2021**. Recurrent Ataxia and Dystonia with Anti-Neurochondrin Autoantibodies. *Neuropediatrics.* 52(3):228-229.

Depierreux, F., Jedidi, H., Hardy, P.-Y., Parmentier, E., Garraux, G. **2020**. Comment j'explore… une dystonie cervicale. *Revue Médicale de Liège*, 75(2), 121-124.

Timmermans, G., **Depierreux, F.**, Wang, F.-C., Hansen, I., Maquet, P. **2019**. Cosmetic injection of botulinum toxin unmasking subclinical myasthenia gravis: a case report and literature review. *Case Reports in Neurology*, 11, 244-251.

Barrea, C., **Depierreux, F.**, Servais, L. **2019**. Odalisque's Position as a Geste Antagoniste in a Variant Phenotype of Ataxia Telangiectasia. *Movement Disorders Clinical Practice*, 6(5), 413-414.

Hardy, P.-Y., **Depierreux, F.**, Ferretti, C. **2019**. Œdème aigu du poumon et traitement par tocolytiques chez la femme enceinte. *Revue Médicale de Liège*, 74(3), 129-133.

Depierreux, F., Parmentier, E., Baquero Duarte, K. A., Balteau, E., Phillips, C., Maquet, P., Garraux, G. **2018**.Validation of new brain MRI biomarkers in Parkinson's Disease: the use of quantitative multi-parameter mapping. *Frontiers in Neuroscience. Conference Abstract: Belgian Brain Congress 2018 – Belgian Brain Council.*

Baquero Duarte, K. A., Guldenmund, J. P., Rouillard, M., **Depierreux, F.**, Balteau, E., Phillips, C., Bahri, M. A., & Garraux, G. **2018**. Degree of Centrality of brain functional connectivity within the motor network for Parkinson's Disease. *Frontiers in Neuroscience. Conference Abstract: Belgian Brain Congress 2018 – Belgian Brain Council.*

Parmentier, E., De Pasqua, V., D'Ostilio, K., **Depierreux, F.**, Garraux, G., Maertens De Noordhout, A. **2018**.Correlation between deep brain stimulation effects on freezing of gait and audio-spinal reflex. *Clinical Neurophysiology*, 129, 2083-2088.

Demonceau, M., Baquero Duarte, K. A., **Depierreux, F.**, Rouillard, M., Croisier J.-L., Bury, T., Jidovtseff, B., Maquet, D., Garraux, G. **2018**. Association between physical fitness and cerebral grey matter integrity in patients suffering from Parkinson's disease, a structural MRI study. *Annals of Physical and Rehabilitation Medicine*, 61 - supplement, 46.

Boutaayamou, M., **Depierreux, F.,** Parmentier, E., Schwartz, C., Bruls, O., Verly, J., Garraux, G. **2018**. Quantification of refined temporal gait parameters in Parkinson's disease using an accelerometer-based ambulatory system. Poster session presented at the Belgian Brain Congress 2018, Liège, Belgium.

Boutaayamou, M., **Depierreux, F**., Parmentier, E., Schwartz, C., Bruls, O., Verly, J., Garraux, G. **2018**. Quantification of gait sub-phase durations using an ambulatory system in Parkinson's disease. Poster session presented at 2nd International Workshop on Freezing of Gait, Leuven, Belgium.

Baquero Duarte, K. A., Guldenmund, P., Rouillard, M., **Depierreux, F.**, Balteau, E., Phillips, C., Bahri, M. A., Garraux, G. **2018**. Degree of Centrality within the motor network for Parkinson's Disease. Poster session presented at OHBM 2018 - Organization for Human Brain Mapping, Singapore.

Lommers, E., **Depierreux, F.**, Hansen, I., Dive, D., Maquet, P. **2018**. NMOSD with anti-MOG antibodies following anti-TNFα therapy: A case report. *Multiple Sclerosis and Related Disorders*, 26, 37-39.

Jedidi, H., Laverdeur, C., **Depierreux, F.**, Beckers, A. **2018**. Une petite histoire de la syphilis. La maladie a travers l'art et l'artiste. *Revue Médicale de Liège,* 73(7-8), 363-369.

Gillain, S., Boutaayamou, M., Dardenne, N., Schwartz, C., Demonceau, M., Gerontitis, C., **Depierreux, F.**, Salmon, E., Garraux, G., Bruyère, O., Bruls, O., Croisier, J.-L., Petermans, J. **2017**. Data set

of healthy old people assessed for three walking conditions using accelerometric and opto-electronic methods. *Aging Clinical and Experimental Research*, 29(6), 1201-1209.

Baquero Duarte, K. A., Guldenmund, P., Rouillard, M., **Depierreux, F.**, Balteau, E., Phillips, C., Bahri, M. A., Garraux, G. 2017. Mean and variance of Dynamic Functional Connectivity in Parkinson's Disease. Poster session presented at Organization for Human Brain Mapping OHBM 2017, Vancouver, Canada.

Leroy, P., Daron, A., & **Depierreux, F**. 2017. Dystonie de type 11 à début précoce. Paper presented at the 45ème Réunion de la Société Européenne de Neuropédiatrie - 2017, Turin, Italy.

Baquero Duarte, K. A., Rouillard, M., **Depierreux, F.**, Guldenmund, P., Bahri, M. A., Balteau, E., Garraux, G. 2016. A time--frequency analysis of resting-state BOLD fMRI activity in Parkinson's disease. Poster session presented at Organization for Human Brain Mapping OHBM 2016, Geneva, Switzerland.

Baquero Duarte, K. A., Rouillard, M., **Depierreux, F.**, Guldenmund, P., Bahri, M. A., Balteau, E., Phillips, C., Garraux, G. 2016. How to find a biomarker to accurately diagnose early stage Parkinson's Disease? Analysis of time-frequency functional activity and connectivity using resting-state fMRI. Poster session presented at The Machine Learning Summer School 2016, Cadiz, Spain.

Jedidi, H., Rostomyan, L., Potorac, I., **Depierreux, F.**, Petrossians, P., Beckers, A. 2016. Advances in diagnosis and management of familial pituitary adenomas. International Journal of Endocrine Oncology, 3(4), 313-323

Himri, K., **Depierreux, F.**, Garraux, G. 2015. Développement de nouveaux marqueurs neuroradiologiques de la maladie de Parkinson

par reconnaissance de motifs. Poster session presented at 2015 GIGA day, Liège, Belgium.

Gillain, S., Wojtasik, V., **Depierreux, F.**, Schwartz, C., Boutaayamou, M., Demonceau, M., Schmitz, X., Dardenne, N., Bruyère, O., Garraux, G., Petermans, J. 2015. Baseline characteristics of a two-year prospective study aiming to link clinical components, cognitive and gait performances in healthy old people: the GABY Study. Poster session presented at 11th International Congress of the European Union Geriatric Medicine Society, Oslo, Norway.

Gillain, S., Wojtasik, V., **Depierreux, F.**, Schwartz, C., Boutaayamou, M., Demonceau, M., Schmitz, X., Dardenne, N., Bruyère, O., Garraux, G., Petermans, J. 2015. Physical and mental determinants of falls inhealthy old people: baseline date of the gabi study. Poster session presented at the 11th Congress of EUGMS, Oslo, Norway.

Jedidi, H., **Depierreux, F.**, Jedidi, Z., Beckers, A. 2015. La pollution lumineuse, entre écologie et santé. Revue Médicale de Liège, 70(11), 557-562.

Depierreux, F., Fanielle, J., Lecomte, M., Hans, G., Maquet, P., Poirrier, R. 2014. La Narcolepsie-Cataplexie aujourd'hui. Revue Médicale de Liège, 69(2), 72-81.

Battisti, O., Zigabe, S., Nyamugabo Munyere Nkana, K., GkiougkiI, E., Kefala, K., **Depierreux, F**. 2014. Intérêts de l'observation des réflexes archaïques et des mouvements généraux chez le nouveau-né et le nourrisson. Annales Africaine de Médecine. 7(4): 1828-1832.

Depierreux, F., Cremers, J., Skawiniak, E., Parmentier, E., Delvaux, V., Garraux, G. 2013. Les troubles du contrôle des impulsions associés au traitement dopaminergique substitutif antiparkinsonien. Revue Médicale de Liège, 68 (mai-juin), 221-225.

2 THIRD-CYCLE DISSERTATIONS

Depierreux, F. 2020. Les dystonies focales de l'enfant. Unpublished DEA/DES thesis, Université de Montpellier, Montpellier, France. Jury: Pr Roubertie, A., & Pr Doummar, D**.**

Depierreux, F. 2016. Approche des troubles cognitifs en unité de mouvements anormaux. Unpublished DEA/DES thesis, Université de Paris-Est Créteil, Paris, France. Jury: Pr Lefebvre des Noettes, V.

PART 5

References

Adler CH, Beach TG, Shill HA, Caviness JN, Sue LI, Jacobson SA, et al. Low clinical diagnostic accuracy of early vs advanced Parkinson disease. Neurology 2014; 83: 406–12.

Albin RL, Young AB, Penney JB. The functional anatomy of basal ganglia disorders. Trends Neurosci 1989; 12: 366–75.

Alexander GE. Basal ganglia-thalamocortical circuits: their role in control of movements. J Clin Neurophysiol 1994; 11: 420–31.

Alexander GE, Crutcher MD, DeLong MR. Basal ganglia-thalamocortical circuits: parallel substrates for motor, oculomotor, 'prefrontal' and 'limbic' functions. Prog Brain Res 1990; 85: 119–46.

Andersen HH, Johnsen KB, Moos T. Iron deposits in the chronically inflamed central nervous system and contributes to neurodegeneration. Cell Mol Life Sci 2014; 71: 1607–22.

Antoniades CA, Barker R. The search for biomarkers in Parkinson ' s disease : a critical review. Expert Rev Neurother 2009; 8(12): 1841–52.

Antonini A, Leenders KL, Vontobel P, Maguire RP, Missimer J, Psylla M, et al. Complementary PET studies of striatal neuronal function in the differential diagnosis between multiple system atrophy and Parkinson's disease. Brain 1997; 120 (Pt 1: 2187–95.

Aquino D, Bizzi A, Grisoli M, Garavaglia B, Bruzzone MG, Nardocci N, et al. Age-related iron deposition in the basal ganglia: quantitative analysis in healthy subjects. Radiology 2009; 252: 165–72.

Aquino D, Contarino V, Albanese A, Minati L, Farina L, Grisoli M, et al. Substantia nigra in Parkinson's disease: A multimodal MRI comparison between early and advanced stages of the disease. Neurol Sci 2014; 35: 753–8.

Arnulf I, Bonnet AM, Damier P, Bejjani BP, Seilhean D, Derenne JP, et al. Hallucinations, REM sleep, and Parkinson's disease: a medical

hypothesis. Neurology 2000; 55: 281–8.

Arribarat G, Pasternak O, De Barros A, Galitzky M, Rascol O, Péran P. Substantia nigra locations of iron-content, free-water and mean diffusivity abnormalities in moderate stage Parkinson's disease. Park Relat Disord 2019; 65: 146–52.

Aschermann Z, Perlaki G, Orsi G, Nagy SA, Horvath A, Bone B, et al. Quantitative assessment of brain iron by R2* relaxometry in patients with cervical dystonia. Mov Disord 2015; 30: 1422–6.

Ashburner J. A fast diffeomorphic image registration algorithm. Neuroimage 2007; 38: 95–113.

Ashburner J, Csernansky JG, Davatzikos C, Fox NC, Frisoni GB, Thompson PM. Computer-assisted imaging to assess brain structure in healthy and diseased brains. Lancet Neurol 2003; 2: 79–88.

Ashburner J, Friston KJ. Voxel-based morphometry--the methods. Neuroimage 2000; 11: 805–21.

Ashburner J, Friston KJ. Unified segmentation. Neuroimage 2005; 26: 839–51.

Azuma M, Hirai T, Yamada K, Yamashita S, Ando Y, Tateishi M, et al. Lateral Asymmetry and Spatial Difference of Iron Deposition in the Substantia Nigra of Patients with Parkinson Disease Measured with Quantitative Susceptibility Mapping. Am J Neuroradiol 2016; 37: 782–8.

Bagnato F, Hametner S, Boyd E, Endmayr V, Shi Y, Ikonomidou V, et al. Untangling the R2* contrast in multiple sclerosis: A combined MRI-histology study at 7.0 Tesla. PLoS One 2018; 13: 1–19.

Banati RB, Daniel SE, Blunt SB. Glial pathology but absence of apoptotic nigral neurons in long-standing Parkinson's disease. Mov Disord 1998; 13: 221–7.

Banerjee M, Okun MS, Vaillancourt DE, Vemuri BC. A method for automated classification of Parkinson's disease diagnosis using an ensemble average propagator template brain map estimated from diffusion MRI. PLoS One 2016; 11: 1–11.

Barrea C, Depierreux F. Recurrent Ataxia and Dystonia with Anti-Neurochondrin Autoantibodies. Neuropediatrics 2021

Barrea C, Depierreux F, Servais L. Odalisque's Position as a Geste Antagoniste in a Variant Phenotype of Ataxia-Telangiectasia. Mov Disord Clin Pract 2019; 6: 413–4.

Baudrexel S, Nürnberger L, Rüb U, Seifried C, Klein JC, Deller T, et al. Quantitative mapping of T1 and T2* discloses nigral and brainstem pathology in early Parkinson's disease. Neuroimage 2010; 51: 512–20.

Becker G, Bahri MA, Michel A, Hustadt F, Garraux G, Luxen A, et al. Comparative assessment of 6-[18 F]fluoro-L-m-tyrosine and 6-[18 F]fluoro-L-dopa to evaluate dopaminergic presynaptic integrity in a Parkinson's disease rat model. J Neurochem 2017; 141: 626–35.

Berardelli a, Wenning GK, Antonini A, Berg D, Bloem BR, Bonifati V, et al. EFNS/MDS-ES/ENS recommendations for the diagnosis of Parkinson's disease. Eur J Neurol 2013; 20: 16–34.

Berg D. In vivo detection of iron and neuromelanin by transcranial sonography – a new approach for early detection of substantia nigra damage. J Neural Transm 2006; 113: 775–80.

Berg D. Hyperechogenicity of the substantia nigra: pitfalls in assessment and specificity for Parkinson's disease. J Neural Transm 2011; 118: 453–61.

Berg D, Behnke S, Walter U. Application of Transcranial Sonography in Extrapyramidal Disorders: Updated Recommendations. Ultraschall der Medizin - Eur J Ultrasound 2006; 27: 12–9.

Berg D, Roggendorf W, Schröder U, Klein R, Tatschner T, Benz P, et al. Echogenicity of the Substantia Nigra. Arch Neurol 2002; 59: 999.

Bernheimer H, Birkmayer W, Hornykiewicz O, Jellinger K, Seitelberger F. Brain dopamine and the syndromes of Parkinson and Huntington Clinical, morphological and neurochemical correlations. J Neurol Sci 1973; 20: 415–55.

Biondetti E, Gaurav R, Yahia-Cherif L, Mangone G, Pyatigorskaya N, Valabrègue R, et al. Spatiotemporal changes in substantia nigra neuromelanin content in Parkinson's disease. Brain 2020; 143: 2757–70.

Black KJ, Ongur D, Perlmutter JS. Putamen volume in idiopathic focal dystonia. Neurology 1998; 51: 819–24.

Blazejewska AI, Schwarz ST, Pitiot A, Stephenson MC, Lowe J, Bajaj N, et al. Visualization of nigrosome 1 and its loss in PD: Pathoanatomical correlation and in vivo 7 T MRI. Neurology 2013; 81: 534–40.

Bouwmans AEP, Vlaar AMM, Srulijes K, Mess WH, Weber WEJ. Transcranial Sonography for the Discrimination of Idiopathic Parkinson's Disease from the Atypical Parkinsonian Syndromes. 2010. p. 121–46

Braak H, Rüb U, Gai WP, Del Tredici K. Idiopathic Parkinson's disease: Possible routes by which vulnerable neuronal types may be subject to neuroinvasion by an unknown pathogen. J Neural Transm 2003; 110: 517–36.

Braak H, Sandmann-Keil D, Gai W, Braak E. Extensive axonal Lewy neurites in Parkinson's disease: A novel pathological feature revealed by α-synuclein immunocytochemistry. Neurosci Lett 1999;265: 67–9.

Braak H, Del Tredici K. Neuroanatomy and pathology of sporadic Parkinson's disease. Adv Anat Embryol Cell Biol 2009; 201: 1–119.

Bradley D, Whelan R, Walsh R, Reilly RB, Hutchinson S, Molloy F, et al. Temporal Discrimination Threshold: VBM evidence for an endophenotype in adult onset primary torsion dystonia. Brain 2009; 132: 2327–35.

Brooks DJ, Frey KA, Marek KL, Oakes D, Paty D, Prentice R, et al. Assessment of neuroimaging techniques as biomarkers of the progression of Parkinson's disease. Exp Neurol 2003; 184: 68–79.

Brooks DJ, Ibanez V, Sawle G V., Playford ED, Quinn N, Mathias CJ, et al. Striatal D2 receptor status in patients with Parkinson's disease, striatonigral degeneration, and progressive supranuclear palsy, measured with11C-raclopride and positron emission tomography. Ann Neurol 1992; 31: 184–92.

Brooks DJ, Ibanez V, Sawle G V., Quinn N, Lees AJ, Mathias CJ, et al. Differing patterns of striatal18F-dopa uptake in Parkinson's disease, multiple system atrophy, and progressive supranuclear palsy. Ann Neurol 1990; 28: 547–55.

Brück A, Aalto S, Nurmi E, Vahlberg T, Bergman J, Rinne JO. Striatal subregional 6-[18 F]fluoro- L -dopa uptake in early Parkinson's disease: A two-year follow-up study. Mov Disord 2006; 21: 958–63.

Brück A, Aalto S, Rauhala E, Bergman J, Marttila R, Rinne JO. A follow-up study on 6-[18F]fluoro-L-dopa uptake in early Parkinson's disease shows nonlinear progression in the putamen. Mov Disord 2009; 24: 1009–15.

Califf RM. Minireview Biomarker definitions and their applications. 2018: 213–21.

Callaghan MF, Freund P, Draganski B, Anderson E, Cappelletti M, Chowdhury R, et al. Widespread age-related differences in the human brain microstructure revealed by quantitative magnetic resonance imaging. Neurobiol Aging 2014; 35: 1862–72.

Cassidy CM, Zucca FA, Girgis RR, Baker SC, Weinstein JJ, Sharp ME, et al. Neuromelanin-sensitive MRI as a noninvasive proxy measure of dopamine function in the human brain. Proc Natl Acad Sci U S A 2019; 116: 5108–17.

Castellani RJ, Siedlak SL, Perry G, Smith MA. Sequestration of iron by Lewy bodies in Parkinson's disease. Acta Neuropathol 2000; 100: 111–4.

Castellanos G, Fernández-Seara MA, Lorenzo-Betancor O, Ortega-Cubero S, Puigvert M, Uranga J, et al. Automated Neuromelanin Imaging as a Diagnostic Biomarker for Parkinson's Disease. Mov Disord 2015; 30: 945–52.

Chaudhuri KR, Healy DG, Schapira AH. Non-motor symptoms of Parkinson's disease: diagnosis and management. Lancet Neurol 2006; 5: 235–45.

Chaudhuri KR, Martinez-Martin P, Brown RG, Sethi K, Stocchi F, Odin P, et al. The metric properties of a novel non-motor symptoms scale for Parkinson's disease: Results from an international pilot study. Mov Disord 2007; 22: 1901–11.

Chen X, Huddleston DE, Langley J, Ahn S, Barnum CJ, Factor SA, et al. Simultaneous imaging of locus coeruleus and substantia nigra with a quantitative neuromelanin MRI approach. Magn Reson Imaging 2014; 32: 1301–6.

Cheng HC, Ulane CM, Burke RE. Clinical progression in Parkinson disease and the neurobiology of axons. Ann Neurol 2010; 67: 715–25.

Chu W, Zhou D, Gaba V, Liu J, Li S, Peng X, et al. Design, Synthesis, and Characterization of 3-(Benzylidene)indolin-2-one Derivatives as Ligands for α-Synuclein Fibrils. J Med Chem 2015; 58: 6002–17.

Cigdem O, Beheshti I, Demirel H. Effects of different covariates and contrasts on classification of Parkinson's disease using structural MRI.

Comput Biol Med 2018; 99: 173–81.

Clayton DF, George JM. Synucleins in synaptic plasticity and neurodegenerative disorders. J Neurosci Res 1999; 58: 120–9.

Colloby SJ, McParland S, O'Brien JT, Attems J. Neuropathological correlates of dopaminergic imaging in Alzheimer's disease and Lewy body dementias. Brain 2012; 135: 2798–808.

Crossman AR. Primate models of dyskinesia: the experimental approach to the study of basal ganglia-related involuntary movement disorders. Neuroscience 1987; 21: 1–40.

Damier P, Hirsch EC, Agid Y, Graybiel AM. The substantia nigra of the human brain: I. Nigrosomes and the nigral matrix, a compartmental organization based on calbindin D(28K) immunohistochemistry. Brain 1999; 122: 1421–36.

Damier P, Hirsch EC, Agid Y, Graybiel AM. The substantia nigra of the human brain II . Patterns of loss of dopamine-containing neurons in Parkinson ' s disease. Brain 1999; 122: 1437–48.

DeJesus OT, Endres CJ, Shelton SE, Nickles RJ, Holden JE. Evaluation of fluorinated m-tyrosine analogs as PET imaging agents of dopamine nerve terminals: comparison with 6-fluoroDOPA. J Nucl Med 1997; 38: 630–6.

Deoni SCL, Williams SCR, Jezzard P, Suckling J, Murphy DGM, Jones DK. Standardized structural magnetic resonance imaging in multicentre studies using quantitative T1 and T2 imaging at 1.5 T. Neuroimage 2008; 40: 662–71.

Depierreux F, Jedidi H, Hardy PY, Parmentier E, Garraux G. [How to explore... a cervical dystonia]. Rev Med Liege 2020; 75: 121–4.

Depierreux F, Parmentier É, Hardy P-Y, Leroy P, Maquet P. Successful treatment of hand dystonia with botulinum toxin in a DYT12 patient. Toxicon 2021; 190S1: s16.

Depierreux, Frédérique; Parmentier, Eric; Mackels, Laurane; Baquero Duarte, Katherine; Degueldre, Christian; Balteau, Evelyne; Salmon, Eric; Philips, Christophe; Bahri, Mohamed Ali; Maquet, Pierre; Garraux G. Parkinson's disease multimodal imaging: F-DOPA PET, neuromelanin-sensitive and quantitative iron-sensitive MRI. npj Park Dis 2021: 1–10.

Dexter DT, Wells FR, Agid F, Agid Y, Lees AJ, Jenner P, et al. Increased nigral iron content in postmortem parkinsonian brain. Lancet (London, England) 1987; 2: 1219–20.

Dexter DT, Wells FR, Lee AJ, Agid F, Agid Y, Jenner P, et al. Increased Nigral Iron Content and Alterations in Other Metal Ions Occurring in Brain in Parkinson's Disease. J Neurochem 1989; 52: 1830–6.

Dickson DW, Braak H, Duda JE, Duyckaerts C, Gasser T, Halliday GM, et al. Neuropathological assessment of Parkinson's disease: refining the diagnostic criteria. Lancet Neurol 2009; 8: 1150–7.

Draganski B, Ashburner J, Hutton C, Kherif F, Frackowiak RSJ, Helms G, et al. Regional specificity of MRI contrast parameter changes in normal ageing revealed by voxel-based quantification (VBQ). Neuroimage 2011; 55: 1423–34.

Draganski B, Schneider SA, Fiorio M, Klöppel S, Gambarin M, Tinazzi M, et al. Genotype-phenotype interactions in primary dystonias revealed by differential changes in brain structure. Neuroimage 2009; 47: 1141–7.

Drion E, Depierreux F. Botulinum toxin treatment of focal dystonia in kernicterus-related movement disorders. Toxicon 2021; 190S1: S17–8.

Du G, Lewis MM, Sen S, Wang J, Shaffer ML, Styner M, et al. Imaging nigral pathology and clinical progression in Parkinson's disease. Mov Disord 2012; 27: 1636–43.

Du G, Lewis MM, Sica C, He L, Connor JR, Kong L, et al. Distinct progression pattern of susceptibility MRI in the substantia nigra of Parkinson's patients. Mov Disord 2018; 33: 1423–31.

Du G, Liu T, Lewis MM, Kong L, Wang Y, Connor J, et al. Quantitative susceptibility mapping of the midbrain in Parkinson's disease. Mov Disord 2016; 31: 317–24.

Eimeren T van, Siebner HR. An update on functional neuroimaging of parkinsonism and dystonia. Curr Opin Neurol 2006; 19: 412–9.

Engelhardt E. Lafora and Trétiakoff: the naming of the inclusion bodies discovered by Lewy. Arq Neuropsiquiatr 2017; 75: 751–3.

Erkkinen MG, Kim M, Geschwind MD. Clinical Neurology and Epidemiology of the Major Neurodegenerative Diseases. Cold Spring Harb Perspect Biol 2018; 10: a033118.

Eshuis SA, Maguire RP, Leenders KL, Jonkman S, Jager PL. Comparison of FP-CIT SPECT with F-DOPA PET in patients with de novo and advanced Parkinson's disease. Eur J Nucl Med Mol Imaging 2006; 33: 200–9.

Fahn, S.; Elton R. U program members. Unified Parkinson's Disease Rating Scale. In: Recent developments in Parkinsons disease, vol 2. Macmillan Healthcare Information; 1987. p. 153–63

Fahn S, Jankovic J, Hallett M. Principles and Practice of Movement Disorders, second edition. Elsevier S. 2011

Faucheux BA, Bonnet AM, Agid Y, Hirsch EC. Blood vessels change in the mesencephalon of patients with Parkinson's disease. Lancet (London, England) 1999; 353: 981–2.

Fearnley JM, Lees AJ. Ageing and Parkinson's disease: substantia nigra regional selectivity. Brain 1991; 114 (Pt 5: 2283–301.

Fedorow H, Tribl F, Halliday G, Gerlach M, Riederer P, Double KL. Neuromelanin in human dopamine neurons: comparison with peripheral melanins and relevance to Parkinson's disease. Prog Neurobiol 2005; 75: 109–24.

Fenichel GM, Bazelon M. Studies on neuromelanin. II. Melanin in the brainstems of infants and children. Neurology 1968; 18: 817–20.

Galazka-Friedman J, Bauminger ER, Friedman A, Barcikowska M, Hechel D, Nowik I. Iron in parkinsonian and control substantia nigra?A mössbauer spectroscopy study. Mov Disord 1996; 11: 8–16.

Gallagher CL, Oakes TR, Johnson SC, Chung MK, Holden JE, Bendlin BB, et al. Rate of 6-[18F]fluorodopa uptake decline in striatal subregions in Parkinson's disease. Mov Disord 2011; 26: 614–20.

García-Lorenzo D, Longo-Dos Santos C, Ewenczyk C, Leu-Semenescu S, Gallea C, Quattrocchi G, et al. The coeruleus/subcoeruleus complex in rapid eye movement sleep behaviour disorders in Parkinson's disease. Brain 2013; 136: 2120–9.

Garnett ES, Firnau G, Nahmias C. Dopamine visualized in the basal ganglia of living man. Nature 1983; 305: 137–8.

Garraux G, Bauer A, Hanakawa T, Wu T, Kansaku K, Hallett M. Changes in Brain Anatomy in Focal Hand Dystonia. Ann Neurol 2004; 55: 736–9.

Garraux G, Phillips C, Schrouff J, Kreisler A, Lemaire C, Degueldre C, et al. Multiclass classification of FDG PET scans for the distinction between Parkinson's disease and atypical parkinsonian syndromes. NeuroImage Clin 2013; 2: 883–93.

Gaurav R, Yahia-Cherif L, Pyatigorskaya N, Mangone G, Biondetti E, Valabrègue R, et al. Longitudinal Changes in Neuromelanin MRI Signal in Parkinson's Disease: A Progression Marker. Mov Disord 2021: 1–11.

Gelb DJ, Oliver E, Gilman S. Diagnostic Criteria for Parkinson Disease. Arch Neurol 1999; 56: 33.

Gerlach M, Ben-Shachar D, Riederer P, Youdim MB. Altered brain metabolism of iron as a cause of neurodegenerative diseases? J Neurochem 1994; 63: 793–807.

Gibb WR. Melanin, tyrosine hydroxylase, calbindin and substance P in the human midbrain and substantia nigra in relation to nigrostriatal projections and differential neuronal susceptibility in Parkinson's disease. Brain Res 1992; 581: 283–91.

Gibb WR, Lees AJ. The relevance of the Lewy body to the pathogenesis of idiopathic Parkinson's disease. J Neurol Neurosurg Psychiatry 1988; 51: 745–52.

Gibb WRG, Lees AJ. Anatomy, pigmentation, ventral and dorsal subpopulations of the substantia nigra, and differential cell death in Parkinson's disease. J Neurol Neurosurg Psychiatry 1991; 54: 388–96.

Goetz CG, Tilley BC, Shaftman SR, Stebbins GT, Fahn S, Martinez-Martin P, et al. Movement Disorder Society-sponsored revision of the Unified Parkinson's Disease Rating Scale (MDS-UPDRS): Scale presentation and clinimetric testing results. Mov Disord 2008; 23: 2129–70.

Gorell JM, Ordidge RJ, Brown GG, Deniau J-C, Buderer NM, Helpern JA. Increased iron-related MRI contrast in the substantia nigra in Parkinson's disease. Neurology 1995; 45: 1138–43.

Gracien RM, Petrov F, Hok P, van Wijnen A, Maiworm M, Seiler A, et al. Multimodal quantitative mri reveals no evidence for tissue pathology in idiopathic cervical dystonia. Front Neurol 2019; 10: 4–11.

Graham JM, Paley MN, Grünewald RA, Hoggard N, Griffiths PD. Brain iron deposition in Parkinson's disease imaged using the PRIME magnetic resonance sequence. Brain 2000; 123 Pt 12: 2423–31.

Gramsch C, Reuter I, Kraff O, Quick HH, Tanislav C, Roessler F, et al. Nigrosome 1 visibility at susceptibility weighted 7T MRI-A dependable diagnostic marker for Parkinson's disease or merely an inconsistent, age-dependent imaging finding? PLoS One 2017; 12: e0185489.

Gröger A, Berg D. Does structural neuroimaging reveal a disturbance of iron metabolism in Parkinson's disease? Implications from MRI and TCS studies. J Neural Transm 2012; 119: 1523–8.

Haacke EM, Xu Y, Cheng YCN, Reichenbach JR. Susceptibility weighted imaging (SWI). Magn Reson Med 2004; 52: 612–8.

Haber SN. The place of dopamine in the cortico-basal ganglia circuit. Neuroscience 2014; 282: 248–57.

Hagenah JM, König IR, Becker B, Hilker R, Kasten M, Hedrich K, et al. Substantia nigra hyperechogenicity correlates with clinical status and number of Parkin mutated alleles. J Neurol 2007; 254: 1407–13.

Hallgren B, Sourander P. The effect of age on the non-haemine iron in the human brain. J Neurochem 1958; 3: 41–51.

Hallgren B, Sourander P. The effect of age on the non-haemin iron in the human brain. J Neurochem 1958; 3: 41–51.

Halliday G, Lees A, Stern M. Milestones in Parkinson ' s Disease — Clinical and Pathologic Features. Mov Disord 2011; 26: 1015–21.

Hardy PY, Hallet C, Kirsch M, Samalea Suarez N, Hick G, Petry J, et al. Anesthetic Management of a Child With Rapid-Onset Dystonia-Parkinsonism (DYT12-ATP1A3): A Case Report. A&A Pract 2021; 15: e01440.

Hare DJ, Double KL. Iron and dopamine: A toxic couple. Brain 2016; 139: 1026–35.

Hasegawa K, Kowa H. Autosomal dominant familial Parkinson disease: older onset of age, and good response to levodopa therapy. Eur Neurol 1997; 38 Suppl 1: 39–43.

Hassler R. Zur Normalanatomie der Substantia nigra. J für Psychol und Neurol 1937: 1–56.

He X, Yablonskiy DA. Biophysical mechanisms of phase contrast in gradient echo MRI. Proc Natl Acad Sci U S A 2009; 106: 13558–63.

Helms G, Draganski B, Frackowiak R, Ashburner J, Weiskopf N. Improved segmentation of deep brain grey matter structures using magnetization transfer (MT) parameter maps. Neuroimage 2009; 47: 194–8.

Herb JN, Rane S, Isaacs DA, Van Wouwe N, Roman OC, Landman BA, et al. Cortical Implications of Advancing Age and Disease Duration in Parkinson's Disease Patients with Postural Instability and Gait Dysfunction. J Parkinsons Dis 2016; 6: 441–51.

Hirsch EC, Brandel J -P, Galle P, Javoy-Agid F, Agid Y. Iron and Aluminum Increase in the Substantia Nigra of Patients with Parkinson's Disease: An X-Ray Microanalysis. J Neurochem 1991; 56: 446–51.

Hirsch EC, Graybiel AM, Agid Y. Melanized dopaminergic neurons are differentially affected in Parkinson's disease. Nature 1988; 334: 345–348.

Hirsch EC, Hunot S. Neuroinflammation in Parkinson's disease: a target for neuroprotection? Lancet Neurol 2009; 8: 382–97.

Hirtz D, Thurman DJ, Gwinn-Hardy K, Mohamed M, Chaudhuri AR, Zalutsky R. How common are the 'common' neurologic disorders? Neurology 2007; 68: 326–37.

Hoehn MM, Yahr MD. Parkinsonism: onset, progression, and mortality. Neurology 1967; 17: 427–427.

Hopes L, Grolez G, Moreau C, Lopes R, Ryckewaert G, Carrière N, et al. Magnetic resonance imaging features of the nigrostriatal system: Biomarkers of Parkinson's disease stages? PLoS One 2016; 11

Hughes AJ, Daniel SE, Kilford L, Lees a J. Accuracy of clinical diagnosis of idiopathic Parkinson's disease: a clinico-pathological study of 100 cases. J Neurol Neurosurg Psychiatry 1992; 55: 181–4.

Innis RB, Seibyl JP, Scanley BE, Laruelle M, Abi-Dargham A, Wallace E, et al. Single photon emission computed tomographic imaging demonstrates loss of striatal dopamine transporters in Parkinson disease. Proc Natl Acad Sci U S A 1993; 90: 11965–9.

Isaias IU, Trujillo P, Summers P, Marotta G, Mainardi L, Pezzoli G, et al. Neuromelanin imaging and dopaminergic loss in parkinson's disease. Front Aging Neurosci 2016; 8: 1–12.

Ishikawa T, Dhawan V, Kazumata K, Chaly T, Mandel F, Neumeyer J, et al. Comparative nigrostriatal dopaminergic imaging with iodine-123-βCIT- FP/SPECT and fluorine-18-FDOPA/PET. J Nucl Med 1996; 37: 1760–5.

Ito H, Kodaka F, Takahashi H, Takano H, Arakawa R, Shimada H, et al. Relation between presynaptic and postsynaptic dopaminergic functions measured by positron emission tomography: Implication of dopaminergic tone. J Neurosci 2011; 31: 7886–90.

Ito Y, Fujita M, Shimada S, Watanabe Y, Okada T, Kusuoka H, et al. Comparison between the decrease of dopamine transporter and that of L-DOPA uptake for detection of early to advanced stage of Parkinson's disease in animal models. Synapse 1999; 31: 178–85.

Jakobson Mo S, Axelsson J, Jonasson L, Larsson A, Ögren MJ, Ögren M, et al. Dopamine transporter imaging with [18F]FE-PE2I PET and [123I]FP-CIT SPECT—a clinical comparison. EJNMMI Res 2018; 8

Jellinger K, Paulus W, Grundke-Iqbal I, Riederer P, Youdim MBH. Brain iron and ferritin in Parkinson's and Alzheimer's diseases. J Neural Transm - Park Dis Dement Sect 1990; 2: 327–40.

Jenkinson C, Fitzpatrick R, Peto V, Greenhall R, Hyman N. The Parkinson's Disease Questionnaire (PDQ-39): development and validation of a Parkinson's disease summary index score. Age Ageing 1997; 26: 353–7.

Jokinen P, Helenius H, Rauhala E, Br A. Simple Ratio Analysis of 18 F-Fluorodopa Uptake in Striatal Subregions Separates Patients with Early Parkinson Disease from Healthy Controls. J Nucl Med 2009; 50: 893–9.

Kaasinen V, Vahlberg T. Striatal dopamine in Parkinson disease: A meta-analysis of imaging studies. Ann Neurol 2017; 82: 873–82.

Karimi M, Tian L, Brown CA, Flores HP, Loftin SK, Videen TO, et al. Validation of nigrostriatal positron emission tomography measures: Critical limits. Ann Neurol 2013; 73: 390–6.

Kashihara K, Shinya T, Higaki F. Reduction of neuromelanin-positive nigral volume in patients with MSA, PSP and CBD. Intern Med 2011; 50: 1683–7.

Kashihara K, Shinya T, Higaki F. Neuromelanin magnetic resonance imaging of nigral volume loss in patients with Parkinson's disease. J Clin Neurosci 2011; 18: 1093–6.

Kastner A, Hirsch EC, Lejeune O, Javoy-Agid F, Rascol O, Agid Y. Is the vulnerability of neurons in the substantia nigra of patients with Parkinson's disease related to their neuromelanin content? J Neurochem 1992; 59: 1080–9.

Keogh MJ, Aribisala BS, He J, Tulip E, Butteriss D, Morris C, et al. Voxel-based analysis in neuroferritinopathy expands the phenotype and determines radiological correlates of disease severity. J Neurol 2015; 262: 2232–40.

Kilbourn MR. 11C- and 18F-radiotracers for in vivo imaging of the dopamine system: Past, present and future. Biomedicines 2021; 9: 1–15.

Killilea DW, Wong SL, Cahaya HS, Atamna H, Ames BN. Iron accumulation during cellular senescence. Ann N Y Acad Sci 2004; 1019: 365–7.

Kish SJ, Shannak K, Hornykiewicz O. Uneven Pattern of Dopamine Loss in the Striatum of Patients with Idiopathic Parkinson's Disease. N Engl J Med 1988; 318: 876–80.

Kitao S, Matsusue E, Fujii S, Miyoshi F, Kaminou T, Kato S, et al. Correlation between pathology and neuromelanin MR imaging in Parkinson's disease and dementia with Lewy bodies. Neuroradiology 2013; 55: 947–53.

Kordower JH, Olanow CW, Dodiya HB, Chu Y, Beach TG, Adler CH, et al. Disease duration and the integrity of the nigrostriatal system in Parkinson's disease. Brain 2013; 136: 2419–31.

Kosta P, Argyropoulou MI, Markoula S, Konitsiotis S. MRI evaluation of the basal ganglia size and iron content in patients with Parkinson's disease. J Neurol 2006; 253: 26–32.

Kotzbauer PT, Tu Z, Mach RH. Current status of the development of PET radiotracers for imaging alpha synuclein aggregates in Lewy bodies and Lewy neurites. Clin Transl Imaging 2017; 5: 3–14.

Kraemmer J, Kovacs GG, Perju-Dumbrava L, Pirker S, Traub-Weidinger T, Pirker W. Correlation of striatal dopamine transporter imaging with post mortem substantia nigra cell counts. Mov Disord 2014; 29: 1767–73.

Kudo Y, Okamura N, Furumoto S, Tashiro M, Furukawa K, Maruyama M, et al. 2-(2-[2-Dimethylaminothiazol-5-yl]ethenyl)-6- (2-[fluoro]ethoxy)benzoxazole: a novel PET agent for in vivo detection of dense amyloid plaques in Alzheimer's disease patients. J Nucl Med 2007; 48: 553–61.

Kuya K, Shinohara Y, Miyoshi F, Fujii S, Tanabe Y, Ogawa T. Correlation between neuromelanin-sensitive MR imaging and 123I-FP-CIT SPECT in patients with parkinsonism. Neuroradiology 2016; 58: 351–6.

De La Fuente-Fernández R, Furtado S, Guttman M, Furukawa Y, Lee CS, Calne DB, et al. VMAT2 binding is elevated in dopa-responsive dystonia: Visualizing empty vesicles by PET. Synapse 2003; 49: 20–8.

Lafora GR. Nuevas invstigaciones sobre los cuerpos amiláceos del interior de las células nerviosas. Trab Lab Invest Biol Univers Madrid 1913; 11: 29–42.

Langkammer C, Krebs N, Goessler W, Scheurer E, Ebner F, Yen K, et al. Quantitative MR Imaging of Brain Iron: A Postmortem Validation Study. Radiology 2010; 257: 455–62.

Langkammer C, Schweser F, Krebs N, Deistung A, Goessler W, Scheurer E, et al. Quantitative susceptibility mapping (QSM) as a means to measure brain iron? A post mortem validation study. Neuroimage 2012; 62: 1593–9.

Langley J, He N, Huddleston DE, Chen S, Yan F, Crosson B, et al. Reproducible detection of nigral iron deposition in 2 Parkinson's disease cohorts. Mov Disord 2019; 34: 416–9.

Langley J, Huddleston DE, Chen X, Sedlacik J, Zachariah N, Hu X. A multicontrast approach for comprehensive imaging of substantia nigra. Neuroimage 2015; 112: 7–13.

Langley J, Huddleston DE, Liu CJ, Hu X. Reproducibility of locus coeruleus and substantia nigra imaging with neuromelanin sensitive MRI. Magn Reson Mater Physics, Biol Med 2017; 30: 121–5.

de Lau LM, Breteler MM. Epidemiology of Parkinson's disease. Lancet Neurol 2006; 5: 525–35.

Lee CS, Samii A, Sossi V, Ruth TJ, Schulzer M, Holden JE, et al. In vivo positron emission tomographic evidence for compensatory changes in presynaptic dopaminergic nerve terminals in Parkinson's disease. Ann Neurol 2000; 47: 493–503.

Lee HM, Kwon K-Y, Kim M-J, Jang J-W, Suh S, Koh S-B, et al. Subcortical grey matter changes in untreated, early stage Parkinson's disease without dementia. Parkinsonism Relat Disord 2014; 20: 622–6.

Lees AJ, Selikhova M, Andrade LA, Duyckaerts C. The black stuff and Konstantin Nikolaevich Tretiakoff. Mov Disord 2008; 23: 777–83.

Lehéricy S, Sharman MA, Dos Santos CL, Paquin R, Gallea C. Magnetic resonance imaging of the substantia nigra in Parkinson's disease. Mov Disord 2012; 27: 822–30.

Lewis MM, Du G, Baccon J, Snyder AM, Murie B, Cooper F, et al. Susceptibility MRI captures nigral pathology in patients with parkinsonian syndromes. Mov Disord 2018; 33: 1432–9.

Lewy FJH. Paralysis agitans. 1. Pathologische Anatomie. In: Lewandowsky M, editor(s). Handbuch der Neurologie, Dritter Band, Spezielle Neurologie I. Berlin: Julius Springer; 1912. p. 920–933

Lewy FJH. Zur pathologischen Anatomie der Paralysis agitans. Dtsch Ztschr Nervenheilkd 1914; 50: 50–5.

Lhermitte J, Kraus WM, McAlpine D. On the occurrence of abnormal deposits of iron in the brain in parkinsonism with special reference to its localisation. J Neurol Neurosurg Psychiatry 1924; S1-5: 195–208.

Li G, Zhai G, Zhao X, An H, Spincemaille P, Gillen KM, et al. 3D texture analyses within the substantia nigra of Parkinson's disease patients on quantitative susceptibility maps and R2* maps. Neuroimage 2019; 188: 465–72.

Li L, Leigh JS. Quantifying arbitrary magnetic susceptibility distributions with MR. Magn Reson Med 2004; 51: 1077–82.

Li X, Xing Y, Martin-Bastida A, Piccini P, Auer DP. Patterns of grey matter loss associated with motor subscores in early Parkinson's disease. NeuroImage Clin 2018; 17: 498–504.

Litvan I, MacIntyre A, Goetz CG, Wenning GK, Jellinger K, Verny M, et al. Accuracy of the clinical diagnoses of Lewy body disease, Parkinson disease, and dementia with Lewy bodies: a clinicopathologic study. Arch Neurol 1998; 55: 969–78.

Di Lorenzo Alho AT, Suemoto CK, Polichiso L, Tampellini E, de Oliveira KC, Molina M, et al. Three-dimensional and stereological characterization of the human substantia nigra during aging. Brain Struct Funct 2016; 221: 3393–403.

Lutti A, Hutton C, Finsterbusch J, Helms G, Weiskopf N. Optimization and validation of methods for mapping of the radiofrequency transmit field at 3T. Magn Reson Med 2010; 64: 229–38.

Lutti A, Stadler J, Josephs O, Windischberger C, Speck O, Bernarding J, et al. Robust and fast whole brain mapping of the RF transmit field B1 at 7T. PLoS One 2012; 7: 1–7.

Mandel S, Grunblatt E, Riederer P, Amariglio N, Jacob-Hirsch J, Rechavi G, et al. Gene expression profiling of sporadic Parkinson's disease substantia nigra pars compacta reveals impairment of ubiquitin-proteasome subunits, SKP1A, aldehyde dehydrogenase, and chaperone HSC-70. Ann N Y Acad Sci 2005; 1053: 356–75.

Mann DMA, Yates PO. Lipoprotein pigments - their relationship to ageing in the human nervous system II. The Melanin Content of Pigmented Nerve Cells. Brain 1974; 97: 489–98.

Martín-Bastida A, Lao-Kaim NP, Roussakis AA, Searle GE, Xing Y, Gunn RN, et al. Relationship between neuromelanin and dopamine terminals within the Parkinson's nigrostriatal system. Brain 2019; 142: 2023–36.

Martin-Bastida A, Pietracupa S, Piccini P. Neuromelanin in parkinsonian disorders: an update. Int J Neurosci 2017; 127: 1116–23.

Martin WRW, Wieler M, Gee M. Midbrain iron content in early Parkinson disease: A potential biomarker of disease status. Neurology 2008; 70: 1411–7.

Martins-Branco D, Esteves AR, Santos D, Arduino DM, Swerdlow RH, Oliveira CR, et al. Ubiquitin proteasome system in Parkinson's disease: a keeper or a witness? Exp Neurol 2012; 238: 89–99.

Mathis CA, Lopresti BJ, Ikonomovic MD, Klunk WE. Small-molecule PET Tracers for Imaging Proteinopathies. Semin Nucl Med 2017; 47: 553–75.

Matsuura K, Maeda M, Tabei K-I, Umino M, Kajikawa H, Satoh M, et al. A longitudinal study of neuromelanin-sensitive magnetic resonance imaging in Parkinson's disease. Neurosci Lett 2016; 633: 112–7.

Matsuura K, Maeda M, Yata K, Ichiba Y, Yamaguchi T, Kanamaru K, et al. Neuromelanin Magnetic Resonance Imaging in Parkinson's Disease and Multiple System Atrophy. Eur Neurol 2013; 70: 70–7.

McGeer PL, McGeer EG, Suzuki JS. Aging and Extrapyramidal Function. Arch Neurol 1977; 34: 33–5.

McNaught KSP, Belizaire R, Isacson O, Jenner P, Olanow CW. Altered proteasomal function in sporadic Parkinson's disease. Exp Neurol 2003; 179: 38–46.

Mondino F, Filippi P, Magliola U, Duca S. Magnetic resonance relaxometry in Parkinson's disease. Neurol Sci 2002; 23: s87–8.

Moore RY, Whone AL, Brooks DJ. Extrastriatal monoamine neuron function in Parkinson's disease: an 18F-dopa PET study. Neurobiol Dis 2008; 29: 381–90.

Morrish PK, Rakshi JS, Bailey DL, Sawle G V, Brooks DJ. Measuring the rate of progression and estimating the preclinical period of Parkinson ' s disease with [18 F] dopa PET. J Neurol Neurosurg Psychiatry 1998; 64: 314–9.

Morrish PK, Sawle G V., Brooks DJ. An [18F]dopa-PET and clinical study of the rate of progression in Parkinson's disease. Brain 1996; 119: 585–91.

Morrish PK, Sawle V, Brooks J. Clinical and [18F]dopa PET findings in early Parkinson's disease. J Neurol Neurosurg Psychiatry 1995; 59: 597–600.

Mudali D, Teune LK, Renken RJ, Leenders KL, Roerdink JBTM. Classification of Parkinsonian syndromes from FDG-PET brain data using decision trees with SSM/PCA features. Comput Math Methods Med 2015; 2015

Nandhagopal R, Kuramoto L, Schulzer M, Mak E, Cragg J, Lee CS, et al. Longitudinal progression of sporadic Parkinson's disease: A multi-tracer positron emission tomography study. Brain 2009;132: 2970–9.

Nandhagopal R, Kuramoto L, Schulzer M, Mak E, Cragg J, McKenzie J, et al. Longitudinal evolution of compensatory changes in striatal dopamine processing in Parkinson's disease. Brain 2011;134:3290–8.

Nandhagopal R, Mak E, Schulzer M, McKenzie J, McCormick S, Sossi V, et al. Progression of dopaminergic dysfunction in a LRRK2 kindred: a multitracer PET study. Neurology 2008; 71: 1790–5.

Neychev VK, Gross RE, Lehéricy S, Hess EJ, Jinnah HA. The functional neuroanatomy of dystonia. Neurobiol Dis 2011; 42: 185–201.

Nurmi E, Ruottinen HM, Bergman J, Haaparanta M, Solin O, Sonninen P, et al. Rate of progression in Parkinson's disease: A 6-[18F]fluoro-L-dopa PET study. Mov Disord 2001; 16: 608–15.

Obeso JA, Lanciego JL. Past, present, and future of the pathophysiological model of the basal ganglia. Front Neuroanat 2011; 5: 1–6.

Obeso JA, Marin C, Rodriguez-Oroz C, Blesa J, Benitez-Temiño B, Mena-Segovia J, et al. The basal ganglia in Parkinson's disease: current concepts and unexplained observations. Ann Neurol 2008; 64 Suppl 2: S30-46.

Ohtsuka C, Sasaki M, Konno K, Kato K, Takahashi J, Yamashita F, et al. Differentiation of early-stage parkinsonisms using neuromelanin-sensitive magnetic resonance imaging. Parkinsonism Relat Disord 2014; 20: 755–60.

Ohtsuka C, Sasaki M, Konno K, Koide M, Kato K, Takahashi J, et al. Changes in substantia nigra and locus coeruleus in patients with early-stage Parkinson's disease using neuromelanin-sensitive MR imaging. Neurosci Lett 2013; 541: 93–8.

Okuzumi A, Hatano T, Kamagata K, Hori M, Mori A, Oji Y, et al. Neuromelanin or DaT-SPECT: which is the better marker for discriminating advanced Parkinson's disease? Eur J Neurol 2019; 26: 1408–16.

Oliveira FPM, Castelo-Branco M. Computer-aided diagnosis of Parkinson's disease based on [(123)I]FP-CIT SPECT binding potential images, using the voxels-as-features approach and support vector machines. J Neural Eng 2015; 12: 026008.

Patel UK, Anwar A, Saleem S, Malik P, Rasul B, Patel K, et al. Artificial intelligence as an emerging technology in the current care of neurological disorders. J Neurol 2021; 268: 1623–42.

Patlak CS, Blasberg RG. Graphical evaluation of blood-to-brain transfer constants from multiple-time uptake data. Generalizations. J Cereb Blood Flow Metab 1985; 5: 584–90.

Péran P, Cherubini A, Luccichenti G, Hagberg G, Démonet JF, Rascol O, et al. Volume and iron content in basal ganglia and thalamus. Hum Brain Mapp 2009; 30: 2667–75.

Perlmutter JS, Norris SA. Neuroimaging biomarkers for Parkinson disease: Facts and fantasy. Ann Neurol 2014; 76: 769–83.

Polymeropoulos MH, Lavedan C, Leroy E, Ide SE, Dehejia A, Dutra A, et al. Mutation in the alpha-synuclein gene identified in families with Parkinson's disease. Science 1997; 276: 2045–7.

Postuma R, Berg D, Stern M, Poewe W, Olanow CW, Oertel W, et al. MDS clinical diagnostic criteria for Parkinson's disease. Mov Disord 2015; 30: 1591–601.

Postuma RB, Poewe W, Litvan I, Lewis S, Lang AE, Halliday G, et al. Validation of the MDS clinical diagnostic criteria for Parkinson's disease. Mov Disord 2018; 33: 1601–8.

Prange S, Metereau E, Thobois S. Structural Imaging in Parkinson's Disease: New Developments. Curr Neurol Neurosci Rep 2019; 19

Prasad S, Saini J, Yadav R, Pal PK. Motor asymmetry and neuromelanin imaging: Concordance in Parkinson's disease. Parkinsonism Relat Disord 2018; 53: 28–32.

Prashanth R, Dutta Roy S, Mandal PK, Ghosh S. Automatic classification and prediction models for early Parkinson's disease diagnosis from SPECT imaging. Expert Syst Appl 2014; 41: 3333–42.

Pringsheim T, Jette N, Frolkis A, Steeves TDL. The prevalence of Parkinson's disease: A systematic review and meta-analysis. Mov Disord 2014; 29: 1583–90.

Priovoulos N, Jacobs HIL, Ivanov D, Uludağ K, Verhey FRJ, Poser BA. High-resolution in vivo imaging of human locus coeruleus by magnetization transfer MRI at 3T and 7T. Neuroimage 2018; 168: 427–36.

Pyatigorskaya N, Gallea C, Garcia-Lorenzo D, Vidailhet M, Lehericy S. A review of the use of magnetic resonance imaging in Parkinson's disease. Ther Adv Neurol Disord 2014; 7: 206–20.

Pyatigorskaya N, Sanz-Morère CB, Gaurav R, Biondetti E, Valabregue R, Santin M, et al. Iron imaging as a diagnostic tool for parkinson's disease: A systematic review and meta-analysis. Front Neurol 2020; 11

Pyatigorskaya N, Sharman M, Corvol JC, Valabregue R, Yahia-Cherif L, Poupon F, et al. High nigral iron deposition in LRRK2 and Parkin mutation carriers using R2* relaxometry. Mov Disord 2015; 30: 1077–84.

Raghavendra U, Acharya UR, Adeli H. Artificial Intelligence Techniques for Automated Diagnosis of Neurological Disorders. Eur Neurol 2020; 82: 41–64.

Reimão S, Ferreira S, Nunes RG, Pita Lobo P, Neutel D, Abreu D, et al. Magnetic resonance correlation of iron content with neuromelanin in the substantia nigra of early-stage Parkinson's disease. Eur J Neurol 2016; 23

Reimão S, Pita Lobo P, Neutel D, Guedes LC, Coelho M, Rosa MM, et al. Substantia nigra neuromelanin-MR imaging differentiates essential tremor from PD. Mov Disord 2015; 30: 953–9.

Riederer P, Wuketich S. Time course of nigrostriatal degeneration in parkinson's disease - A detailed study of influential factors in human brain amine analysis. J Neural Transm 1976; 38: 277–301.

Rizzo G, Copetti M, Arcuti S, Martino D, Fontana A, Logroscino G. Accuracy of clinical diagnosis of Parkinson disease: A systematic review and meta-analysis. Neurology 2016; 86: 566–76.

Rizzo G, Copetti M, Arcuti S, Martino D, Fontana A, Logroscino G. Accuracy of clinical diagnosis of Parkinson disease: A systematic review and meta-analysis. Neurology 2016; 86: 566–76.

Rossi M, Ruottinen H, Elovaara I, Ryymin P, Soimakallio S, Eskola H, et al. Brain Iron Deposition and Sequence Characteristics in Parkinsonism. Invest Radiol 2010; 45: 795–802.

Saari L, Kivinen K, Gardberg M, Joutsa J, Noponen T, Kaasinen V. Dopamine transporter imaging does not predict the number of nigral neurons in Parkinson disease. Neurology 2017; 88: 1461–7.

Sampedro F, Marín-Lahoz J, Martínez-Horta S, Pagonabarraga J, Kulisevsky J. Dopaminergic degeneration induces early posterior cortical thinning in Parkinson's disease. Neurobiol Dis 2019; 124: 29–35.

Sasaki M, Shibata E, Tohyama K, Takahashi J, Otsuka K, Tsuchiya K, et al. Neuromelanin magnetic resonance imaging of locus ceruleus and substantia nigra in Parkinson's disease. Neuroreport 2006; 17: 1215–8.

Scherfler C, Khan NL, Pavese N, Lees AJ, Quinn NP, Brooks DJ, et al. Upregulation of dopamine D2 receptors in dopaminergic drug-naive patients with Parkin gene mutations. Mov Disord 2006; 21: 783–8.

Schmidt MA, Engelhorn T, Marxreiter F, Winkler J, Lang S, Kloska S, et al. Ultra high-field SWI of the substantia nigra at 7T: reliability and consistency of the swallow-tail sign. BMC Neurol 2017; 17: 194.

Schmierer K, Scaravilli F, Altmann DR, Barker GJ, Miller DH. Magnetization transfer ratio and myelin in postmortem multiple sclerosis brain. Ann Neurol 2004; 56: 407–15.

Schwarz ST, Afzal M, Morgan PS, Bajaj N, Gowland PA, Auer DP. The 'swallow tail' appearance of the healthy nigrosome - A new accurate test of Parkinson's disease: A case-control and retrospective cross-sectional MRI study at 3T. PLoS One 2014; 9

Schwarz ST, Rittman T, Gontu V, Morgan PS, Bajaj N, Auer DP. T1-weighted MRI shows stage-dependent substantia nigra signal loss in Parkinson's disease. Mov Disord 2011; 26: 1633–8.

Schwarz ST, Xing Y, Tomar P, Bajaj N, Auer DP. In Vivo assessment of brainstem depigmentation in Parkinson disease: Potential as a severity marker for multicenter studies. Radiology 2017; 283: 789–98.

Segovia F, Górriz JM, Ramírez J, Martínez-Murcia FJ, Levin J, Schuberth M, et al. Multivariate Analysis of 18F-DMFP PET Data to Assist the Diagnosis of Parkinsonism. Front Neuroinform 2017; 11: 23.

Shah M, Seibyl J, Cartier A, Bhatt R, Catafau AM. Molecular imaging insights into neurodegeneration: Focus on α-synuclein radiotracers. J Nucl Med 2014; 55: 1397–400.

Shamoto-Nagai M, Maruyama W, Akao Y, Osawa T, Tribl F, Gerlach M, et al. Neuromelanin inhibits enzymatic activity of 26S proteasome in human dopaminergic SH-SY5Y cells. J Neural Transm 2004; 111: 1253–65.

Shamoto-Nagai M, Maruyama W, Yi H, Akao Y, Tribl F, Gerlach M, et al. Neuromelanin induces oxidative stress in mitochondria through release of iron: mechanism behind the inhibition of 26S proteasome. J Neural Transm 2006; 113: 633–44.

Sian-Hülsmann J, Mandel S, Youdim MBH, Riederer P. The relevance of iron in the pathogenesis of Parkinson's disease. J Neurochem 2011; 118: 939–57.

Simões RM, Castro Caldas A, Grilo J, Correia D, Guerreiro C, Pita Lobo P, et al. A distinct neuromelanin magnetic resonance imaging pattern in parkinsonian multiple system atrophy. BMC Neurol 2020; 20: 1–12.

Snow BJ, Tooyama I, McGeer EG, Yamada T, Calne DB, Takahashi H, et al. Human positron emission tomographic [18F]Fluorodopa studies correlate with dopamine cell counts and levels. Ann Neurol 1993; 34: 324–30.

Sofic E, Riederer P, Heinsen H, Beckmann H, Reynolds G, Hebenstreit G, et al. Increased iron (II1) and total iron content in post mortem substantia nigra of parkinsonian brain. J Neural Transm 1988; 74: 199–205.

Sofic E, Riederer P, Heinsen H, Beckmann H, Reynolds GP, Hebenstreit G, et al. Increased iron (III) and total iron content in post mortem substantia nigra of parkinsonian brain. J Neural Transm 1988; 74: 199–205.

Spatz H. Über den eisennachweis im gehirn, besonders in zentren des extrapyramidal-motorischen systems. I. Teil. Zeitschrift für die gesamte Neurol und Psychiatr 1922; 77: 261–390.

Spillantini MG, Crowther RA, Jakes R, Hasegawa M, Goedert M. α-Synuclein in filamentous inclusions of Lewy bodies from Parkinson's disease and dementia with Lewy bodies. Proc Natl Acad Sci U S A 1998; 95: 6469–73.

Spillantini MG, Goedert M. The alpha-synucleinopathies: Parkinson's disease, dementia with Lewy bodies, and multiple system atrophy. Ann N Y Acad Sci 2000; 920: 16–27.

Spillantini MG, Schmidt ML, Lee VM-Y, Trojanowski JQ, Jakes R, Goedert M. α-Synuclein in Lewy bodies. Nature 1997; 388: 839–40.

Stefanis L. Alpha-Synuclein in Parkinson's Disease. Cold Spring Harb Perspect Med 2012; 2: a009399–a009399.

Sterling NW, Du G, Lewis MM, Dimaio C, Kong L, Eslinger PJ, et al. Striatal shape in Parkinson's disease. Neurobiol Aging 2013; 34: 2510–6.

Stoessl AJ, Lehericy S, Strafella AP. Imaging insights into basal ganglia function, Parkinson's disease, and dystonia. Lancet (London, England) 2014; 384: 532–44.

Stüber C, Morawski M, Schäfer A, Labadie C, Wähnert M, Leuze C, et al. Myelin and iron concentration in the human brain: a quantitative study of MRI contrast. Neuroimage 2014; 93 Pt 1: 95–106.

Sulzer D, Cassidy C, Horga G, Kang UJ, Fahn S, Casella L, et al. Neuromelanin detection by magnetic resonance imaging (MRI) and its promise as a biomarker for Parkinson's disease. NPJ Park Dis 2018; 4: 11.

Sulzer D, Zecca L. Intraneuronal dopamine-quinone synthesis: A review. Neurotox Res 1999; 1: 181–95.

Sulzer D, Zecca L. Intraneuronal dopamine-quinone synthesis: a review. Neurotox Res 2000; 1: 181–95.

Tabelow K, Balteau E, Ashburner J, Callaghan MF, Draganski B, Helms G, et al. hMRI - A toolbox for quantitative MRI in neuroscience and clinical research. Neuroimage 2019; 194: 191–210.

Takahashi H, Ohama E, Suzuki S, Horikawa Y, Ishikawa A, Morita T, et al. Familial juvenile parkinsonism: clinical and pathologic study in a family. Neurology 1994; 44: 437–41.

Taniguchi D, Hatano T, Kamagata K, Okuzumi A, Oji Y, Mori A, et al. Neuromelanin imaging and midbrain volumetry in progressive supranuclear palsy and Parkinson's disease. Mov Disord 2018; 33: 1488–92.

Thobois S, Guillouet S, Broussolle E. Contributions of PET and SPECT to the understanding of the pathophysiology of Parkinson's disease. Neurophysiol Clin 2001; 31: 321–40.

Thomas M, Jankovic J, Suteerawattananon M, Wankadia S, Caroline KS, Vuong KD, et al. Clinical gait and balance scale (GABS): validation and utilization. J Neurol Sci 2004; 217: 89–99.

Tomlinson CL, Stowe R, Patel S, Rick C, Gray R, Clarke CE. Systematic review of levodopa dose equivalency reporting in Parkinson's disease. Mov Disord 2010; 25: 2649–53.

Tretiakoff KN. Contribution a l'étude de l'anatomie pathologique du Locus Niger de Soemmering avec quelques déductions relative à la pathogénie des troubles du tonus muscularaire et de la maladie de Parkinson. 1919

Trujillo P, Summers PE, Ferrari E, Zucca FA, Sturini M, Mainardi LT, et al. Contrast mechanisms associated with neuromelanin-MRI. Magn Reson Med 2017; 78: 1790–800.

Tysnes OB, Storstein A. Epidemiology of Parkinson's disease. J Neural Transm 2017; 124: 901–5.

Tzourio-Mazoyer N, Landeau B, Papathanassiou D, Crivello F, Etard O, Delcroix N, et al. Automated anatomical labeling of activations in SPM using a macroscopic anatomical parcellation of the MNI MRI single-subject brain. Neuroimage 2002; 15: 273–89.

Uitti RJ, Rajput AH, Rozdilsky B, Bickis M, Wollin T, Yuen WK. Regional Metal Concentrations in Parkinson's Disease, Other Chronic Neurological Diseases, and Control Brains. Can J Neurol Sci / J Can des Sci Neurol 1989; 16: 310–4.

Ulla M, Bonny JM, Ouchchane L, Rieu I, Claise B, Durif F. Is R2* a New MRI Biomarker for the Progression of Parkinson's Disease? A Longitudinal Follow-Up. PLoS One 2013; 8: 1–8.

Uversky VN, Li J, Fink AL. Metal-triggered structural transformations, aggregation, and fibrillation of human α-synuclein: A possible molecular link between parkinson's disease and heavy metal exposure. J Biol Chem 2001; 276: 44284–96.

Uzuegbunam BC, Librizzi D, Yousefi BH. PET radiopharmaceuticals for Alzheimer's disease and Parkinson's disease diagnosis, the current and future landscape. 2020

Venegas-Francke P. Transcranial Sonography in the Discrimination of Parkinson's Disease Versus Vascular Parkinsonism. 2010;147–56.

Vlaar AMM, van Kroonenburgh MJPG, Kessels AGH, Weber WEJ. Meta-analysis of the literature on diagnostic accuracy of SPECT in parkinsonian syndromes. BMC Neurol 2007; 7: 27.

Wallis LI, Paley MNJ, Graham JM, Grünewald RA, Wignall EL, Joy HM, et al. MRI assessment of basal ganglia iron deposition in Parkinson's disease. J Magn Reson Imaging 2008; 28: 1061–7.

Walter U, Behnke S, Eyding J, Niehaus L, Postert T, Seidel G, et al. Transcranial brain parenchyma sonography in movement disorders: State of the art. Ultrasound Med Biol 2007; 33: 15–25.

Walter U, Klein C, Hilker R, Benecke R, Pramstaller PP, Dressler D. Brain parenchyma sonography detects preclinical parkinsonism. Mov Disord 2004; 19: 1445–9.

Wang J, Zhuang Q, Zhu L, Zhu H, Li T, Li R. Meta-analysis of brain iron levels of Parkinson ' s disease patients determined by postmortem and MRI measurements. Nat Publ Gr 2016: 1–13.

Wang Y, Liu T. Quantitative susceptibility mapping (QSM): Decoding MRI data for a tissue magnetic biomarker. Magn Reson Med 2015; 73: 82–101.

Ward RJ, Zucca FA, Duyn JH, Crichton RR, Zecca L. The role of iron in brain ageing and neurodegenerative disorders. Lancet Neurol 2014; 13: 1045–60.

Weiskopf N, Mohammadi S, Lutti A, Callaghan MF. Advances in MRI-based computational neuroanatomy: From morphometry to in-vivo histology. Curr Opin Neurol 2015; 28: 313–22.

Weiskopf N, Suckling J, Williams G, Correia M. MM, Inkster B, Tait R, et al. Quantitative multi-parameter mapping of R1, PD*, MT, and R2* at 3T: A multi-center validation. Front Neurosci 2013: 1–11.

Whone AL, Watts RL, Stoessl AJ, Davis M, Reske S, Nahmias C, et al. Slower progression of Parkinson's disease with ropinirole versus levodopa: The REAL-PET study. Ann Neurol 2003; 54: 93–101.

Wieler M, Gee M, Martin WRW. Longitudinal midbrain changes in early Parkinson's disease: Iron content estimated from R2*/MRI. Parkinsonism Relat Disord 2015; 21: 179–83.

Wilms H, Rosenstiel P, Sievers J, Deuschl G, Zecca L, Lucius R. Activation of microglia by human neuromelanin is NF-kappaB dependent and involves p38 mitogen-activated protein kinase: implications for Parkinson's disease. FASEB J 2003; 17: 500–2.

Xing Y, Sapuan A, Dineen RA, Auer DP. Life span pigmentation changes of the substantia nigra detected by neuromelanin-sensitive MRI. Mov Disord 2018; 33: 1792–9.

Xu J, Jia Z, Knutson MD, Leeuwenburgh C. Impaired iron status in aging research. Int J Mol Sci 2012; 13: 2368–86.

Yu L, Cui J, Padakanti PK, Engel L, Bagchi DP, Kotzbauer PT, et al. Synthesis and in vitro evaluation of α-synuclein ligands. Bioorg Med Chem 2012; 20: 4625–34.

Zaharchuk G, Gong E, Wintermark M, Rubin D, Langlotz CP. Deep learning in neuroradiology. Am J Neuroradiol 2018; 39: 1776–84.

Zecca L, Bellei C, Costi P, Albertini A, Monzani E, Casella L, et al. New melanic pigments in the human brain that accumulate in aging and block environmental toxic metals. Proc Natl Acad Sci U S A 2008; 105: 17567–72.

Zecca L, Berg D, Arzberger T, Ruprecht P, Rausch WD, Musicco M, et al. In vivo detection of iron and neuromelanin by transcranial sonography: a new approach for early detection of substantia nigra damage. Mov Disord 2005; 20: 1278–85.

Zecca L, Fariello R, Riederer P, Sulzer D, Gatti A, Tampellini D. The absolute concentration of nigral neuromelanin, assayed by a new sensitive method, increases throughout the life and is dramatically decreased in Parkinson's disease. FEBS Lett 2002; 510: 216–20.

Zecca L, Pietra R, Goj C, Mecacci C, Radice D, Sabbioni E. Iron and other metals in neuromelanin, substantia nigra, and putamen of human brain. J Neurochem 1994; 62: 1097–101.

Zecca L, Stroppolo A, Gatti A, Tampellini D, Toscani M, Gallorini M, et al. The role of iron and copper molecules in the neuronal vulnerability of locus coeruleus and substantia nigra during aging. Proc Natl Acad Sci U S A 2004; 101: 9843–8.

Zecca L, Stroppolo A, Gatti A, Tampellini D, Toscani M, Gallorini M, et al. The role of iron and molecules in the neuronal vulnerability of locus coeruleus and substantia nigra during aging. Proc Natl Acad Sci U S A 2004; 101: 9843–8.

Zecca L, Youdim MBH, Riederer P, Connor JR, Crichton RR. Iron, brain ageing and neurodegenerative disorders. Nat Rev Neurosci 2004; 5: 863–73.

Zhang W, Phillips K, Wielgus AR, Liu J, Albertini A, Zucca FA, et al. Neuromelanin activates microglia and induces degeneration of dopaminergic neurons: implications for progression of Parkinson's disease. Neurotox Res 2011; 19: 63–72.

Zucca FA, Basso E, Cupaioli FA, Ferrari E, Sulzer D, Casella L, et al. Neuromelanin of the human substantia Nigra: An update. Neurotox Res 2014; 25: 13–23.

Zucca FA, Segura-Aguilar J, Ferrari E, Muñoz P, Paris I, Sulzer D, et al. Interactions of iron, dopamine and neuromelanin pathways in brain aging and Parkinson's disease. Prog Neurobiol 2017; 155: 96–119.

Zucca FA, Vanna R, Cupaioli FA, Bellei C, De Palma A, Di Silvestre D, et al. Neuromelanin organelles are specialized autolysosomes that accumulate undegraded proteins and lipids in aging human brain and are likely involved in Parkinson's disease. NPJ Park Dis 2018; 4: 17.